

AWS/TN-87/002

REVISED

Supersedes  
AD-A 184 814

(2)

AD-A207 904



## ISENTROPIC ANALYSIS AND INTERPRETATION:

OPERATIONAL APPLICATIONS TO SYNOPTIC  
AND MESOSCALE FORECAST PROBLEMS

**S DTIC ELECTE MAY 22 1989 D**  
By  
Dr. James T. Moore

Saint Louis University  
Department of Earth and Atmospheric Sciences  
P.O. Box 8099-Laclede Station  
St. Louis, Missouri 63156

**AUGUST 1987**

**REVISED MAY 1989**

APPROVED FOR PUBLIC RELEASE; DISTRIBUTION IS UNLIMITED.

**AIR WEATHER SERVICE (MAC)  
Scott Air Force Base, Illinois, 62225-5008**

89 5 14 007

**REVIEW AND APPROVAL STATEMENT**

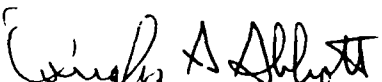
AWS/TN-87/002, *Isentropic Analysis and Interpretation: Operational Applications to Synoptic and Mesoscale Forecast Problems*, August 1987, is approved for public release. There is no objection to unlimited distribution of this document to the public at large, or by the Defense Technical Information Center (DTIC) to the National Technical Information Service (NTIS).

This document has been reviewed and is approved for publication.



**GEORGE TANIGUCHI, GM-13**  
Forecasting Services Division  
Directorate of Aerospace Services,  
DCS/Aerospace Sciences  
Reviewing Official

FOR THE COMMANDER



**DOUGLAS A. ABBOTT, Colonel, USAF**  
Asst DCS/Aerospace Sciences

**UNCLASSIFIED****REPORT DOCUMENTATION PAGE**

1a. Report Security Classification: UNCLASSIFIED  
3. Distribution/Availability of Report: Approved for public release; distribution is unlimited.  
4. Performing Organization Report Number: AWS/TN-87/002  
6a. Name of Performing Organization: HQ AWS  
6b. Office Symbol: DNTS  
6c. Address: Scott AFB, IL 62208-5008  
11. Title: Isentropic Analysis and Interpretation: Operational Applications to Synoptic and Mesoscale Forecast Problems  
12. Personal Author: Dr James T. Moore, Saint Louis University, Department of Earth and Atmospheric Sciences, P.O. Box 8099-LaClede Station, St Louis, MO 63156  
13a. Type of Report: Technical note  
14. Date of Report: August 1987  
15. Page Count: 93  
17. COSATI Codes: Field--04, Group--02  
18. Subject Terms: METEOROLOGY, WEATHER FORECASTING, AVIATION FORECASTING, WEATHER ANALYSIS, ISENTROPIC ANALYSIS, ISENTROPIC COORDINATE SYSTEM, CONSTANT PRESSURE ANALYSIS, TRAJECTORY ANALYSIS, TROPOPAUSE FOLDING PROCESS, psi charts, sigma charts, thermal wind, static stability, vorticity, condensation pressure, condensation ratio, condensation difference, streamlines, trajectories, freezing level, icing, clear air turbulence, overrunning convection.  
19. Abstract: A basic review of the isentropic coordinate system, including its advantages and disadvantages for operational use. The primitive equations in isentropic coordinate form are discussed with emphasis on their physical meaning and interpretation. Isentropic analysis techniques for "horizontal" and cross sectional perspectives are described as aids for diagnostic analysis of synoptic scale weather systems. Numerous diagnostic variables are discussed; all can be excellent tools in identifying synoptic scale features helpful in forecasting cyclogenesis and regions susceptible to strong convection. The final section presents specialized applications of isentropic techniques to weather analysis and forecasting, including: trajectory analysis, tropopause folding process, short-term forecasting of severe weather threat areas, and aviation forecasting.  
20. Distribution/Availability of Abstract: Same as report  
21. Abstract Security Classification: UNCLASSIFIED  
22a. Name of Responsible Individual: George Taniguchi  
22b. Telephone: 618 256-4741 (A576-4741)  
22c. Office Symbol: AWS/DNTS



Accession For	
NTIS	CRA&I <input checked="" type="checkbox"/>
DTIC	TAB <input type="checkbox"/>
Unannounced <input type="checkbox"/>	
Justification	
By	
Distribution	
Availability Codes	
Dist	Avail and/or Special
A-1	

## PREFACE

Before the changeover to pressure coordinates in the early 1940's, isentropic analysis was utilized extensively for diagnosing and forecasting weather systems. Since that time the advantages of the isentropic coordinate system and isentropic analysis techniques have been neglected in the curricula of both universities and training centers. The 1960's and 1970's saw a resurgence of isentropic analysis in the research community as it was well-suited to the needs of those studying atmospheric flow on both the synoptic and mesoscales of motion. This monograph has been written with the goal of presenting the isentropic viewpoint and methods of diagnosis in one volume that can be easily accessible to the practicing operational meteorologist. It is the author's hope that this information will help increase the use of isentropic analysis techniques in the field as a *supplement* to standard constant pressure analyses as forecasters attempt to diagnose and predict the three dimensional flow associated with precipitation systems.

I would like to acknowledge that motivation for this paper came from Dr. Lawrence Wilson of the Atmospheric Environment Service in Canada who wrote a similar shorter paper for Canadian meteorologists. Several examples discussed in this text are borrowed from his training paper. Also, Anderson (1984) wrote a paper for the National Weather Service (NWS) Western Region describing isentropic analysis which is frequently referenced.

The author would like to thank St. Louis University for offering a sabbatic leave during which time he was able to work on this manuscript. The people at the NSSFC were also very supportive and offered ideas on strengthening the text. Dr. Joe Schaefer of SSD in CRH gave helpful suggestions which were appreciated. Friends at the NWSTC including Daryl Covey, Pete Chaston, and Dan Berkowitz who will be implementing this material into the NWS training program are all appreciated for their support and enthusiasm for this project. Also, Dr. Dale Meyer, Mr. George Taniguchi, Mr. George Horn and Mr. Michael Squires of the Air Weather Service are to be thanked for their proofreading of the text. Last, but not least, the expert typing of Ms. Juanita Ryles and the assistance of Mr. Richard Molinaro are deeply appreciated.

**NOTE: THE MAY 1989 REVISION REQUIRED REPLACEMENT  
OF THE FOLLOWING PAGES: 9, 10, 45, 46, 49, 83, 84, 85.**

## CONTENTS

1. INTRODUCTION.....	1
2. ISENTROPIC COORDINATE SYSTEM.....	2
A. Definition.....	2
B. History of Isentropic Analysis.....	4
C. Advantages of Isentropic Analysis.....	6
D. Disadvantages of Isentropic Analysis.....	13
E. Primitive Equations in Isentropic Coordinates.....	18
F. Constructing an Isentropic Data Set from Rawinsonde Data.....	26
3. ISENTROPIC ANALYSIS TECHNIQUES.....	28
A. Psi Charts.....	28
B. Sigma Charts.....	31
C. Cross Section Analysis Techniques.....	37
1. Thermal Wind Relationship in Isentropic Coordinates.....	37
2. Isentropic Topography in the Vicinity of Upper Level Fronts and Jet Streaks.....	38
D. Useful Diagnostic Variables Computed From Isentropic Data.....	44
1. Static Stability.....	44
2. Moisture Advection/Convergence.....	44
3. Adiabatic Vertical Motion.....	44
4. Static Stability Tendency.....	45
5. Absolute Vorticity.....	45
6. Potential Vorticity.....	45
7. Condensation Pressure.....	46
8. Condensation Ratio.....	46
9. Condensation Difference.....	46
10 Streamlines.....	49
4. SPECIALIZED APPLICATIONS OF ISENTROPIC ANALYSES TO DIAGNOSTIC/FORECAST PROBLEMS.....	52
A. Isentropic Trajectories.....	52
1. Implicit Approach.....	52
2. Explicit Approach.....	56
3. Trajectory-derived Variables.....	57
B. Potential Vorticity and Tropopause Folding.....	60
C. Short Term Forecasting of Severe Convection Using Isentropic Analyses.....	69
D. Additional Applications.....	70
1. Freezing Level and Icing.....	74
2. Clear Air Turbulence.....	74
3. Overrunning Convection.....	78
5. CONCLUDING COMMENTS.....	80
6. REFERENCES.....	81

## FIGURES

Figure 1a.	Salem, IL (SLO) Sounding for 1200 GMT 8 September 1986.....	7
Figure 1b.	Albuquerque, NM (ABQ) Sounding for 0000 GMT 5 September 1986.....	7
Figure 2.	Typical vertical cross section diagrams.....	11
Figure 3.	Cross section showing how isentropic surfaces appear in the vicinity of regions with superadiabatic (SA) and neutral (N) lapse rates.....	14
Figure 4.	Cross section showing how the vertical resolution of an area may vary within a very stable (VS) and less stable (LS) region.....	16
Figure 5.	Soundings for progressively later time periods into the night (t <sub>1</sub> , t <sub>2</sub> , t <sub>3</sub> ) illustrating how radiational influences may change the pressure level at which a given isentropic surface is found.....	16
Figure 6.	Schematic diagram depicting the stability changes that can take place in the presence of diabatic heating/cooling.....	22
Figure 7.	Geostrophic wind scale for an isentropic surface on a polar stereographic projection with a 1:15 million map scale.....	24
Figure 8.	Geostrophic wind scale for an isentropic surface on a polar stereographic projection with a 1:10 million map scale.....	25
Figure 9.	Station model plot for psi charts.....	29
Figure 10.	Isobaric topography in the vicinity of fronts (a) and isobaric topography associated with frontogenesis in the warm sector (b).....	30
Figure 11a.	Isentropic pressure pattern in the vicinity of a strong, mature cold front.....	30
Figure 11b.	Isentropic pressure pattern in the vicinity of a frontolysing cold front .....	32
Figure 11c.	Isentropic pressure pattern in the vicinity of an occluding frontal system.....	32
Figure 12.	Fronts indicated at the surface and schematic flow pattern around an occluded cyclone as shown by the moisture lines in an isentropic surface in mid-air.....	33
Figure 13.	Illustrating probable upslope motion of a moist current as deduced from the relation of the moisture lines to the isobars on an isentropic surface.....	33
Figure 14.	Flow pattern at different isentropic surfaces which leads to increasing convective instability.....	33
Figure 15.	Station model plot for sigma charts.....	35
Figure 16.	Wilson (1985) station model plot.....	36
Figure 17.	Plotting model used by ISENT (NWS Southern Region isentropic plotting program used on AFOS), Little (1985).....	36
Figure 18.	Schematic showing how stations are depicted with respect to the regression line and their original positions.....	39
Figure 19.	Cross section illustrating the relationship between sloping isentropic surfaces and the vertical wind shear.....	40
Figure 20.	Cross section plotting model.....	41
Figure 21.	Idealized and averaged picture for the annual mean or the spring and autumn seasons....	42
Figure 22.	Condensation pressure (mb) vs. specific humidity for 283, 293, 303, and 313 K isentropic surfaces.....	47
Figure 23a.	Isentropic condensation pressure pattern over a mature, strong cold front.....	48
Figure 23b.	Isentropic condensation pressure pattern over an occluding frontal system.....	48
Figure 24.	Condensation-pressure spread to cloud-conversion table.....	50
Figure 25a.	Isentropic streamlines in the vicinity of a strengthening cold front.....	51
Figure 25b.	Isentropic streamlines in the vicinity of a weakening cold front.....	51
Figure 26a.	Isentropic surface, $\theta = 45^{\circ}\text{C}$ , 0300 GMT 8 January 1953.....	54
Figure 26b.	Isentropic surface, $\theta = 45^{\circ}\text{C}$ , 1500 GMT 8 January 1953.....	55
Figure 27a.	330 K isentropic surface for 1200 GMT 10 May and 0000 GMT 11 May 1973.....	58
Figure 27b.	Trajectories computed for 1200 GMT 10 May through 0000 GMT 11 May 1973 on 330 K isentropic surface using discrete model technique.....	59
Figure 28a.	312 K 3-hour isentropic trajectories beginning 1700 GMT 10 April 1979.....	61
Figure 28b.	312 K 3-hour delta M field for 1700-2000 GMT 10 April 1979.....	61
Figure 28c.	312 K 3-hour vertical motion field for 1700-2000 GMT 10 April 1979.....	62
Figure 29a.	500 mb surface for 0300 GMT 13 December 1953.....	64
Figure 29b.	Cross section along line A-B in Figure 29a.....	64
Figure 29c.	500 mb surface for 0300 GMT 14 December 1953.....	65
Figure 29d.	Cross section along line C-D in Figure 29c.....	65
Figure 29e.	500 mb surface for 0300 GMT 15 December 1953.....	66
Figure 29f.	Cross section along line E-F in Figure 29e.....	66
Figure 30a-b	Vertical cross section from International Falls, MN (INL) to Denver, CO (DEN) for 1200 GMT 18 February 1979.....	67
Figure 30c-d	Vertical cross sections from Green Bay, WI (GRB) to Apalachicola, FL (AQO) for 0000 GMT 19 February 1979.....	68
Figure 31a.	National Weather Service radar summary for 2035 GMT 10 April 1979.....	71
Figure 31b.	Isentropic cross section for 1700 GMT 10 April 1979.....	71
Figure 31c.	The Montgomery streamfunction for 306 K surface at 1700 GMT 10 April 1979.....	71
Figure 31d.	Adiabatic vertical motion and specific humidity for 306 K surface at 1700 GMT 10 April 1979.....	72

Figure 31e. Horizontal moisture convergence and low level stability for 306 K surface at 1700 GMT 10 April 1979.....	72
Figure 31f. Low level stability flux for 304-308 K layer at 1700 GMT 10 April 1979.....	73
Figure 31g. Composite chart for 1700 GMT 10 April 1979.....	73
Figure 32. Schematic illustration of regions of clear air turbulence in the vicinity of an upper level jet core and frontal zone.....	76
Figure 33. Cross sections of potential temperature and wind speed and direction at 0000 GMT 20 April 1971.....	77
Figure 34. Cross section of equivalent potential temperature and wind components parallel to the plane of the cross section.....	79

## 1. INTRODUCTION

The motivation behind this paper is simple--I wanted to lay down the basic concepts of isentropic analysis and interpretation for those people in the "front lines" of meteorology, the practicing forecasters. Since the demise of the isentropic coordinate system in the 1940's, few academic institutions or training centers have taught isentropic meteorology as part of their synoptic or weather analysis and forecasting laboratory courses. More recently, that situation has been changing. However, there are several generations of meteorologists who have never been shown the advantages of isentropic analyses in diagnosing the current weather. Therefore, they are naturally reluctant to incorporate these charts into their daily forecasting scheme. The success of systems such as AFOS (Automation of Field Operations and Services) and McIDAS (Man-Computer Interactive Display Acquisition System) show that new and varied computer products can be incorporated into the operational environment. However, if these products are to be efficiently and intelligently utilized, the end users (i.e., the forecasters) must be knowledgeable about the advantages and disadvantages of each new tool. As Doswell (1986) notes, we need to consider training at least as much as technology. The technology makes it very easy for us to create isentropic data sets and analyses. The training makes this not-so-new method of diagnosing atmospheric flow easy to use, understandable and useful.

Toward that end I will try to illustrate the advantages *and* disadvantages of isentropic analysis in the diagnosis of weather patterns *as a supplement to* standard constant pressure analyses. I will draw heavily on the work of other researchers (e.g., Danielsen, Reiter, Uccellini, Petersen, Namias, Rossby, Wilson, Anderson) who have proven isentropic analyses effectiveness in diagnostic work through numerous case studies. References will be given so that the adventuresome reader can delve into some of the topics we discuss in greater detail. For that reason this paper does not attempt to be an exhaustive guide for isentropic meteorology. Mathematics will be used but minimized for fear of boring or disenfranchising the reader. Emphasis instead will be placed upon *conceptualization* of ideas rather than heady dynamics. This is especially important in isentropic analysis since isentropic surfaces are truly three-dimensional, unlike the quasi two-dimensional pressure surfaces. Our experience at St. Louis University in the synoptic laboratory is that it takes several weeks for students to get over their two-dimensional, constant pressure biases to visualize three-dimensional isentropic flow. It is much like the transition for A. Square, the key character in *Flatland* by Edwin A. Abbott (1952), in going from Flatland to the three-dimensional world of *Sphereland* (Burger, 1965). This author encourages the reader to read both *Flatland* and *Sphereland* as they are useful exercises in visualization; references are given at the end of this paper.

Finally, I want to acknowledge that motivation for this paper came from Dr. Laurence Wilson of the Atmospheric Environment Service in Canada who wrote a similar shorter paper for Canadian meteorologists. Several examples discussed in this text are borrowed from his training paper. Also Anderson (1984) wrote a paper describing isentropic analysis for the National Weather Service's (NWS) Western Region which is frequently referenced.

## 2. ISENTROPIC COORDINATE SYSTEM

### A. Definition

One must first begin with the concept of an *adiabatic* process as applied to a fictitious parcel of air with a volume of roughly  $1 \text{ m}^3$ . During an adiabatic process an air parcel will experience no heat exchange with its environment; i.e., no heat is added or taken away from the parcel. In terms of the first law of thermodynamics we write,

$$dh = 0 = C_p dT - \alpha dP \quad (1)$$

Since  $\alpha = RT/P$  we can write (1) as:

$$\frac{dT}{T} = \frac{R}{C_p} \frac{dP}{P} \quad (2)$$

Following Hess (1959), if we integrate from some temperature,  $T$ , and pressure,  $P$ , to a temperature,  $\theta$ , at 1000 mb, we obtain:

$$\Theta = T \left( \frac{1000}{P} \right)^\kappa \quad (3)$$

where  $\kappa = R/C_p$ .

The temperature,  $\theta$ , is physically defined as the temperature that a parcel of air would have if it were compressed (or expanded) adiabatically from its original pressure to 1000 mb. It is known as *potential temperature* and is a conservative property for parcels of air with *no* changes in heat due to such processes as solar/terrestrial radiation, mixing with environmental air that has a different temperature, and latent heating/evaporative cooling. Although these restrictions would seem to make the application of this thermodynamic variable limited there is empirical evidence that such "diabatic" heating and cooling processes are usually secondary in importance for temporal scales on the order of the synoptic. Some people (such as the author) would also argue that one could extend this approximation to meso  $\alpha$  scales of motion under certain conditions.

Hess (1959) also shows that the entropy of an air parcel,  $\phi$ , is related to its potential temperature as:

$$\phi = C_p \ln \Theta + \text{const} \quad (4)$$

So a parcel which moves dry adiabatically not only conserves its potential temperature but also its entropy. A surface composed of parcels whose potential temperatures are equal is described as an equal entropy or isentropic surface. In

thermodynamics we are told that entropy is a measure of the disorder of a system. However, operational meteorologists have little use for this concept. Thus, aside from using the term *isentropic*, we meteorologists prefer to use *potential temperature* as a variable rather than *entropy*, which carries more of a mystical aspect!

In the troposphere the atmosphere is, on the average, stable; i.e.,  $-\partial T/\partial Z = \gamma_{\text{envir}} < 9.5^{\circ}\text{C}/\text{km}$ , typically  $\gamma_{\text{envir}} = 6.5^{\circ}\text{C}/\text{km}$ . In such an atmosphere the potential temperature can be shown by (5) to increase with height.

$$\frac{1}{\Theta} \frac{\partial \Theta}{\partial z} = \frac{(\Gamma_d - \gamma)}{T} \quad (5)$$

In (5)  $\Gamma_d$  is the dry adiabatic lapse rate and  $\gamma$  is the actual or environmental lapse rate. Under stable conditions  $\gamma < \Gamma_d$ , so  $\partial \theta / \partial z > 0$  meaning  $\theta$  increases with height. If the lapse rate is neutral then  $\gamma = \Gamma_d$  and  $\partial \theta / \partial z = 0$ ; i.e.,  $\theta$  is constant with height. If  $\gamma > \Gamma_d$  the lapse rate is superadiabatic and  $\theta$  decreases with height. Furthermore, as Rossby, et al., (1937) note, the potential temperature also increases southward at about the same rate as the dry bulb temperature. So the troposphere may be envisioned as being composed of a great number of isentropic layers which gradually descend from cold polar regions to warmer subtropical latitudes. As one ascends from the troposphere into the stratosphere, where the atmosphere is very stable, isentropic surfaces become compacted in the vertical. This attribute makes them extremely valuable for resolving upper-level stable frontal zones in the presence of upper tropospheric wind maxima or jet streaks. Thus, in a stably stratified atmosphere; i.e.,  $-\partial T/\partial Z < 9.8^{\circ}\text{C}/\text{km}$ , potential temperature can be an excellent vertical coordinate--especially since it increases with height, thereby avoiding the headaches of dealing with a vertical coordinate (namely pressure) which decreases with height.

Rossby, et al., (1937) and later Blackadar and Dutton (1970) note that it is necessary to "tag" a parcel with more than its potential temperature since on an isentropic surface all parcels "look alike". A second natural "tag" would be mixing ratio or specific humidity, both quantities which are also conserved during dry adiabatic ascent/descent. Another possible "tag" (which will be discussed later) is *potential vorticity*. It should be no surprise, then, that the three-dimensional transport of moisture on a vertically sloping isentropic surface should display good spatial and temporal continuity. As will be shown later, this has important diagnostic and prognostic implications for the movement of both moist and dry tongues in low-middle levels of the troposphere.

Meanwhile, one might ask why isentropic analysis was ever abandoned if, as recognized way back in the 1930's, it showed such great promise? Perhaps even more importantly, why has it regained favor today?

## B. History of Isentropic Analysis

The rise and fall and subsequent rebirth of isentropic analysis for the study of synoptic scale systems is quite interesting. The historical perspective discussed by Bleck (1973) is summarized here. Apparently, as the story goes, in the 1930's once upper air observations became available there was quite a debate over what vertical coordinate system would be most useful for weather analysis and forecasting. German meteorologists and several European colleagues favored a constant pressure coordinate system while the British Commonwealth and the United States favored using a constant height system. But, several vociferous meteorologists (e.g., C. G. Rossby and J. Namias) urged the adoption of isentropic coordinates. Consider their arguments:

"It can hardly be doubted that the isentropic charts represent the true motion of the air more faithfully by far than synoptic charts for any fixed level in the free atmosphere. At a fixed level in the middle of the troposphere entire air masses may, as a result of slight vertical displacements, appear or disappear in the time interval between two consecutive charts, making that entire method of representation futile."  
(Rossby, et al, 1937).

"While maps of atmospheric pressure at various levels have been found especially helpful in weather forecasting, the use of temperatures and humidities on such constant level charts has hardly done more than make atmospheric disturbances seem more complicated in vertical structure than surface weather analyses would indicate."  
(Namias, 1939).

One researcher (Spilhaus, 1938) even suggested in a short paper for the Bulletin of the American Meteorological Society that airplanes fly along isentropic surfaces using a "thetameter" to keep track of the potential temperature for the pilots!

According to Bleck (1973) the U. S. Weather Bureau did respond in the late 1930's to these arguments (and other advantages noted in the next section) and transmitted data needed for isentropic analysis over the weather teletype network. However, after a number of years (by the mid 1940's) this service was discontinued and a constant pressure coordinate was used. Bleck (1973) and Wilson (1985) note several reasons for this action.

- (1) The second world war created an impetus for a standardization to a common vertical coordinate system and analysis procedures. The demands of the aviation community were for winds on constant pressure surfaces.

- (2) In the pre-computer age isentropic charts were difficult and time-consuming to prepare within operational time constraints.
- (3) Perhaps most significantly, the Montgomery streamfunction, which defines geostrophic flow on an isentropic surface, was being erroneously computed. This resulted in a geostrophic wind law on isentropic surfaces which did not work. Undoubtedly, this led to disenchantment with isentropic analysis and its eventual demise.

Reiter (1972) discusses the last problem in some detail. Briefly, the Montgomery streamfunction (which is basically equivalent to heights on a constant pressure surface, in terms of its relationship to the geostrophic wind) is defined by Montgomery (1937) as:

$$M = \Phi + C_p T_\theta \quad (6)$$

In the early isentropic years  $M$  was computed by interpolating the two terms,  $\Phi$  and  $C_p T_\theta$ , separately, using for  $\Phi$  the conventional pressure-geopotential calculations (Bleck, 1973). As Danielsen (1959) discovered, the two terms in (6) are related through the hydrostatic equation in isentropic coordinates. Therefore, computing these terms independently resulted in unacceptable errors of as much as 20% in their sum (Wilson, 1985). Bleck (1973) believes that this lack of a workable geostrophic wind relationship contributed to the disuse of isentropic analysis--especially in the operational community.

After Danielsen's (1959) discovery of this error in computing the Montgomery streamfunction, the path was cleared for a resurgence of isentropic analysis--at first notably in diagnostic work and later in predictive models. Some examples of research which used isentropic analysis techniques include:

- (1) Studies of exchange processes between the stratosphere and troposphere, especially along "breaks" or "folds" in the tropopause (Danielsen, 1959, 1968; Reiter, 1972, 1975; Staley, 1960; Reed, 1955; Shapiro, 1980; Uccellini, *et al.*, 1985; and others).
- (2) Studies of air flow associated with extratropical cyclones attempting to explain the characteristic cloud patterns observed by satellite imagery (Carlson, 1980; Carr and Millard, 1985; Danielsen, 1966; Danielsen and Bleck, 1967; Browning, 1986; and others).
- (3) The construction of isentropic trajectories used to diagnose Lagrangian vertical motions and ageostrophic flow associated with jet streak activity (Danielsen, 1961; Petersen and Uccellini, 1979; Haagenson and Shapiro, 1979; Kocin, *et al.*, 1981; Moore and Squires, 1982; Uccellini, *et al.*, 1985; and others). The relationship of isentropic upslope flow to cloud patterns has been noted by many Satellite Field Service Stations (SFSS) in their daily messages.

- (4) Utilization of isentropic analysis to obtain better resolution of winds and moisture in the vicinity of frontal zones above the surface for diagnostic work or model initialization (Petersen, 1986).
- (5) Experiments in numerical weather prediction using models with equations formulated in isentropic coordinates (Eliassen and Raustein, 1968; Bleck, 1973; Homan and Petersen, 1985; Uccellini and Johnson, 1979; and others).
- (6) Studies of frontogenesis in inviscid, adiabatic flow, notably by Hoskins and Bretherton (1972).

We will now explore some of the advantages of this unique isentropic viewpoint.

### C. Advantages of Isentropic Analysis

The advantages of using an isentropic perspective in diagnosing atmospheric flow have been discussed by Saucier (1955), Bleck (1973), Uccellini (1976), Wilson (1985), and Moore (1985). These advantages include:

- (1) Over synoptic (and to a degree, subsynoptic) spatial and temporal scales, isentropic surfaces act like "material surfaces", (Rossby, *et al.*, 1937). That is, air parcels are thermodynamically "bound" to their isentropic surface in the absence of diabatic processes such as terrestrial/solar radiation, latent heating/evaporative cooling, and sensible heat exchanges in the planetary boundary layer. The only other thermodynamic surfaces that act as material surfaces are surfaces of equivalent potential temperature and wet bulb potential temperature, both conservative properties for either "dry" or "wet" parcels. However, the latter are unwieldy to use in diagnostic work since they are typically multi-valued with respect to pressure; i.e., they are folded in the vertical. The only times that an isentropic surface has a non-unique value of pressure is if the environment is neutral ( $\partial\theta/\partial Z = 0$ ) or if it is unstable ( $\partial\theta/\partial Z < 0$ ). This is illustrated by Figure 1a and 1b.

Of the diabatic processes most apt to restrict the applicability of isentropic analysis, the release of latent heat is the most significant. As we would expect this takes place in saturated, ascending air. The problems with isentropic surfaces within the planetary boundary is that they are subject to greater diurnal cycles of solar/terrestrial heating/cooling which causes the isentropic surface to move up/down thereby losing its continuity. Thus, airflow in the troposphere is best diagnosed by choosing the most appropriate isentropic surface in the area of interest above the planetary boundary layer.

- (2) Isentropic surfaces can vary with respect to height (Z) or pressure (P). Therefore, "horizontal" flow along isentropic surfaces contains the *adiabatic* component of vertical motion which would otherwise be computed as a separate component in either a Cartesian or isobaric coordinate system. This will be explained in

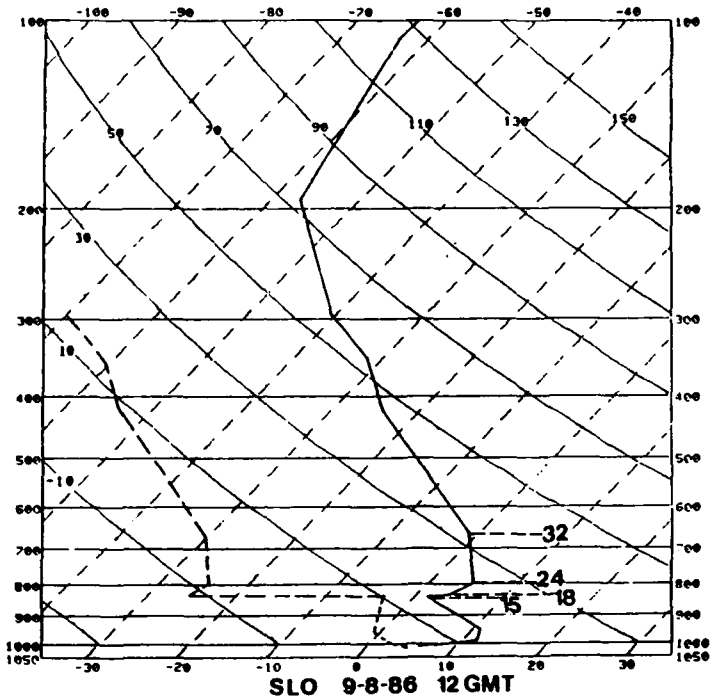


Figure 1a. Salem, IL (SLO) sounding for 1200 GMT, 8 September 1986. This skew-T, log P diagram shows how potential temperature changes in the vertical in the vicinity of a stable region. Numbers adjacent to the temperature sounding are potential temperature in °C.

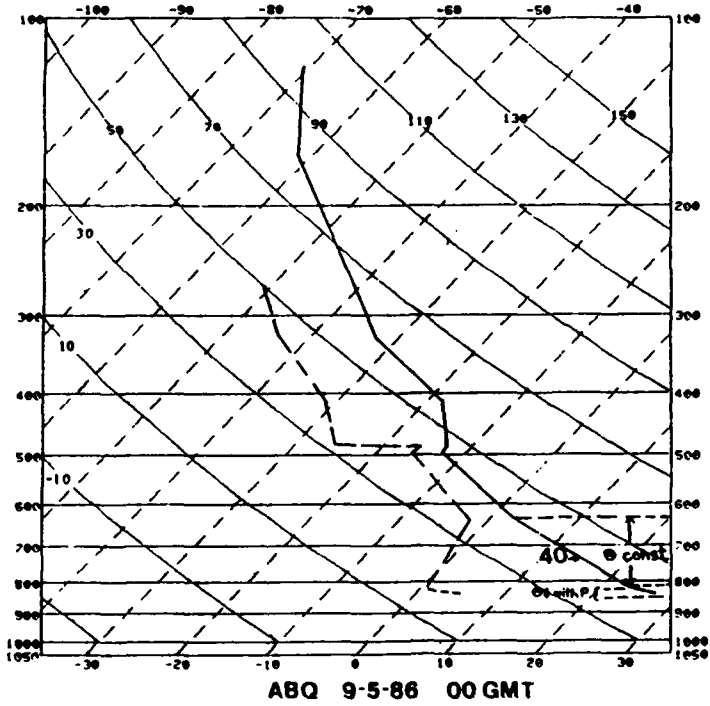


Figure 1b. Albuquerque, NM (ABQ) sounding for 0000 GMT, 5 September 1986. This skew-T, log P diagram shows how neutral and superadiabatic layers appear on a sounding. Note:  $40 = 313$  °C = potential temperature of the layer; below that layer, lapse rate is superadiabatic.

greater detail as it is important for understanding how vertical motions appear on isentropic surfaces.

Vertical motion with respect to pressure in isentropic coordinates is expressed as:

$$\omega = \left( \frac{\partial P}{\partial t} \right)_e + \vec{V} \cdot \nabla_e P + \frac{\partial P}{\partial \Theta} \frac{d\Theta}{dt}$$

**A      B      C**

(7)

As described by Moore (1986), terms A, B, C can be physically described as:

- (A) Local pressure tendency: This represents the effect of an isentropic surface moving up or down at a specific point (local derivative). With standard rawinsonde data this term can be evaluated over a 12-hour period as a backward time derivative. However, that is really a poor estimate of a local time derivative.
- (B) Advection of pressure on the isentropic surface: This term can be qualitatively evaluated by noting the cross-isobar flow on an isentropic surface. Air flowing from high to low pressure represents upward vertical motion ( $\omega < 0$ ), while air flowing from low to high pressure indicates downward vertical motion ( $\omega > 0$ ). Since an isobar on an isentropic surface is also an isotherm, this is equivalent to thermal advection. This can be proven easily by considering Poisson's equation (3) derived earlier:

$$\Theta = T \left( \frac{1000}{P} \right)^{\kappa} \quad (3)$$

If one considers an isobar ( $P$ ) on an isentropic surface ( $\theta$ ) it becomes clear that since  $P$  and  $\theta$  are constant along that isobar,  $T$  must be also. Carrying this one step further--if we consider the equation of state,

$$P = \rho R T \quad (8)$$

One can see that since  $P$  and  $T$  are constant, so must be  $\rho$ , the density. Thus, an isobar drawn on an isentropic surface is also an isotherm and an isopycnic (isostere).

- (C) Diabatic heating/cooling term: This term measures the contribution to vertical motion by diabatic processes such as those listed earlier, notably latent heating. When this term is non-zero, it forces the parcel to "jump" off the isentropic surface. In a stable atmosphere  $\partial P / \partial \theta < 0$  since  $\theta$  increases as  $P$  decreases. Therefore, the sign of term "C" depends totally upon the sign of the diabatic term, " $d\theta/dt$ ", which is  $> 0$  for heating and  $< 0$  for cooling.

Thus, diabatic heating will cause upward motion *with respect to the isentropic surface* and diabatic cooling will cause downward motion. This is the only true vertical motion *with respect to* the isentropic surface. Just as  $w = dZ/dt$  measures vertical motion with respect to constant height surfaces and  $\omega = dP/dt$  measures vertical motion with respect to constant pressure surfaces,  $d\theta/dt$  is a measure of vertical motion with respect to an isentropic surface. Unfortunately, measuring  $d\theta/dt$ , especially within the confines of an operational environment, is not easy. Fortunately, at synoptic scales of motion and in the pre-severe storm or convective environment, it plays a secondary role in forcing changes in  $\omega$ . However, Moore (1986) has shown that once convection begins this term can be equal to or greater than terms A and B combined. It is modulated to a great extent by the static stability,  $\partial P/\partial \theta$ ; i.e., in stable regions it is small, but in less stable regions it can be quite large.

If only term B of (7) is considered one can define the adiabatic vertical motion as:

$$\omega_{\text{adiabatic}} \approx \vec{V} \cdot \nabla_{\theta} P \quad (9)$$

Wilson (1985) notes that the advection term and the local pressure tendency term are usually opposite in sign but that the advection term typically dominates, especially in regions of strong advection. He offers the following illustration:

Example: Vicinity of Maniwaki, 0000 GMT January 14, 1980 300K

Wind speed = 50 knots =  $25 \text{ m s}^{-1}$  towards decreasing pressure

magnitude of  $\nabla P = 50 \text{ mb} / (3 \text{ deg latitude})$

Pressure on 300 K surface at YMW at January 13/1200 GMT = 530 mb

Pressure on 300 K surface at YMW at January 14/0000 GMT = 610 mb

Pressure on 300 K surface at YMW at January 14/1200 GMT = 650 mb

This represents a warming trend over the 24 hour period.

$$(\partial P/\partial t)_{\theta} = (650 \text{ mb} - 530 \text{ mb})/24 \text{ hours} = +1.39 \mu\text{bars/s}$$

$$\vec{V} \cdot \nabla P = V \frac{\partial P}{\partial n} \cos \theta$$

$$\begin{aligned} \vec{V} \cdot \nabla P &= 2500 \text{ cm/s} \times (50 \times 10^3 \mu\text{bars}) \\ &\quad / (3^\circ \text{ lat} \times (111 \text{ km}/1^\circ \text{ lat}) \times 10^5 \text{ cm/km}) \\ &\quad \times \cos 180^\circ \end{aligned}$$

$$\nabla \cdot \nabla P = -3.75 \text{ } \mu\text{bars/s}$$

Also,  $\partial P / \partial \theta d\theta / dt = 0$  for dry ascent

$> 0$  for moist ascent, solar heating, etc.

$< 0$  for evaporative cooling, terrestrial cooling,

etc.

$$\text{Therefore, } \omega = +1.39 \text{ } \mu\text{bars/s} - 3.75 \text{ } \mu\text{bars/s} = -2.36 \text{ } \mu\text{bars/s}$$

This is a typical synoptic scale value for omega. Normally, we would only have the t and t - 12 hour maps which would permit us to extrapolate  $\partial P / \partial t$  (i.e., use backward differencing). Note that if the air is saturated, the third term would amplify the vertical motion as latent heat would take the parcel up and off the isentropic surface. However, this effect would be compensated by increases in term A of (7) as the isentropic surface descends when diabatically heated.

Typically a forecaster would not compute vertical motion as above (although a computer could generate this product easily). However, it can quickly be estimated from the advection pattern by noting (a) the strength of the winds, (b) their component across the isobars, and (c) the strength of the isobar gradient.

(3) Because moisture transport on isentropic surfaces includes the vertical advection component, which is often missed or forgotten in pressure coordinates, moisture transport tends to display a more coherent pattern in space-time on isentropic surfaces than on standard 850 mb or 700 mb charts (Oliver and Oliver, 1951; Namias, 1938). Wilson, *et al.*, (1980) note that since isentropic parcels conserve their mixing ratio or specific humidity values one can forecast the motion of dry-lines and moist tongues using the component of the wind perpendicular to the isohumes. Although we all try to do this on constant pressure charts it is really inappropriate since we have no way of estimating vertical advection on pressure charts.

This advantage is probably one of the greatest of isentropic analysis. Many a forecaster probably has seen patches of moisture "pop up" on 850 or 700 mb charts, especially during warm air advection (overrunning) situations. Undoubtedly this moisture is coming up from below the 850/700 mb surfaces--a process one cannot see within a constant pressure perspective. Isentropic uplifting typically represents not only vertical motion but moisture advection as well. Similarly, subsidence and drying out of air behind frontal systems (or associated with jet streak secondary circulations) can be seen quite nicely on isentropic analyses.

(4) Frontal discontinuities are virtually nonexistent on isentropic surfaces, since frontal zones tend to run parallel to the isentropic surfaces (Bleck, 1973). This property of isentropic surfaces makes them extremely useful in diagnosing kinematic and dynamic variables, especially in baroclinic zones. Since the isentropic surfaces run parallel to the frontal zone, the variations of basic quantities (e.g., wind, moisture, temperature) take place more gradually along them; i.e., over larger scales (see Figure 2). Constant pressure surfaces literally cut through

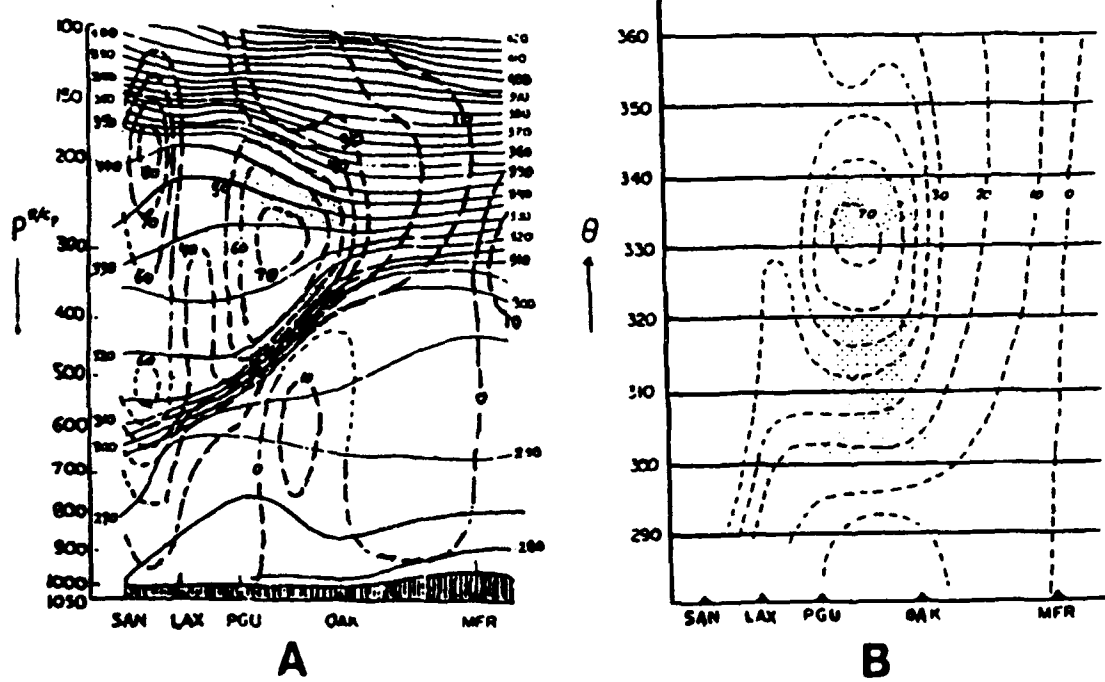


Figure 2. Typical vertical cross section diagrams. The diagram on the left (A) shows potential temperature and normal wind components. The diagram on the right (B) is the same except with potential temperature shown as the vertical coordinate (Wilson, 1984).

frontal zones causing quantities associated with a frontal zone to change more radically over subsynoptic spatial scales. An interesting result of this property of isentropic surfaces is that derived quantities (e.g., vorticity, divergence) tend to display weaker gradients and be oriented quite differently than on corresponding constant pressure charts. One must always remember that although the isentropic chart is two-dimensional it represents a vertically tilted three-dimensional surface. This tends to make people uncomfortable since constant pressure maps are quasi-horizontal depictions or slices of the atmosphere. Novices tend to ask, "but what level am I looking at?", to which we must reply, "one isentropic level--but several pressure levels". It is a bit like studying a foreign language--if you try to translate everything to English you are in trouble. You have to try to *think* in the foreign language and not revert back to English. Similarly one should try *not* to understand isentropic analysis within a constant pressure framework, but should attempt to *think* in an isentropic perspective. This may take some time. Don't be disappointed when it all looks strange at first.

(5) The vertical separation between consecutive isentropic surfaces is a measure of the static stability. This can be represented in two ways. One method is by simply viewing a cross section and noting regions of strong (weak) stability wherever isentropic surfaces are close together (far apart). This is useful in locating upper level frontal zones, inversions, and vertical changes in stability. In many ways this is much better than using standard stability indices which are parcel-related or only computed using certain levels of the atmosphere. A second method of using this advantage is through horizontal plots of the distance between two consecutive isentropic surfaces separated by 10 K or 15 K.

Also noteworthy is the fact that static stability,  $\partial P / \partial \theta$ , is related via the continuity equation in isentropic coordinates (see 13) to divergence/convergence taking place in the layer. Divergence in the layer *increases* the static stability while convergence in the layer *reduces* the static stability. An important fact to think about is that divergence/convergence is *not* related to vertical motion in an isentropic framework, unlike in pressure coordinates where vertical motion is related to the vertical profile of the divergence. Divergence/convergence in a layer affects the static stability by changing the amount of mass between consecutive isentropic surfaces.

(6) The slope of an isentropic surface in the vertical is directly related to the thermal wind. This result will be discussed more rigorously in Section 3.C.1; however, this statement should not be surprising. We are all familiar with the fact that in pressure coordinates the thermal wind is proportional to the gradient of the thickness or mean temperature of the layer in question. A vertically sloping isentropic surface is indicative of a strong thermal contrast which is represented on the isentropic surface as a tight packing of isobars or isotherms. Thus, where isentropic surfaces tilt up or down significantly one can diagnose a frontal zone and a commensurate change in the wind speed with height.

In a cross section analysis, *even in the absence of wind data*, one could diagnose regions of strong or weak wind shear. In a quasi-barotropic atmosphere the

isentropic surfaces would be quasi-horizontal, indicative of weak thermal winds.

(7) Parcel trajectories may be computed on isentropic surfaces using either implicit (Danielsen, 1961) or explicit (Petersen and Uccellini, 1979) methods. These trajectories and their Lagrangian change fields have been shown by the above researchers and others to be faithful to and highly correlated with the four-dimensional flow associated with mid-latitude synoptic and even subsynoptic scale motions.

Although this result is more useful to the research community in their post analysis of storm systems it also has applications in the operational environment. Even 12-hourly isentropic data sets can be used to generate the recent history of air parcels and their 12-hour change fields to help diagnose present cloud and precipitation fields. Danielsen's and this author's work with vertical motion fields derived from changes in pressure along parcel trajectories reveal excellent correlation to cloud patterns and precipitation. Since Lagrangian omega fields are calculated over time, typically 12 hours, and are plotted at the trajectory midpoint, they are more representative of long periods of lifting/descent than instantaneous vertical motions generated by other methods.

#### D. Disadvantages of Isentropic Analysis

As useful as isentropic analysis can be to the meteorologist, like any tool it has its drawbacks. However, knowing the following pitfalls will allow one to become a more intelligent user and therefore a better meteorologist. So, lest the author be accused of painting too rosy a picture--here is the other side of the story.

Experience has shown the following drawbacks to the use of isentropic analysis:

(1) Isentropic surfaces become ill-defined in regions where the lapse rate is neutral-superadiabatic; i.e.,  $\partial\theta/\partial Z < 0$ . In the neutral case, the isentropic surface is vertical (see the portion of the 305 K surface labeled N in Figure 3) while in the superadiabatic case it is folded (see the 300 K surface in Figure 3). In the latter case the folded surface is said to be multi-valued with respect to pressure. This is a serious problem because a vertical coordinate should change monotonically with height. Obviously in these cases it doesn't. These type of troublesome lapse rates are often seen in the desert southwest of the U. S. (e.g, El Paso, TX; Midland, TX) especially in the 0000 GMT soundings in low levels.

One method of dealing with this problem is to eliminate the neutral and superadiabatic lapse rates before processing by checking for them in each sounding and readjusting the temperature profile to make the lapse rates slightly less than neutral. At St. Louis University we average all variables pertaining to the isentropic surface over the layer in question and assign a mean pressure to the isentropic surface. This is done to simulate the vertical mixing (or averaging) that takes place within neutral-superadiabatic layers in the atmosphere.

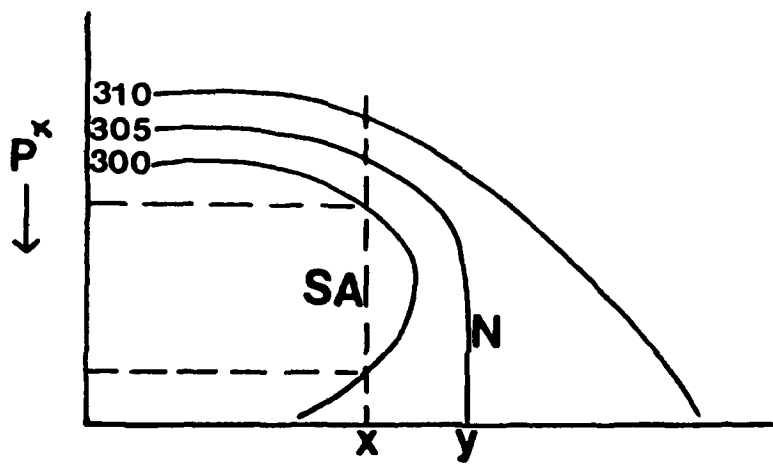


Figure 3. Cross section showing how isentropic surfaces appear in the vicinity of regions with superadiabatic (SA) and neutral (N) lapse rates.

(2) In near-neutral lapse rate regions there is poor vertical resolution of the atmosphere. As noted earlier the vertical difference between two isentropic surfaces is greater in less stable regions than in stable ones (see Figure 4). Since frontal zones are baroclinic, in stable regions of the atmosphere isentropes tend to be compacted in the vertical and slope substantially in the vertical. So in these regions (as well as in upper level fronts associated with jet streaks) there is favorable vertical and horizontal resolution.

(3) The continuity of isentropic analysis is disrupted significantly by the presence of diabatic processes (Namias, 1940). This problem tends to show up mostly in the presence of (a) radiation, (b) evaporation and condensation, and (c) convection. An example of radiative effects is given in Figure 5.

Due to cooling of the air nearest the earth's surface overnight the 300 K isentropic surface is found at progressively higher levels ( $A \rightarrow B \rightarrow C$ ) with time. Without taking radiative cooling into account, a forecaster might attribute this decrease in pressure on the isentropic surface to advection.

Other variables will be affected by the diabatic effect as well. Since moisture typically decreases with elevation as the isentropic surface rises, the mixing ratio observed in the vicinity of this station will decrease with time. Similarly wind speed may increase and the direction veer as the surface rises (especially in the planetary boundary layer). Again, the unsuspecting observer would attribute these changes erroneously to some advective or developmental affect.

The opposite would be true during the diurnal heating cycle during which the pressure would increase, moisture increase, speed decrease, and wind direction back with time on the 300 K surface. This is a good reason for trying to avoid using isentropic surfaces too close to or within the planetary boundary layer.

If an isentropic surface is known to lie within a region of latent heating or evaporative cooling, significant changes can occur as well. When latent heat is liberated, the potential temperature of the substantial surface, say 300 K, is raised to say, 304 K. Therefore, the 300 K isentropic surface will be found at a lower level where the mixing ratio and wind may be quite different, leading to possible erroneous interpretation by the analyst.

Similarly, when precipitation falls through an isentropic sheet which is not saturated, evaporative cooling will take place as the mixing ratio increases. As Namias (1940) notes, this lowers the potential temperature of the substantial surface from, say 300 K to, say 296 K, and therefore raises the isentropic surface. Now it is possible, if this evaporative cooling took place beneath a warm frontal inversion, that this process will raise the isentropic surface to within the frontal zone. In this case mixing ratio values will likely increase while the wind veers and strengthens with height. If this process was occurring beneath a cold frontal surface, the winds would likely back and strengthen with height. These scenarios vary with the strength and depth of the frontal zone.

Convection is disruptive to the continuity of isentropic surfaces mostly because it can effectively sustain the transport of moisture to higher levels. Namias (1940) notes that these vertical currents transport moisture to higher

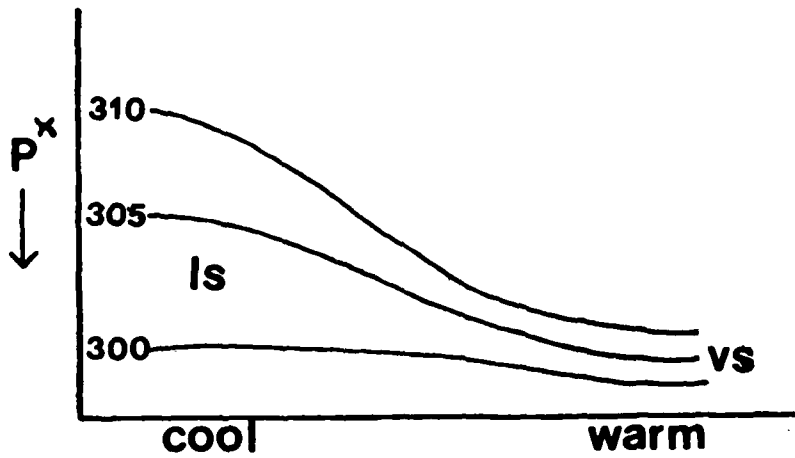


Figure 4. Cross section showing how the vertical resolution of an area may vary within a very stable (VS) and less stable (LS) region.

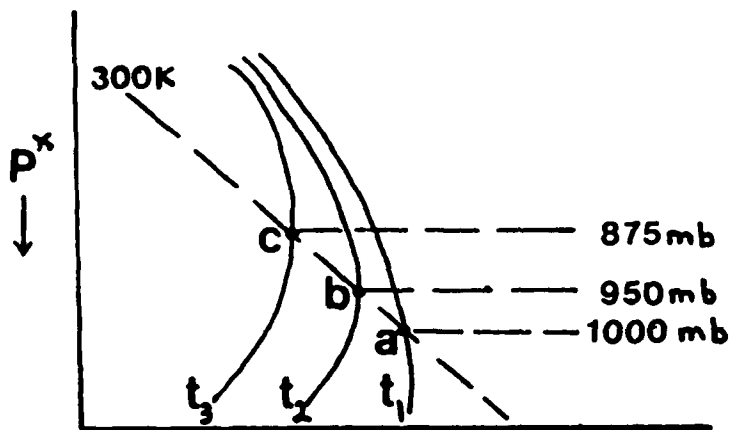


Figure 5. Soundings for progressively later time periods into the night ( $t_1, t_2, t_3$ ) illustrating how radiational influences may change the pressure level at which a given isentropic surface is found (Namias, 1940).

levels and replenish the moisture being precipitated out with cold frontal squall lines or even air mass type convective systems. However, he also mentions that the case of widespread convection can be quite different. The vertical transport of moisture from widespread convection can actually change the moisture pattern aloft. Such would be the case, for instance, in a Mesoscale Convective Complex (MCC) environment when convective scale feedback alters the synoptic scale flow and moisture significantly. So on a limited scale, within a squall line, the disruption of the moisture continuity on an isentropic surface is minimized as convection transports moisture vertically within the moist tongue to replenish moisture lost through precipitation. However, widespread convection can definitely contaminate the moisture continuity over larger scales of motion, rendering the analysis less useful. It is important to note that wintertime convection in unstable continental arctic/polar air masses is usually quite shallow and has very limited influence on isentropic surfaces in the free atmosphere.

(4) Isentropic surfaces tend to intersect the ground at steep angles causing analyses near where they intersect the ground to be suspect. One must be careful about over-interpreting analyses made near where the isentropic surface intersects the earth. One would do best to choose isentropic levels which never reach the ground. However, to depict moist/dry tongues associated with synoptic scale systems one tries to go as low as possible without hitting the ground. So there are trade-offs; as usual, there are no quick-fixes!

(5) Choosing the "proper" isentropic surfaces is not trivial. Generally, as in constant pressure analyses, one would like to use at least two or three isentropic surfaces to analyze. However, unlike constant pressure analyses, one has to choose different isentropic levels depending upon the time of year. Namias (1940) suggests the following *low level* isentropic surface for each season:

Season	Low Level Potential Temperature
Winter	290-295 K
Spring	295-300 K
Summer	310-315 K
Fall	300-305 K

The abrupt increase from spring to summer values is due to the normal rapid increase of free air temperature as summer convection sets in.

From experience the author has found that rather than guessing at what levels to use, one should create an isentropic cross section through the area of interest, preferably with winds and mixing ratio displayed. It is then relatively easy to choose the "right" isentropic levels in areas of jet streaks, moist tongues, etc. What this author *likes* about this so-called disadvantage is that it forces the meteorologist to think three-dimensionally and reason out his ideas for choosing certain isentropic levels to analyze. In the author's view this is better than using routinely generated, standard constant pressure charts simply because they are familiar or easier to take off the computer! The isentropic thinking process

thereby avoids the setting in of "meteorological cancer" so often discussed in the literature (Doswell, 1986).

(6) Isentropic analyses are not generally available and require computations which can only be done in real-time by a computer. This problem has gradually been solved, especially over the last decade with the explosion of computer power. Creation of an isentropic database from standard constant pressure rawinsonde data can now be done in minutes on a minicomputer. Once the constant pressure rawinsonde data has been decoded, sorted, and arranged into direct access files on our minicomputer, we create a real-time isentropic data set in less than 5 minutes at St. Louis University. The AFOS system now supports an isentropic analysis program (Anderson, 1984 and Little, 1985) while the Centralized Storm Information System (CSIS) System at the National Severe Storms Forecast Center (NSSFC) supports most isentropic analysis already. Wilson (1985) reports that an isentropic generation/analysis system is being used in Quebec within the Atmospheric Environment Service in Canada on a routine basis. So the computer problem is really no problem any more. The availability is actually a function of the demand which is addressed in the next section.

(7) The "inertia" problem as described by Wilson (1985) is that most meteorologists today have been brought up on constant pressure analyses and quasi-horizontal thinking. Effort is required to change one's viewpoint. Although it should be stressed that isentropic analysis does not *replace* isobaric analysis, it is meant as a supplement to aid in diagnosis. The two viewpoints can and *should* work together. Many features seen on constant pressure charts can be located on isentropic charts, so the changeover is not as radical as it first would seem.

(8) Finally, there is the problem of lack of numerical model forecast products in isentropic coordinate form, useful for forecasting. As Wilson (1985) notes, this would not be very hard to do. Currently none of the NWP models uses pressure coordinates; all forecast data must be interpolated to isobaric surfaces before dissemination to the forecast community. Why not also interpolate the model data to isentropic coordinates and send a few key levels out for 12-24-36-48 hours? This could easily be done if there was demand from the forecast community. This should be the new crusade for those of us interested in isentropic analysis.

#### E. Primitive Equations in Isentropic Coordinates

The primitive equations in isentropic coordinates are as follows:

##### *Momentum Equations*

$$\frac{\partial u_\Theta}{\partial t} + \nabla_\Theta \cdot \nabla_\Theta u + \frac{d\Theta}{dt} \frac{\partial u}{\partial \Theta} = - \frac{\partial M}{\partial x} + fv_\Theta + F_x \quad (10)$$

$$\frac{\partial v_\theta}{\partial t} + \vec{V}_\theta \cdot \nabla_\theta v + \frac{d\Theta}{dt} \frac{\partial v}{\partial \Theta} = -\frac{\partial M}{\partial y} - fu_\theta + F_y \quad (11)$$

*Hydrostatic Equation*

$$\frac{\partial M}{\partial \Theta} = C_p \left( \frac{P}{P_0} \right)^\kappa = \frac{C_p T}{\Theta} \quad (12)$$

*Mass Continuity Equation*

$$\frac{\partial}{\partial t} \left( \frac{\partial P}{\partial \Theta} \right) + \vec{V} \cdot \nabla \frac{\partial P}{\partial \Theta} + \frac{d\Theta}{dt} \frac{\partial}{\partial \Theta} \left( \frac{\partial P}{\partial \Theta} \right) = -\frac{\partial P}{\partial \Theta} \nabla \cdot \vec{V}_\theta - \frac{\partial P}{\partial \Theta} \frac{\partial}{\partial \Theta} \left( \frac{d\Theta}{dt} \right) \quad (13)$$

*Thermodynamic Equation*

$$\frac{dQ}{dt} = C_p T_\theta \frac{d \ln \Theta}{dt} \quad (14)$$

*Definition of Montgomery Streamfunction*

$$M = C_p T_\theta + g z_\theta \quad (15)$$

*Poisson's Equation*

$$\Theta = T \left( \frac{P_0}{P} \right)^\kappa \quad (16)$$

*Other Useful Diagnostic Expressions*

*Geostrophic Wind Relationship*

$$\vec{V}_{geo} = \frac{\hat{k}}{f} \times \nabla_\theta M \quad (17)$$

*Thermal Wind Relationship*

$$\vec{V}_T = \frac{\partial \vec{V}_{geo}}{\partial \Theta} = \frac{R}{f} \left( \frac{P^{\kappa-1}}{P_0^\kappa} \right) (\hat{k} \times \nabla_\theta P) \quad (18)$$

### Gradient Wind Relationships

$$\hat{s}: \frac{dV}{dt} = fv_{geo} \sin\beta \quad (19)$$

$$\hat{n}: -\frac{V^2}{R} = -fv_{geo} \cos\beta + fv \quad (20)$$

### Potential Vorticity

$$P_\Theta = \frac{-(\zeta_\Theta + f)}{\frac{\partial P}{\partial \Theta}} \quad (21)$$

### Description of Equations

First, we should note that the total derivative in isentropic coordinates is written as:

$$\frac{d(\ )}{dt} = \mathbf{A} \frac{\partial(\ )}{\partial t} + \mathbf{B} \frac{\partial(\ )}{\partial x} + \mathbf{C} \frac{\partial(\ )}{\partial y} + \mathbf{D} \frac{\partial(\ )}{\partial \Theta} + \mathbf{E} \frac{d\Theta}{dt} \frac{\partial(\ )}{\partial \Theta} \quad (22)$$

where: term A is the total derivative (Lagrangian)

term B is the local derivative (Eulerian)

term C+D are the horizontal advection terms and

term E is the vertical advection term.

The expression  $d\theta/dt$  represents all non-adiabatic heating/cooling (diabatic effects). It essentially represents vertical motion with respect to the isentropic surfaces. Since isentropic surfaces tilt substantially in the vertical, this "vertical motion", curiously enough, may have a horizontal component (horizontal with respect to Cartesian coordinates!). For strictly adiabatic processes term E is absent. Finally, keep in mind that the u and v wind components are measured on isentropic surfaces.

*Momentum Equations (10 and 11):* On the left-hand side (LHS) of (10) and (11) are the local time tendency of u (v) momentum, the inertial-advection term, and the vertical advection term. Notice that the latter term acts upon the vertical wind shear measured with respect to potential temperature. These three terms together are equal to the total (Lagrangian) time tendency of u (v) momentum. On the righthand side (RHHS) of (10) and (11) there is the gradient of the Montgomery streamfunction in the X (Y) direction, the Coriolis term, and the frictional term. The Montgomery streamfunction is analogous to height on a constant pressure surface and serves to define the geostrophic flow on an isentropic

surface.

*Hydrostatic Equation (12):* This is the equation used to compute  $M$  on the isentropic surfaces. In pressure coordinates one integrates the hydrostatic equation  $\partial P / \partial Z = -\rho g$  to obtain the hypsometric equation used to obtain heights on pressure surfaces. To do this it is necessary to integrate up from the earth's surface using the temperature profile obtained by the rawinsonde. Similarly, here, one obtains  $M$  by integrating (12) with respect to  $\theta$ . Thus, the Montgomery stream-function consists of a thermal term ( $C_p T$  = enthalpy) and a geopotential energy term ( $gZ$ ) which are *not* independent but related through the hydrostatic equation.

*Mass Continuity Equation (13):* This equation describes the change in mass between two isentropic surfaces, as measured by  $\Delta P$ , as a function of several processes. One can also think of this expression as a static stability tendency equation since  $\partial P / \partial \theta$  is the static stability. On the LHS there are the local time tendency and horizontal and vertical advection of stability terms. Together they form the total derivative of stability which would be useful if one were following parcels as in trajectory calculations.

On the RHS there are the divergence and diabatic terms. The divergence term changes stability in the following manner: divergence (convergence) in the layer ( $\Delta P$ ) causes the isentropic surfaces to compact (separate) in the vertical thereby causing the stability of the column to increase (decrease). This shrinking/stretching of the column between two isentropic surfaces in response to divergence/convergence in the layer maintains mass continuity.

The diabatic term looks complex but can be described easily in physical terms. Note that it is *not* just diabatic heating that is measured but its change in the vertical. Thus, if the diabatic heating/cooling was uniform in the layer this term would be zero. However, let us say that there was diabatic cooling in lower levels due to evaporation and diabatic heating in upper levels due to latent heating. Then, as seen in Figure 6, the static stability would increase with time. Essentially what happens is that in the presence of latent heating the 310 K surface is warmed to 314 K, meaning that the 310 K surface becomes redefined at a *higher* pressure. At the same time the 305 K surface is being cooled to 301 K, redefining the 305 K surface to a *lower* pressure. The net result is to increase the stability as the two surfaces approach each other in the vertical. Other examples of this nature could be shown depicting diurnal stability increases/decreases in the presence of solar heating and terrestrial cooling processes.

*Thermodynamic Equation (14):* As Wilson (1985) notes, all adiabatic advection and vertical motion is accounted for in the horizontal momentum equations through  $M$ . The thermodynamic equation in isentropic coordinates states that diabatic heating ( $dQ/dt > 0$ ) causes isentropic surfaces to propagate through the atmosphere in a direction *toward* lower potential temperature values. The explanation for this is that adding heat to a parcel will increase its potential temperature ( $d\ln\theta/dt > 0$ ). Alternately, the surface in the presence of diabatic heating

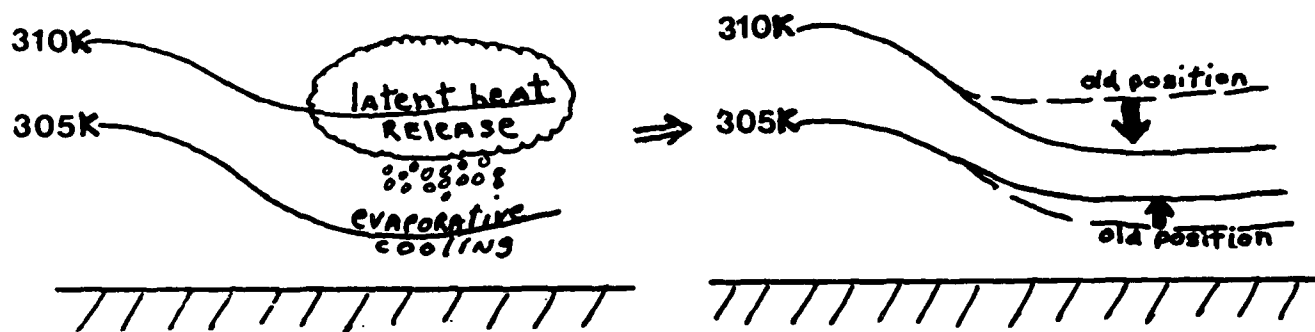


Figure 6. Schematic diagram depicting the stability changes that can take place in the presence of diabatic heating/cooling.

will become "redefined" at a lower level of the atmosphere. Conversely, in regions of diabatic cooling isentropic surfaces propagate upwards towards higher potential temperature levels.

*Montgomery Streamfunction (15):* This expression states that the streamfunction on an isentropic surface is the sum of the enthalpy,  $C_p T$ , and the geopotential at that level. Again, these terms are related to each other through the hydrostatic equation (12).

*Poisson's Equation (16):* This equation is the sounding expression for isentropic coordinates. It enables one to compare parcels of air by computing the temperature they would have if they were brought up (down) to 1000 mb--a base state level.

*Geostrophic Wind Relationship (17):* This expression relates the geostrophic wind to the pattern of Montgomery streamfunction. The relationship is similar to that on a constant pressure surface--the geostrophic wind blows parallel to the Montgomery streamfunction with lower values to the left of the wind (in the northern hemisphere). The geostrophic wind is also proportional to the gradient of Montgomery streamfunction and inversely proportional to the Coriolis parameter,  $f$ . One can create a geostrophic wind scale, similar to those used on constant pressure surfaces, which helps the analyst isopleth lines of constant  $M$  on an isentropic surface. Examples are given in Figures 7-8 for two different polar stereographic scales (1:15 million and 1:10 million). To use them, place one point of a compass on one point on the Y axis at the latitude in question and the other point to the right on the isotach value you want. The distance measured between the points is the distance two  $M$  lines should be apart (if drawn at intervals of  $60 \times 10^5$  ergs/gm) to support the given wind speed.

*Thermal Wind Relationship (18):* The thermal wind (the vertical shear of the geostrophic wind) in isentropic coordinates is proportional to the mean pressure gradient in the layer. Since isobars on an isentropic surface are equivalent to isotherms, the thermal wind is also proportional to the mean temperature gradient in the layer as is the case with pressure coordinates. The strength of the thermal wind is related to the vertical tilt of the isentropic surfaces, which is related to the pressure gradient recorded on them. The thermal wind "blows" parallel to the mean isobars in the layer with low pressure (cold temperatures) on the left and high pressure (warm temperatures) on the right looking downwind. This diagnostic relationship is very useful in interpreting cross sectional analyses and will be discussed in greater detail in Section 3.C.1.

*Gradient Wind Relationships (19-20):* The gradient wind equations are useful for studying accelerated and curved flow. Equation (19) shows that acceleration (deceleration) takes place when the wind blows across the isopleths of Montgomery streamfunction towards lower (higher) values,  $\beta > 0$  ( $\beta < 0$ ). For geostrophic flow  $\beta = 0$  and there is no acceleration. Equation (20) describes curved flow as it includes the centrifugal force (term 1). For  $\beta = 0$  it reduces to

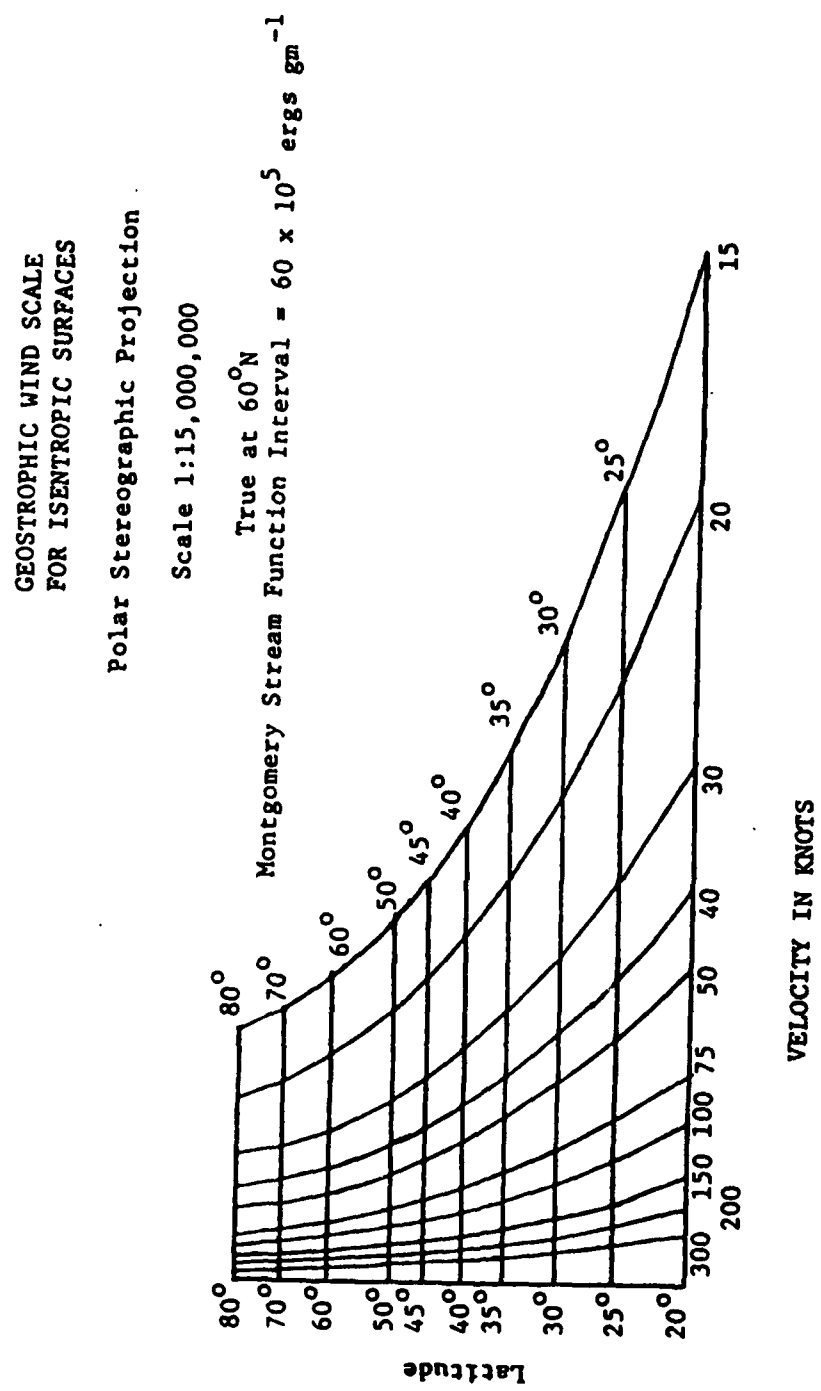


Figure 7. Geostrophic wind scale for an isentropic surface on a polar stereographic map projection with a 1:15 million map scale.

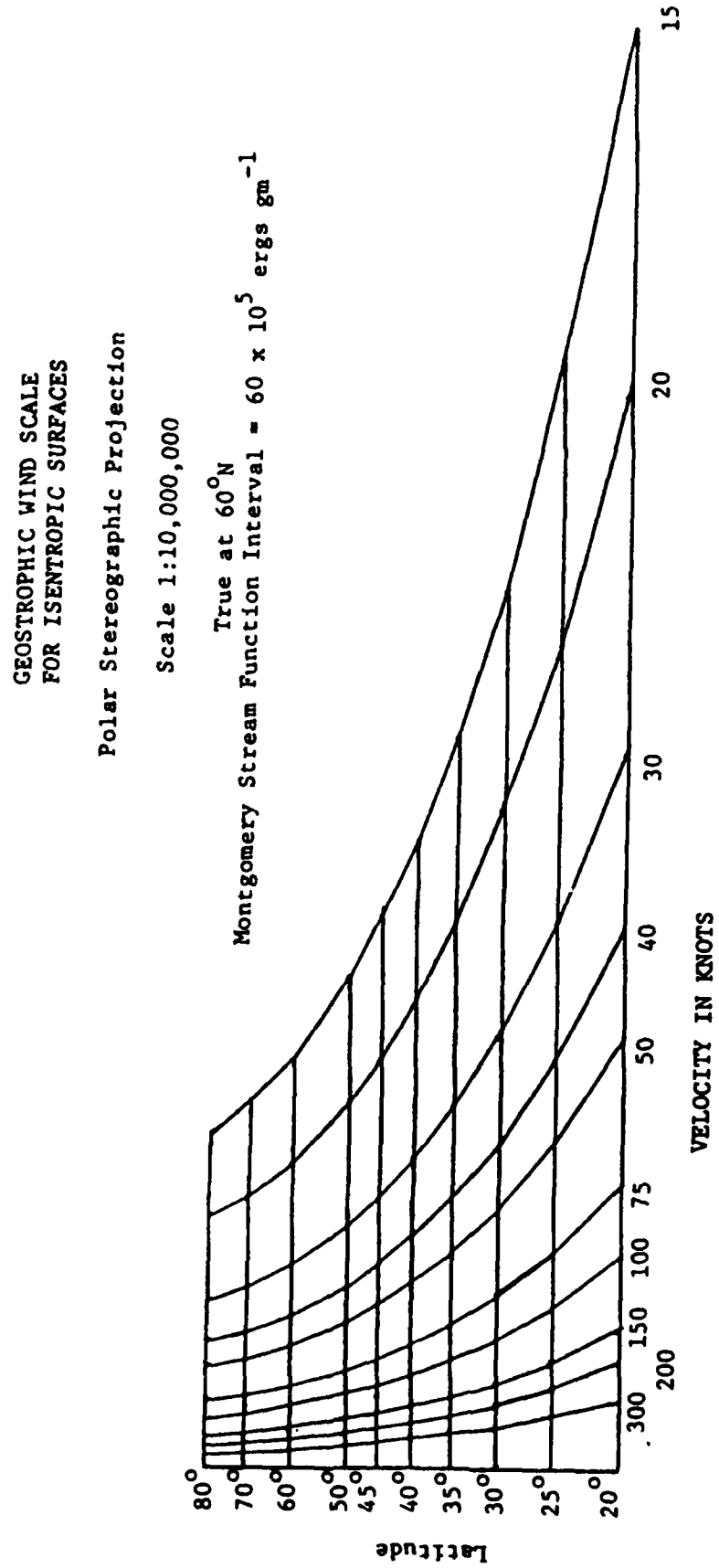


Figure 8. Geostrophic wind scale for an isentropic surface on a polar stereographic map projection with a 1:10 million map scale.

the standard gradient wind equation.

*Potential Vorticity (21):* Potential vorticity is defined as the ratio of the absolute vorticity, represented as  $\zeta + f$ , and the static stability in the column bounded by two isentropic surfaces. Under adiabatic, frictionless flow, potential vorticity is conserved, making it a useful "tag" for parcels. Reiter (1972) discusses how conservation of potential vorticity can be used to trace air parcels out of the stratosphere into the troposphere along tropopause "folds." Much of Danielsen's work referenced earlier used this conservation principle. Holton (1972, p. 69-73) uses conservation of potential vorticity to describe lee side cyclogenesis. Under conservation of potential vorticity, if a layer bounded by two isentropic surfaces shrinks (stretches) in the vertical the absolute vorticity of the column must decrease (increase) in response. After an isentropic layer has crossed the Rocky Mountains, for example, it generally increases in depth as the lowest level follows the topography while the uppermost level remains relatively fixed, leading to increased vorticity to the lee of the mountains.

#### F. Constructing an Isentropic Data Set from Rawinsonde Data

The isentropic analysis program that creates isentropic station data from rawinsonde data came originally from a research program written for Danielsen's work in the 1960's. The versions of this program used at St. Louis University (SLU) and by the Atmospheric Environment Service in Canada are nearly the same. The total computation time to run the program on the University mini-computer is on the order of 5-10 minutes. Standard and significant level rawinsonde data are needed. In the SLU version, wind data at constant height intervals (PPBB group) are used to interpolate winds to significant levels (TTBB group). This creates a complete sounding of pressure, height, temperature, dewpoint, wind direction, and wind speed for processing. The user can select the interval between isentropic levels in the troposphere and stratosphere.

The actual procedures for the computation and interpolation of isentropic data are described in Duquet (1964) and in Wilson, *et al.*, (1980). Interpolation of all variables except wind is done assuming linearity with respect to  $P^{\kappa}$  where  $\kappa = R/C_p = 0.286$ . Winds are interpolated linearly with respect to height; direction and speed are interpolated separately. Duquet (1964) notes that the latter method of interpolation tends to smooth the wind hodograph. For each sounding the following variables are computed at each isentropic level:

- (1) Montgomery streamfunction ( $M$ ) in units of  $10^5$  ergs/gm.
- (2) Pressure ( $P$ ) in millibars.

- (3) Virtual Temperature ( $T_v$ ) in degrees C.
- (4) Height (Z) in gpm. The height is determined by integrating the hypsometric equation from the ground up.
- (5) Actual specific humidity (q) in gm/kg. This is obtained by computing  $e_s$  (the saturation vapor pressure) from the Clausius-Clapeyron equation using the interpolated *dew point* temperature and then finding q from the relation:

$$q = \frac{.622 e}{P - .378 e} \quad (23)$$

- (6) Saturation specific humidity ( $q_s$ ) in gm/kg. This is found as in (5) except using the interpolated *virtual temperature*.
- (7) Relative humidity in percent computed as the ratio of  $e/e_s$  or  $q/q_s$ .
- (8) Wind speed and direction in degrees and  $m s^{-1}$ .
- (9) Stability, upper and lower, measured as the distance in mb to the adjacent higher and lower isentropic levels.
- (10) Wind shear at a given level is determined from the winds and streamfunctions at the levels immediately above and below the isentropic surface. Directions are given in degrees. Speed shears are multiplied by appropriate constants and displayed in millibars per degree latitude. These unusual units are useful to the analyst since they relate the vertical wind shear to the isobaric gradient on an isentropic surface as discussed earlier in (18).

With respect to the Montgomery streamfunction it should be noted that when stated in units of  $10^5$  ergs/gm, a difference of *one* in the last digit corresponds to a height difference of *1 meter*. Therefore, a difference of  $60 \times 10^5$  ergs/gm, which is a typical contour interval for M, corresponds to 60 meters in height on a constant pressure surface.

As noted earlier in the SLU version of the Duquet program, neutral-superadiabatic lapse rates will result in multiple pressure levels for one isentropic surface. We prefer to average the variables for that level, applying them to a mean pressure value instead of "adjusting" the sounding.

### 3. ISENTROPIC ANALYSIS TECHNIQUES

In this section we will explore various analysis procedures for both vertical and "horizontal" plots of isentropic data. Emphasis will be placed on practical applications to everyday forecast problems.

There are basically three different charts used in isentropic analysis: the psi chart, the sigma chart, and the isentropic cross section. The psi chart is named after  $\psi$ , which typically represents a streamfunction--in this case the Montgomery streamfunction. In this set of notes we have used M instead of  $\psi$ . The sigma chart is so named because static stability ( $\partial P/\partial \theta$ ) is often represented as  $\sigma$ . It should be noted that several researchers/analysts prefer to plot all their isentropic surface data on one map rather than split it up into two charts. This is a user-selectable feature and therefore is left to the reader. For completeness we will show several station models so that the reader may compare the various options.

#### A. Psi Charts

On the psi chart the following variables are plotted: Montgomery streamfunction, wind direction and speed, mixing ratio, and relative humidity. The M value can be plotted in cgs or mks units. A typical value is  $30,600 \times 10^5$  ergs/gm or equivalently  $30,600 \times 10^1$  Joules/kg. Either way, the leading digit is usually not plotted--the 3 or 2 preceding it is understood. A typical station model plot is shown in Figure 9.

Contour intervals will vary according to the season but typical values for warm/cold seasons are as follows:

Variable	Contour Interval
Montgomery streamfunction	$30/60 \times 10^1$ J/kg
Pressure	25/50 mb
Wind speed	$10/20 \text{ m s}^{-1}$
Acutal specific humidity	2/1 gm/kg
Relative humidity	50/70/90%

As on any chart a maximum of three types of isopleths is suggested, preferably using a color scheme along with solid, dashed, or dotted lines. The "starting value" of the Montgomery streamfunction is a function of the level. It is usually best to start at an even number; e.g. 31,000 or 29,800, whenever possible and, of course, to be consistent from day to day on the same surface. The Montgomery streamfunction field helps to define the flow of the geostrophic wind and also to identify short/long wave activity much as on a constant pressure chart.

Isobars also should be started at some even number like 600 or 700 mb. They help to define cold and warm tongues on the isentropic surface. Strong gradients of pressure also can be used to locate frontal zones as seen in Figure 10. Anderson (1984) has described various isobar patterns in the vicinity of frontal

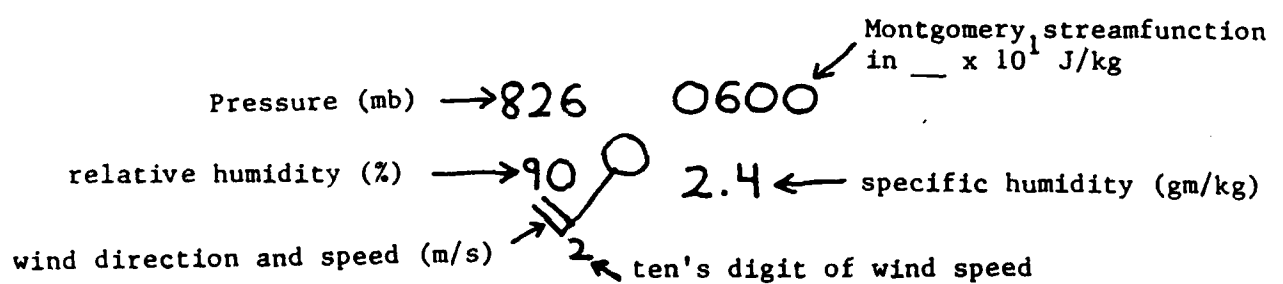


Figure 9. Station model plot for psi charts.

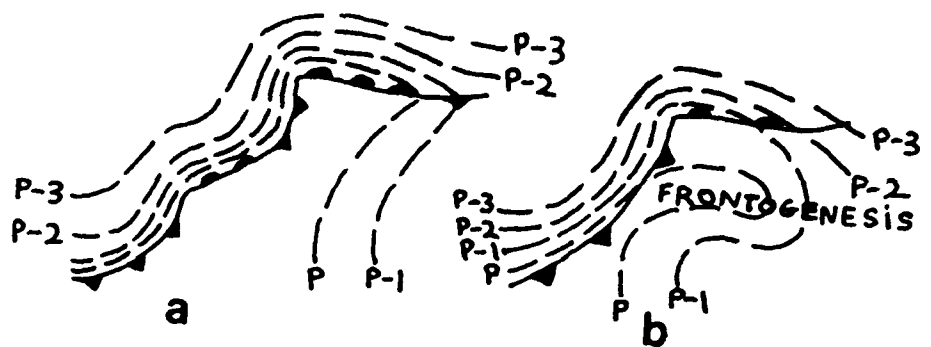


Figure 10. Isobaric topography in the vicinity of fronts (a) and isobaric topography associated with frontogenesis in the warm sector (b) (Namias, 1940).

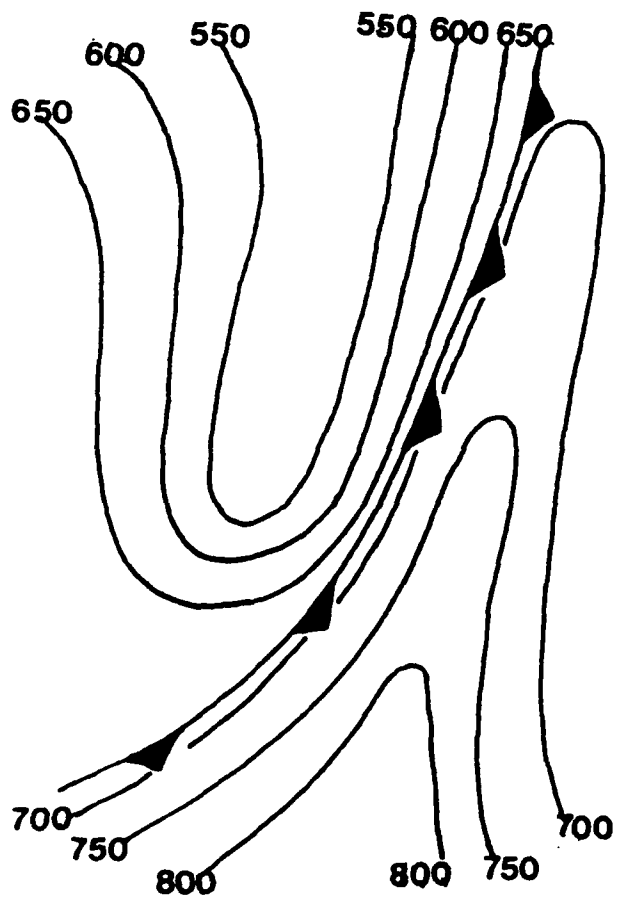


Figure 11a. Isentropic pressure pattern in the vicinity of a strong, mature cold front (Anderson, 1984).

systems. Figure 11a shows a pressure pattern in the vicinity of a strong mature cold front. The cold front is placed at the leading edge of the pressure gradient with the warm (high pressure) thermal ridge extending in a narrow tongue ahead of the front. Isobars are usually found to cross a frontal system undergoing frontolysis (Figure 11b). The lack of structure in the pressure field is indicative of a weakening thermal gradient and decaying frontal zone. In the case of an occluding system warm tongues tend to be diagnosed along the warm front and occlusion portions of the cyclone with a cold (low pressure) trough extending southward behind the cold/occluded fronts (Figure 11c). Also, as discussed earlier, the cross-isobar component of the wind can be used qualitatively to estimate the upslope/downslope adiabatic vertical motion. Isobars are good as reference values, especially for someone just beginning isentropic analysis and remind the analyst of the three-dimensional nature of this "horizontal" surface.

Mixing ratio isopleths (isohumes) are, of course, essential for depicting moist/dry tongues and their advection. Figure 12 depicts an idealized isohume pattern associated with an occluding system. It should be noted that in winter it is not uncommon to receive substantial precipitation out of clouds in which the specific humidity is less than 1 gm/kg (Byers, 1938). Therefore, the isohume contour interval is seasonally dependent and level-dependent as specific humidity values often decrease rapidly with height. A typical isentropic upslope pattern is depicted in Figure 13 with a south-southwesterly flow on this isentropic surface air being lifted as it transports moisture northward.

With two isentropic levels analyzed one can often diagnose regions where convective instability is being increased as dry air aloft is advected over moist air below. Such a situation is shown in Figure 14. Notice how low level moist air is currently being overlain by upper level dry air thereby increasing the convective instability. In other cases it may be possible to predict this pattern based on advection patterns at the two levels.

Relative humidity is helpful to estimate how close some areas are to saturation so that the analyst may be careful in interpretation. To avoid map clutter one may isopleth the 50, 70, 90% values or merely shade in green values exceeding 70%.

Isotachs may be drawn as well to help diagnose jet streaks at low, middle, or high levels. Keep in mind that the jet streak depicted on an isentropic chart is being drawn in its three-dimensional detail so one is not only seeing its length and width, but its depth. One intangible benefit of such an analysis is that it reinforces the view of the atmosphere as a continuous fluid. Such an appreciation is difficult to obtain with constant pressure analyses, which are two-dimensional and quasi-horizontal.

## B. Sigma Charts

The sigma chart is primarily a stability chart. The variables typically plotted on it are pressure, thermal wind, the number of millibars needed to reach the  $\theta + 5K$  isentropic surface, and the number of millibars needed to reach the  $\theta - 5K$

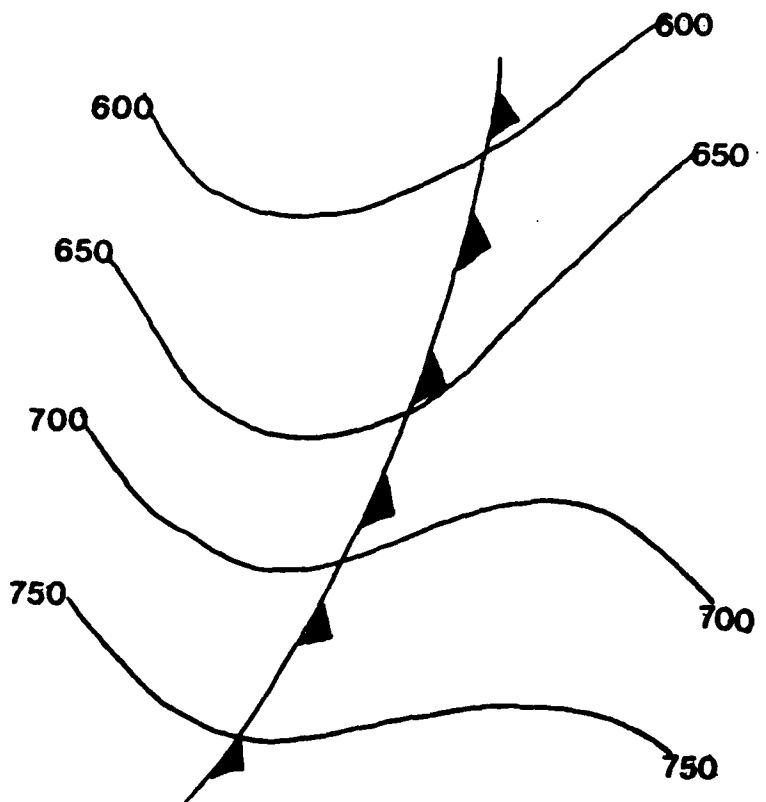


Figure 11b. Isentropic pressure pattern in the vicinity of a frontolysizing cold front (Anderson, 1984).

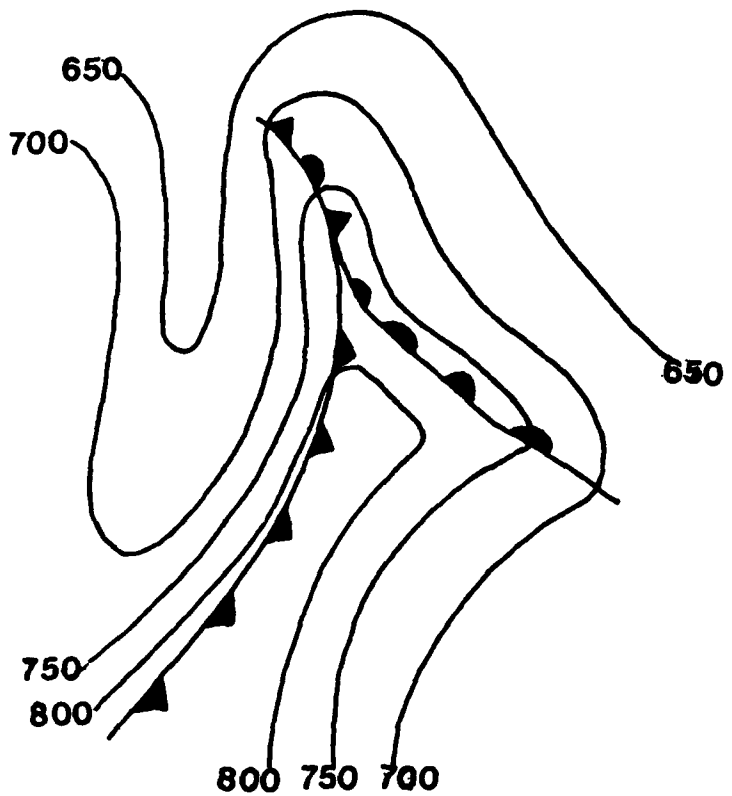


Figure 11c. Isentropic pressure pattern in the vicinity of an occluding frontal system (Anderson, 1984).

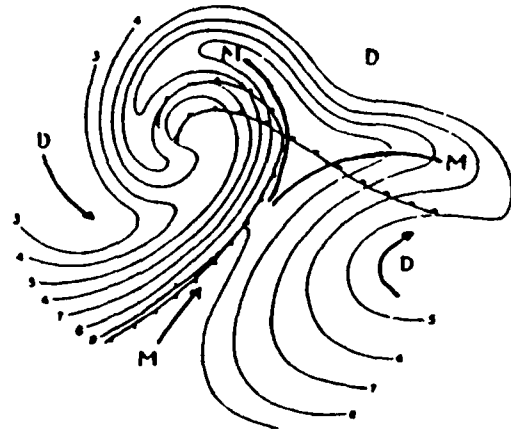


Figure 12. Fronts indicated at the surface and schematic flow pattern around an occluded cyclone as shown by the moisture lines in an isentropic surface in mid-air (Namias, 1940).

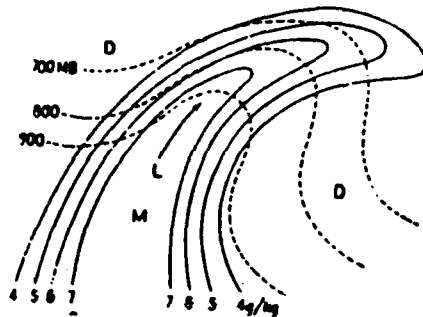


Figure 13. Illustrating probable upslope motion of a moist current as deduced from the relation of the moisture lines to the isobars on an isentropic surface (Namias, 1940).

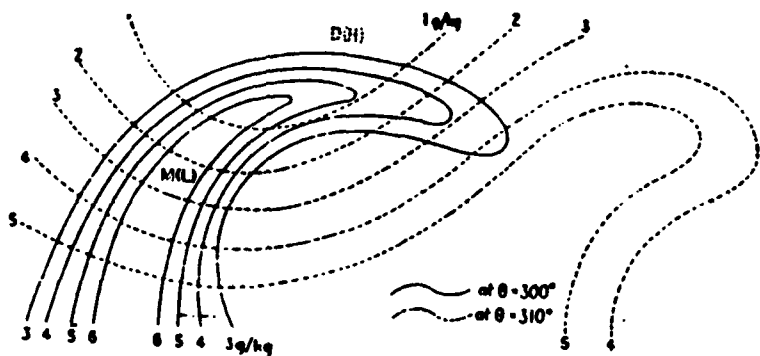


Figure 14. Flow pattern at different isentropic surfaces which leads to increasing convective instability. Solid (dashed) lines are isohumes at low (upper) level (Namias, 1940).

isentropic surface. In this station model we have assumed that the 5K interval was chosen as an option when creating the data set. However, this number depends on the interval chosen, which is up to the researcher/analyst. The plotting model varies among researchers but looks essentially as shown in Figure 15.

Some people plot the total of the two LHS numbers in the bottom right corner, thus indicating the stability over a 10K interval. These numbers indicate the static stability ( $\partial P/\partial \theta$ ) which on a cross section would show up as the distance in millibars between two adjacent isentropic surfaces. The greater the distance between two adjacent isentropic surfaces, the greater the instability. Small distances between isentropic surfaces indicates great stability. In the stratosphere, for instance, the static stability is usually around 10K per 50 mb or less, while tropospheric values are generally around 10K per 100-200 mb! By isoplething the total static stability (the sum of the LHS numbers) we can obtain an excellent diagnosis of the instability.

Typical contour intervals will once again vary with the season but are typically as follows:

Variable	Contour Interval
Pressure	25/50 mb
Static Stability	10/20 mb

Although it might be better to analyze for the total static stability (lower  $\Delta P$  + upper  $\Delta P$ ) it is good to see the breakdown of the two layers to see where the greater instability is located.

The plotted thermal wind is computed for the layer surrounding the actual isentropic level in question. If one were analyzing the 300 K surface, the thermal wind would be valid for the 295-305 K layer (if a 5K interval was chosen). One can use the thermal wind directions to help draw the isobars since, according to (18), the thermal wind over a layer "blows" parallel to the mean isobars of the layer. Similarly, the gradient of the isobars can be qualitatively checked by noting the speed of the thermal wind. Strong (weak) thermal winds are associated with large (small) isobaric gradients on isentropic surfaces. One word of warning--these wind shears are based on the actual wind--not the geostrophic wind. So the degree to which this actual wind shear "obeys" the pressure gradient depends on the degree to which the actual wind "obeys" the geostrophic wind. It is possible for ageostrophic wind components; e.g., those in the vicinity of convective systems or jet streaks, to produce wind shears which are out of balance with the expected geostrophic shear. In any event, forecasters, especially those in aviation, should find these wind shear calculations informative for the diagnosis/prediction of turbulence. Other forecasters may use the wind shear to measure the significance of a frontal boundary or elevated inversion.

For completeness, we also show two other plotting models which essentially combine the features of the psi and sigma charts. Wilson (1985) uses the plotting model shown in Figure 16. He uses one variable that has not been discussed yet--

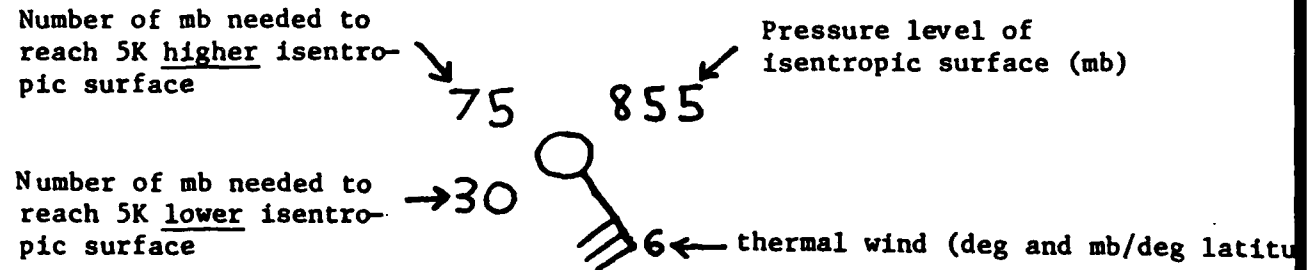


Figure 15. Station model plot for sigma charts.

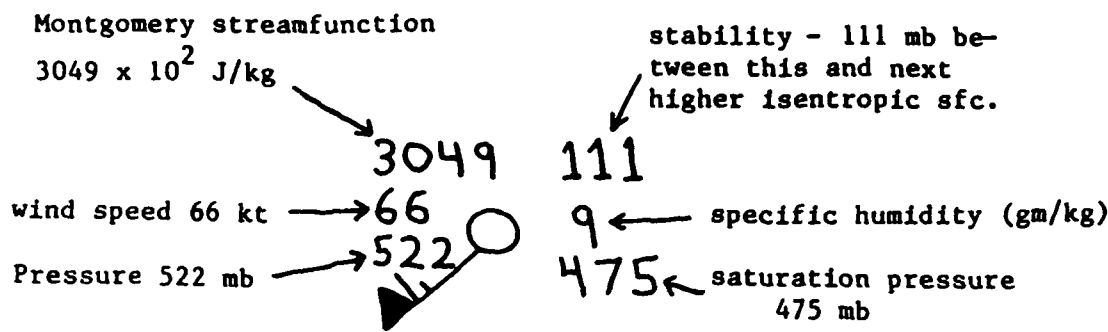


Figure 16. Wilson (1985) station model plot.

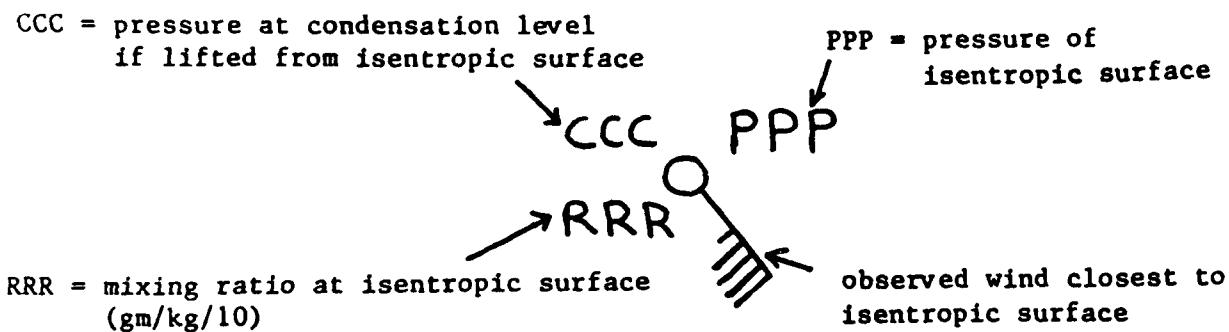


Figure 17. Plotting model used by ISENT (NWS Southern Region isentropic plotting program used on AFOS), Little (1985).

the saturation pressure or lifted condensation pressure. Essentially this is the level to which the parcel must be lifted to achieve saturation. It gives a quick assessment of how close the atmosphere is to saturation at a station. More will be said of this later. Other variables are as described earlier.

Little (1985) describes a program for AFOS called ISENT which plots isentropic data in the form shown in Figure 17.

As with any analysis scheme you should pick the station model(s) that suit your needs. The author usually tries to avoid analyzing more than three variables per map--preferably only two for easier viewing and presentation.

### C. Cross Section Analysis Techniques

We now will turn our attention to vertical "slices" through the atmosphere--cross sections. They usually are the first step in choosing the "horizontal" isentropic surfaces to analyze. One typically chooses the surfaces which are embedded in an interesting feature; e.g., baroclinic zones, jet streaks, or moist tongues. Generally, in addition to the isentropes, it is also interesting to display mixing ratio (or specific humidity) and/or winds on the cross section. The mixing ratio profiles are useful in gauging the depth of the moist layer and possible areas of convective instability (dry air over moist air). The wind profile is useful at depicting the vertical extent of jet streaks or wind maxima but also has an interesting relationship to the tilt of the isentropic surfaces. This is the subject of the next section.

#### 1. Thermal Wind Relationship in Isentropic Coordinates

An isentropic cross section is generally chosen to be *normal* to a jet streak or wind maximum and therefore *across* a baroclinic zone (i.e., frontal zone). This allows one to depict the vertical and horizontal dimensions of the jet streak and attendant baroclinic zone. Mixing ratio profiles are also quite variable and interesting in this area, too. Since the baroclinic zone is, by definition, a region of strong thermal contrast, one would expect to see a great tilt of the isentropic surface from high in the cold air to low in the warm air. From thermal wind consideration this requires strong vertical wind shear through these zones.

From our earlier discussion of the thermal wind you may recall that it "blows" parallel to the mean isobars in the layer or normal to the pressure gradient such that low (cold) pressure is to the left of the thermal wind looking downstream. In a cross section depiction we are graphically representing only a *component* of the total isobaric gradient. There is no guarantee that the chosen cross section is exactly parallel to the isobaric gradient associated with the jet streak. Therefore, we plot on the cross section only the *wind components* normal to the plane of the cross section. Wind components *into* the plane of the cross section are generally designated as positive while those wind components *out of* the plane of the cross section are designated as negative. It is these normal wind components which have a relationship to the pressure gradients depicted in the cross section.

To obtain the normal wind components it is necessary to know the angle between the plane of the cross section and true north-south. However, rawinsonde stations do not generally all lie on a straight line. So what is done? In the SLU cross section program we compute a least squares regression line for the stations chosen. The position of the stations is then chosen on this regression line perpendicular to the original station location as seen in Figure 18. One must intelligently choose stations which are approximately on a line because the regression line computation is "dumb"; i.e., even a series of stations along a curve will be placed on a *line*. Let the user beware!

Figure 19 is a schematic example of how we can relate vertical wind shear to the tilt of isentropic surfaces in a cross section. Notice how the upper isentropic surface slopes down from the cold air (pt. A) to the warmer air (pt. B). Therefore, the gradient of pressure in the plane of this cross section points from A to B. Since the thermal wind points in or out of the cross section with cold air to the left (looking downwind), the thermal wind will point into the page in this case. The net result is that we expect the wind components into the page to *increase* with height in this area of the cross section. This means that for this N-S cross section westerly winds will increase with height. We can now state three general rules:

- (1) When isentropic surfaces slope *down*, the thermal wind is positive; i.e., wind components *into* the plane of the cross section increase with height.
- (2) When isentropic surfaces slope *up*, the thermal wind is negative; i.e., wind components *out of* the plane of the cross section increase with height.
- (3) When isentropic surfaces are horizontal (quasi-barotropic), the thermal wind is approximately zero and the normal wind component does not change with height.

On a typical cross section one plots the potential temperature, specific humidity and normal wind components as shown in Figure 20.

In the troposphere it is useful to draw isentropes at 2-4K intervals, but as one nears the stratosphere it is best to double the interval to at least 4-8K as the stability is very strong. Since water vapor decreases quickly with height a good contour interval for specific humidity is 1-2 gm/kg. Finally, isotachs can be drawn at 5 m/s intervals. Remember that values can be + or -; therefore, a zero line may need to be drawn.

## **2. Isentropic Topography in the Vicinity of Upper-Level Fronts and Jet Streaks**

An averaged, idealized cross section from north to south is shown in Figure 21. There are many interesting features in this cross-section. They include:

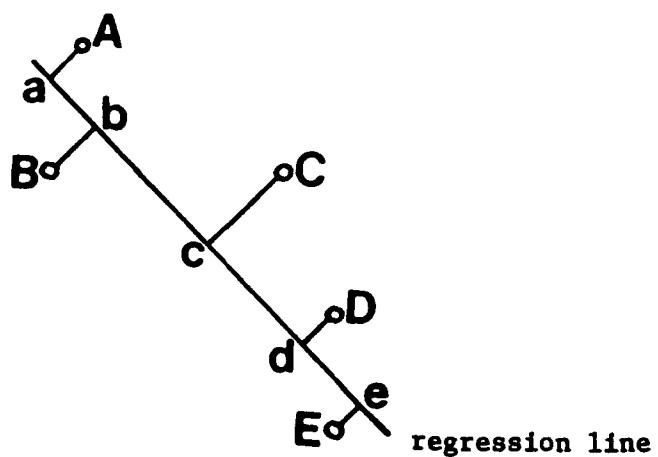


Figure 18. Schematic showing how stations are depicted with respect to the regression line and their original positions.

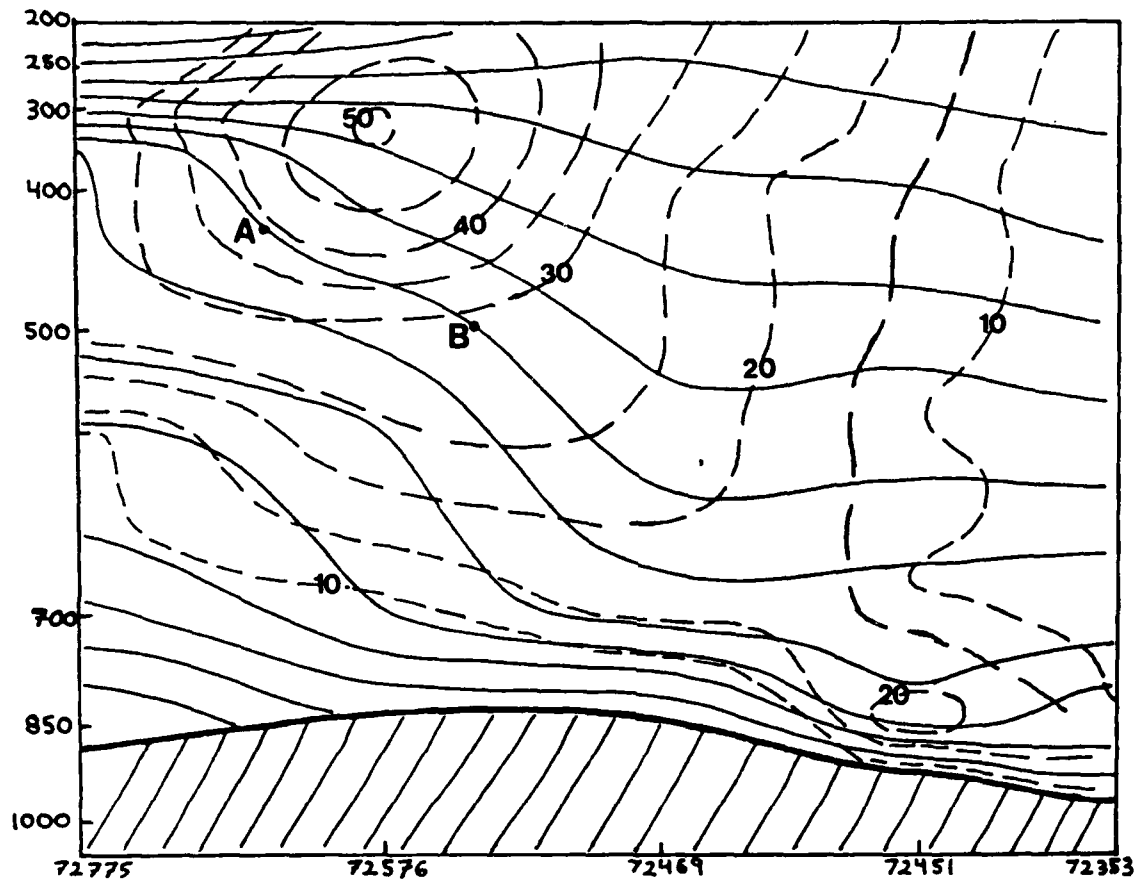


Figure 19. Cross section illustrating the relationship between sloping isentropic surfaces and the vertical wind shear. Solid lines are isentropes and dashed lines are normal wind components where + (-) indicates winds into (out of) the plane of the cross section.

Potential Temperature ( $^{\circ}$ K)  $\rightarrow 296$        $10.6 \leftarrow$  specific humidity (gm/kg)  
     $+ 6.3 \leftarrow$  normal wind component (m/s)

Figure 20. Cross section plotting model.

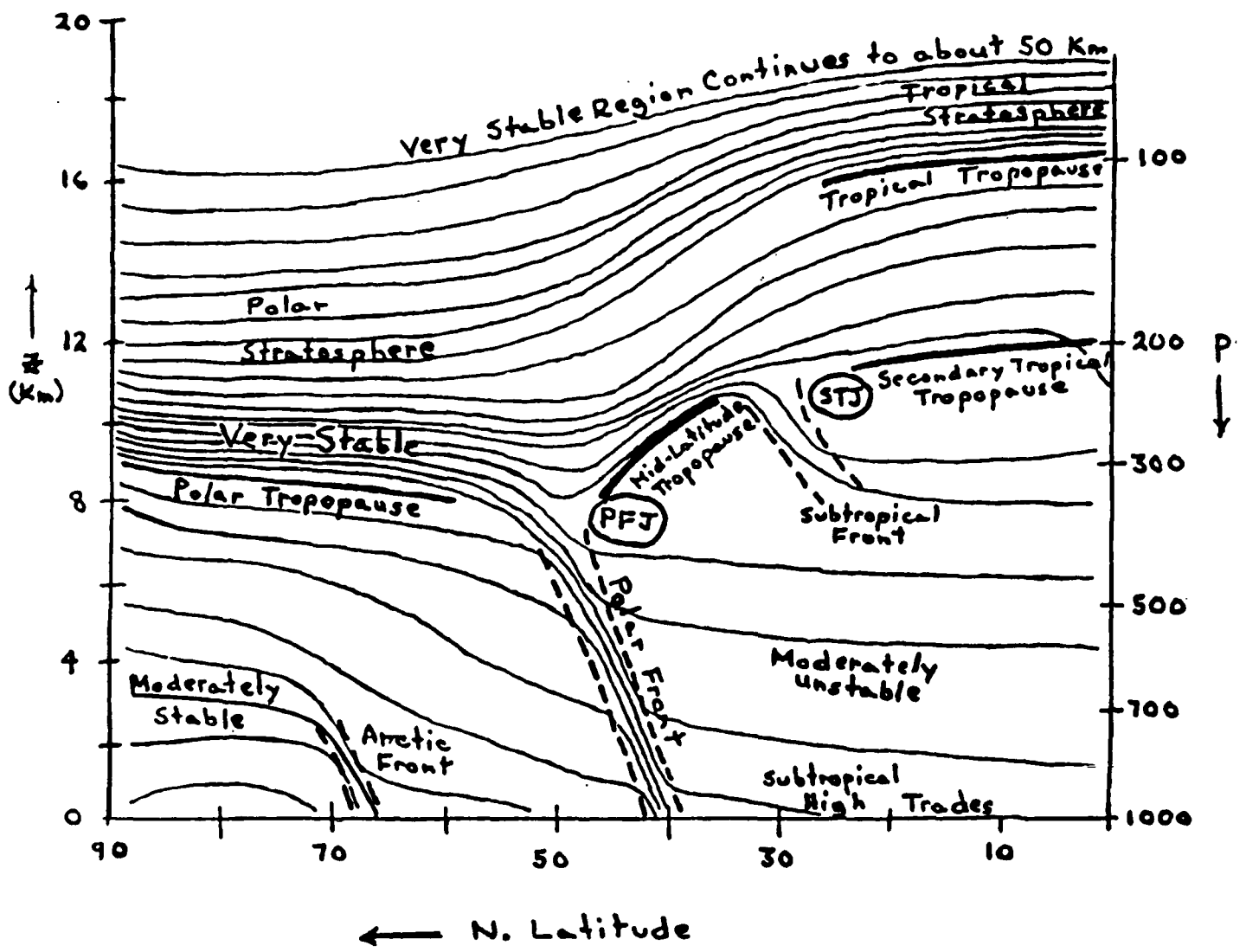


Figure 21. Idealized and averaged picture for the annual mean or the Spring and Autumn seasons. In summer the tropopause lifts at middle and high latitudes, the tropospheric gradients and the Arctic front weaken or vanish, and the associated jet streams weaken or vanish. The subtropical jet (STJ) stream in particular weakens and the subtropical highs shift poleward. In winter the polar frontal jet (PFJ) stream often merges with the STJ stream especially over the continents; the gradients in the troposphere are stronger then and the stability is greater, but nowhere near as stable as the stratosphere. The sloping isentropes imply that the westerlies increase with height in the troposphere, and decrease with height to become easterlies in the stratosphere, except at very high latitudes. There is again a strong seasonal variation in the stratosphere, with westerlies at high latitudes moving southward to middle latitudes and strengthening in winter.

(A) The polar frontal jet (PFJ) and its associated polar front are seen around  $40\text{--}50^{\circ}\text{N}$ . The polar front is depicted as a sloping zone (indicating strong thermal contrast) and as a compacted isentrope zone indicating stability. Although it is shown in Figure 21 as identifiable all the way to the surface, this is not always the case, since the isentropic surfaces lost continuity in the boundary layer. The PFJ is placed at about 350 mb, a little lower in the atmosphere than perhaps it should be. It is above the polar front where the vertically-integrated result of the thermal wind effects is greatest. Note how the isentropes slope up above the PFJ, indicating a reversal of the thermal wind in the stratosphere and a subsequent decrease in westerly momentum. Also notice how there is a gap in the tropopause in the vicinity of the PFJ. In fact the polar front appears as an extension of the strongly stable air of the stratosphere. In this region there is considerable stratospheric-tropospheric air exchange. This shows that the tropopause is not quite the "lid" or impermeable layer it was once thought to be. We will return to this concept later.

(B) The air in the troposphere is much less stable than the stratospheric air. This is seen by comparing the vertical distances between isentropes in both regions. The air in the troposphere is *not* unstable generally but *relatively less stable* --the farther apart the isentropes the less stable the lapse rate. Potential temperature lapse rates of 10 K/100 mb are not uncommon, whereas in the stratosphere lapse rates are generally about 10 K/50 mb or more.

(C) The arctic front shows up as a shallow, few kilometer deep layer of stable air with strong vertical tilt. This is a good example of how one can gauge the depth of systems and perhaps, as in this case, determine whether a system in low levels is vertically coupled to the upper air flow.

(D) The subtropical jet (STJ) is shown to be associated with a weak upper tropospheric front. This is not unexpected since the STJ is not explained through thermal wind arguments as is the PFJ. It comes about as a result of air flowing north in the upper branch of the Hadley cell circulation attempting to conserve its angular momentum. As it flows north its angular velocity increases in response to a shorter distance to the earth's axis of turning. The STJ can be even stronger than the PFJ, with speeds of up to 260 knots observed over Southern Japan (Palmen and Newton, 1969). Palmen and Newton (1969) also observed that the STJ is characterized by great steadiness in both wind direction and geographic location, and tends to have an anticyclonic curvature. The STJ tends to be associated with a "break" between the mid-latitude tropopause at around 250 mb (noticeably higher than the PFJ) and the tropical tropopause typically found at 100 mb. Often on jet charts or 200 mb charts it is difficult to determine if a jet streak is part of the PFJ or STJ. A cross section of winds will help diagnose these two jet streams. However, in the winter it is not uncommon for the two jet systems to merge

as the PFJ moves southward with the polar front.

(E) The tropopause, especially in middle and higher latitudes, is easy to locate, except near significant jet streaks where the tropopause "breaks" occur. The tropopause appears as a zone where the vertical lapse rate of potential temperature increases by about an order of magnitude.

#### D. Useful Diagnostic Variables Computed from Isentropic Data

Once an isentropic data set has been generated from rawinsonde data it is relatively straightforward to interpolate the station data to a grid on a map projection (e.g., lambert conformal, polar stereographic). This can be done using one of the more popular objective analysis schemes (e.g., Barnes, 1973). Details of this procedure will not be discussed in this paper. For an excellent treatment of this subject see Koch, *et al.*, (1983). Once grids of  $u$ ,  $v$ ,  $P$ ,  $q$ ,  $M$  are obtained for a particular isentropic surface numerous diagnostic variables may be computed. In this section we will briefly discuss some of these variables and how they might be used in diagnostic analysis.

1) Static Stability: This variable can be expressed as  $\Delta P = P$  (upper  $\theta$  surface) -  $P$  (lower  $\theta$  surface) which is always  $< 0$ , although some people like to define it in the opposite sense so that it is always  $> 0$ . In any event, it is a relative measure of instability which *does not* take moisture into account. Horizontal plots of this variable on an isentropic surface, using adjacent surfaces for the computation, are "quick and dirty" estimates of stability and stability change. Units are millibars.

2) Moisture Advection/Convergence: Moisture advection is expressed mathematically as  $-\vec{V} \cdot \nabla q$ . Values  $> 0$  (or  $< 0$ ) indicate increasing (or decreasing) moisture locally. Local increases or decreases of moisture; e.g., through evaporation or condensation, are neglected. Essentially it evaluates quantitatively what one can estimate qualitatively by superimposing the flow (streamlines or Montgomery streamfunction) over the isohumes. Units are generally gm/kg-hr  $\times 10$ . Multiplying by 10 inflates the values to bring out important features.

To take this one step further, one can compute moisture convergence on isentropic surfaces expressed as  $-\nabla \cdot q\vec{V} = -\vec{V} \cdot \nabla q - q\vec{V} \cdot \nabla$ . As you can see, it includes the advection of moisture *and* the effect of divergence/convergence on the moisture field. In an isentropic framework this variable measures not only the advection of moisture but also the destabilization (or stabilization) that takes place with convergence (or divergence). Thus, positive values indicate positive moisture advection and/or destabilization due to convergence. This is often useful in forecasting convection. Negative values indicate drying out due to negative moisture advection and/or stabilization associated with divergence. Units are gm/kg-hr  $\times 10$ .

3) Adiabatic Vertical Motion: This variable can be expressed as:

$$\omega_{\text{adiabatic}} \approx \nabla \cdot \nabla_{\theta} P$$

Negative (positive) values imply upward (downward) motion on an isentropic surface. This expression is a reasonable approximation to (7) since, as described by Homan and Uccellini (1987), the local pressure tendency term will always act against the diabatic term in (7). The remaining term shown above is thus a good approximation to vertical motion, especially at the synoptic scale. It is essentially measuring what you would qualitatively estimate from the cross-isobar component of the streamlines or Montgomery streamfunction. Units are generally  $\mu\text{bars/sec}$  to be consistent with standard measures of vertical motion.

4) Static Stability Tendency: This variable is taken from the continuity equation (13) discussed earlier. Assuming no diabatic effects we can write (13) as:

$$\frac{\partial}{\partial t} \left( \frac{\partial P}{\partial \theta} \right) = -\nabla \cdot \nabla \left( \frac{\partial P}{\partial \theta} \right) - \frac{\partial P}{\partial \theta} (\nabla \cdot \nabla) \quad (24)$$

Since  $\partial P / \partial \theta$  is always  $< 0$  (for  $\theta$  to be a valid coordinate!) it flips the sign of the tendency term. If either the advection or the divergence term is *negative* they contribute to *destabilization*. Likewise, *positive* values indicate a tendency towards *stabilization*. The advection term simply moves existing patterns of static stability about, while the divergence term can create or destroy static stability. Divergence in the layer acts to *increase* stability (+ sign) while convergence acts to *decrease* stability. To compute these terms one uses  $\partial P / \partial \theta$  centered on the isentropic surface whose u and v wind components are used. Units can be written as  $\text{mb/K-s} \times 10^{-5}$ .

5) Absolute Vorticity: Absolute vorticity can be computed as:

$$\eta_{\theta} = \zeta_{\theta} + f = \frac{\partial v_{\theta}}{\partial x} - \frac{\partial u_{\theta}}{\partial y} + f \quad (25)$$

using u and v wind components on an isentropic surface. Absolute vorticity is one of the most basic variables used for analysis in synoptic meteorology. Vorticity is useful in diagnosing short waves and their intensity, the same as on isobaric surfaces. It is especially helpful in depicting strong horizontal shear zones associated with westerly jets with little curvature. Units are  $\times 10^{-5} \text{ s}^{-1}$ .

6) Potential Vorticity: This variable is written as shown in equation (21):

$$P_{\theta} = \frac{-(\zeta_{\theta} + f)}{\frac{\partial P}{\partial \theta}}$$

Potential vorticity is useful as a tracer for atmospheric flow under adiabatic, frictionless conditions. It can be especially useful, when interpolated to cross sections, to diagnose the intrusion of stratospheric air which generally has potential vorticity values about one order of magnitude greater than tropospheric values (Reiter, 1972). When air extruding into the troposphere along the polar front experiences convergence, it increases its cyclonic spin in an effort to conserve its potential vorticity. Staley (1960) notes that the potential vorticity of a parcel is changed only by diabatic heating and/or friction. Units are typically  $\text{cm}\cdot\text{s}\cdot\text{K}/\text{gm} \times 10^{-9}$ .

7) Condensation Pressure: This variable was first suggested by Byers (1938) to help better represent moisture on isentropic surfaces. It is simply defined as the pressure to which unsaturated air must be raised dry-adiabatically in order to reach saturation; i.e., the condensation level. It is typically expressed in millibars. The key advantage of condensation pressure over specific humidity is that condensation pressure better represents moisture differences at low values of  $q$ . This can be seen best in Figure 22, which presents condensation pressures vs. specific humidity for various potential temperatures. Note that along each isentropic surface the slope ( $\partial P/\partial q$ ) <sub>$\theta$</sub>  is greatest at low values of  $q$ . Byers (1938) notes that on an isentropic surface a specific humidity between 1 and 0.5 gm/kg is poorly represented, while condensation pressure isobars make it stand out about as much as a 5-10 gm/kg difference. This is important, especially in winter when low specific humidity values are often associated with significant precipitation and clouds. Simple algorithms are available to compute the condensation pressures for unsaturated air.

Anderson (1984) notes that condensation pressure isobars can be useful in identifying frontal positions. A moist tongue, represented as a ridge of condensation pressure is usually present along or slightly ahead of a strong, mature cold front (Figure 23a). As a cyclone occludes the moist tongue will typically branch into two tongues--one turning cyclonically to the northwest and the other anticyclonically to the northeast. The occlusion is usually found in the vicinity of the branching (Figure 23b). Anderson (1984) notes that the precipitation is often heaviest in this area.

8) Condensation Ratio: Byers (1938) defines this variable as the ratio of the condensation pressure ( $P_o$ ) and the actual pressure ( $P$ ) of a point on an isentropic surface. It is a measure of nearness to condensation and is dimensionless. Condensation ratio can then replace relative humidity on the psi chart.

Byers (1938) points out that nearness to condensation can also be estimated by the distance between an isobar ( $P$ ) and an isobar of condensation pressure ( $P_o$ ) having the same value. If the prevailing flow is expected to move a  $P_o$  isobar over a  $P$  isobar of the same value, saturation and precipitation can be expected.

9) Condensation Difference: Anderson (1984) notes that the condensation ratio is not easy to analyze. He suggests computing the condensation difference by subtracting the value of the condensation pressure from the corresponding pressure

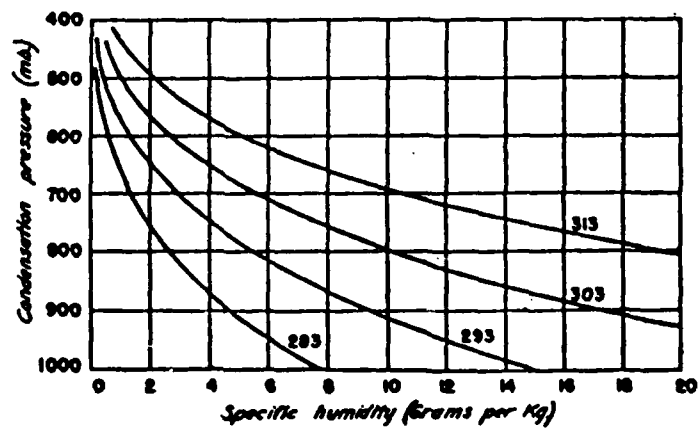


Figure 22. Condensation pressure (mb) vs. specific humidity for 283, 293, 303, and 313 K isentropic surfaces. Note the great slopes for low specific humidities (Byers, 1938).

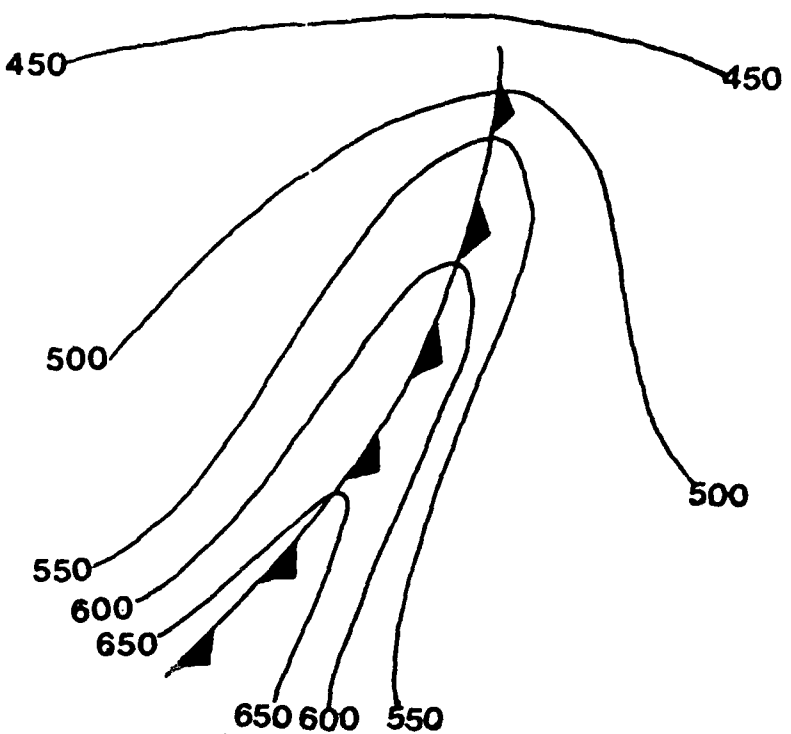


Figure 23a. Isentropic condensation pressure pattern over a mature, strong cold front (Anderson, 1984).

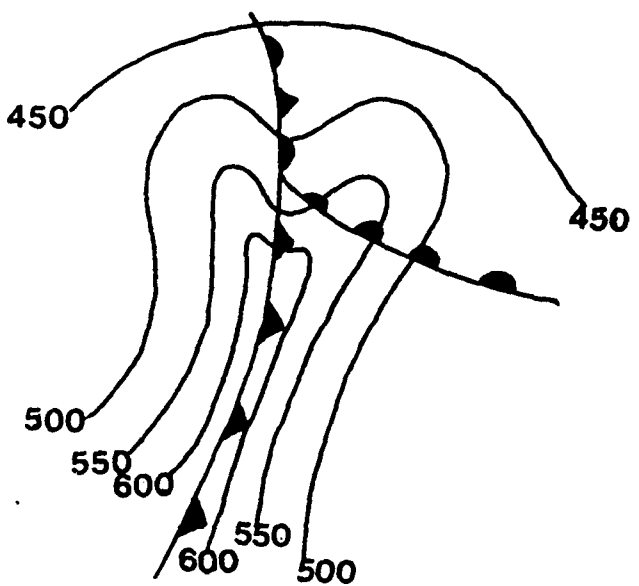


Figure 23b. Isentropic condensation pressure pattern over an occluding frontal system (Anderson, 1984).

value on an isentropic surface. The smaller the value of the condensation difference, the closer the parcel to saturation. Due to smoothing and round-off errors, a difference of less than 20 mb represents saturation. For summer over the western U. S. he found values < 100 mb to be useful indications of near-saturation.

Edson (1966) discusses the use of the "condensation pressure spread" for cloud forecasting. Figure 24 is his diagram illustrating the relationship of this variable to cloud cover for various pressure levels.

10) Streamlines: On the CSIS system and the isentropic program designed by Anderson (1984), a streamline analysis is available for display, usually to overlay with one other variable. Streamlines, it should be remembered are based on the actual wind and display the instantaneous field of motion. They can be overlaid with the Montgomery streamfunction to depict regions of ageostrophic flow. They also are excellent for depicting regions of convergence/divergence which, in an isentropic framework, are associated with destabilization/stabilization. However, they do not display any speed information. So, although streamlines crossing isobars, for instance, generally imply vertical motion, one cannot get a quantitative measure of omega from such a field.

Anderson (1984) states that streamlines will tend to converge in the vicinity of frontal boundaries (Figure 25a), especially in regions of frontogenesis. When streamlines flow across a front as depicted in Figure 25b the front is weak and in the process of frontolysis.

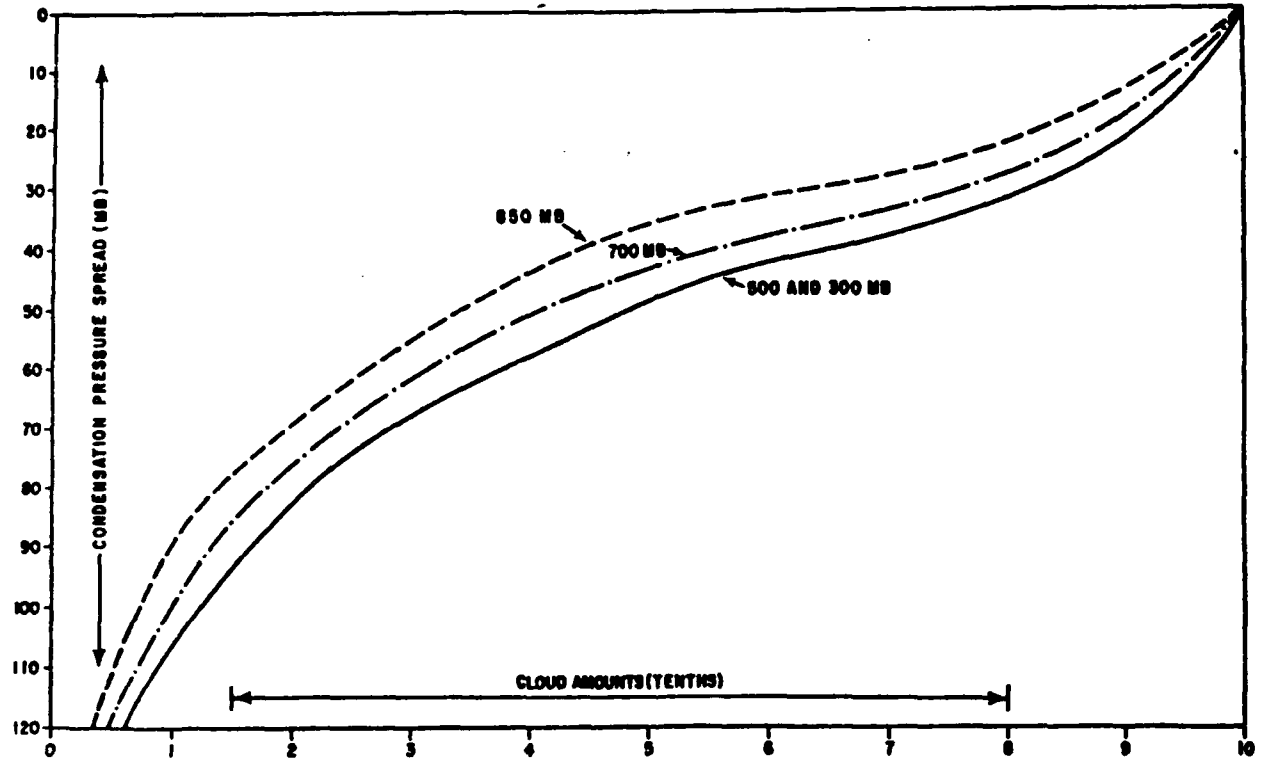


Figure 24. Condensation-pressure spread to cloud-conversion table (Edson, 1966).

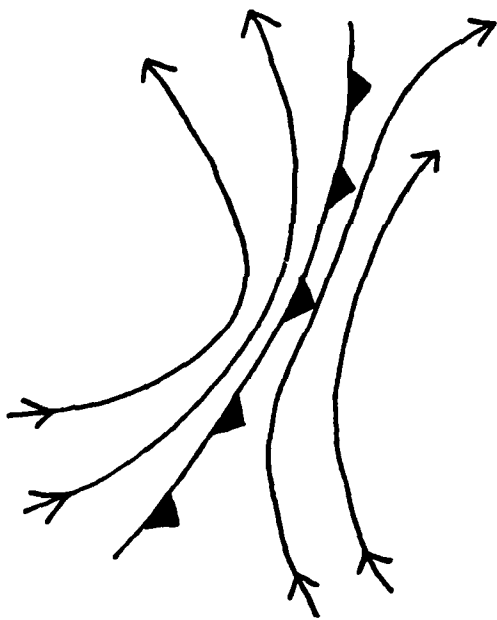


Figure 25a. Isentropic streamlines in the vicinity of a strengthening cold front (Anderson, 1984).

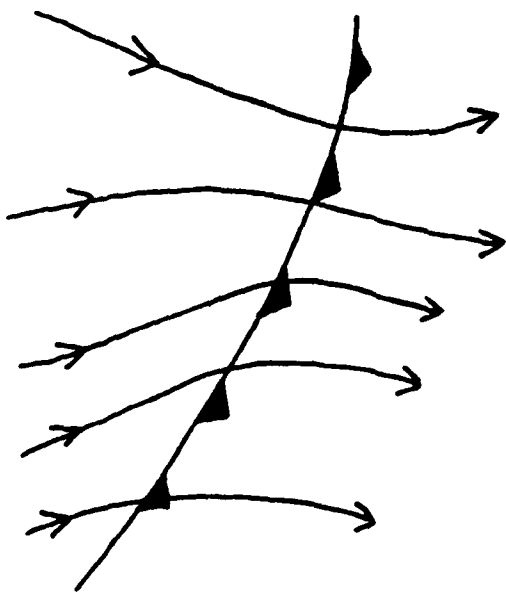


Figure 25b. Isentropic streamlines in the vicinity of a weakening cold front (Anderson, 1984).

#### 4. SPECIALIZED APPLICATIONS OF ISENTROPIC ANALYSES TO DIAGNOSTIC/FORECAST PROBLEMS.

There have been numerous applications of isentropic analysis techniques to the study of extratropical systems and, more recently, to mesoscale systems. In this section we will briefly describe some of these applications, referring the reader to the original papers for a more in-depth treatment of each approach.

##### A. Isentropic Trajectories

There are two basic approaches to computing trajectories on an isentropic surface (Dutton, 1976):

1. If the equations of motion are solved on a grid with fine resolution, then trajectories can be computed for any parcel by geometrical methods. This is known as the explicit method.
2. If a sufficient number of conservation properties of an air parcel can be identified, then we can observe their values in a parcel at one time and then find the parcel's new location at a later time by finding where the same combination of values of these variables occurs.  
This is known as the implicit approach.

##### 1. Implicit Approach

Danielsen (1961) outlined the implicit approach of computing isentropic trajectories which is based on a total energy equation.

We begin with the two dimensional inviscid equations of motion in isentropic coordinates:

$$\frac{d\vec{V}}{dt} = -\vec{\nabla}M - f\hat{k}\times\vec{V} \quad (26)$$

Dotting (26) with  $\vec{V}$  yields:

$$\frac{d}{dt} \left( \frac{V^2}{2} \right) = -\vec{V} \cdot \vec{\nabla}M \quad (27)$$

Next, we write the total derivative of M assuming adiabatic conditions

$$\frac{dM}{dt} = \frac{\partial M}{\partial t} + \vec{V} \cdot \vec{\nabla}M \quad (28)$$

Solving for the advection term in (28) and substituting into (27) results in:

$$\frac{d}{dt} \left( M + \frac{V^2}{2} \right) = \frac{\partial M}{\partial t} \quad (29)$$

This is an energy relationship which can be applied to a parcel trajectory by integrating (29) over time, resulting in:

$$M_f - M_i + \frac{1}{2}(V_f^2 - V_i^2) = \int_{t_1}^{t_2} \frac{\partial M}{\partial t} dt \quad (30)$$

The RHS term of (30) can be approximated at the initial (i), midpoint (m) and final (f) points of the trajectory and weighting the midpoint, i.e.,

$$\int_{t_1}^{t_2} \frac{\partial M}{\partial t} dt = \frac{\Delta M_i + 2\Delta M_m + \Delta M_f}{4} \quad (31)$$

resulting in a finite difference form of the integrated energy relationship:

$$M_f - M_i + \frac{1}{2}(V_f^2 - V_i^2) = \frac{\Delta M_i + 2\Delta M_m + \Delta M_f}{4} \quad (32)$$

This relationship *and* a distance formula written as:

$$D = \frac{V_i + V_f}{2} \Delta t \quad (33)$$

can be used to construct a trajectory. Essentially, the energy relationship (32) and the distance formula (33) must be solved simultaneously by choosing a point on an initial isentropic surface at a certain time, and then exploring the downstream area on the same isentropic level X hours later (usually 12) which balances both equations. This can be done graphically but is quite laborious, even though Daniels' early work was done this way (Daniels, 1966). Later on this process was adapted to a computer as described by Daniels and Bleck (1967) and Haagenson and Shapiro (1979).

Figure 26a displays the initial time period on the 328 K isentropic surface used in a study by Daniels and Reiter (1960) for trajectory calculations. The isentropic trajectory is plotted in Figure 26b to display the same surface 12 hours later over the central U. S. Notice how a trajectory, initially located on the anti-cyclonic side of the jet streak, turns towards higher values of M and descends from approximately 370 mb to 460 mb while slowing down enroute. Its path

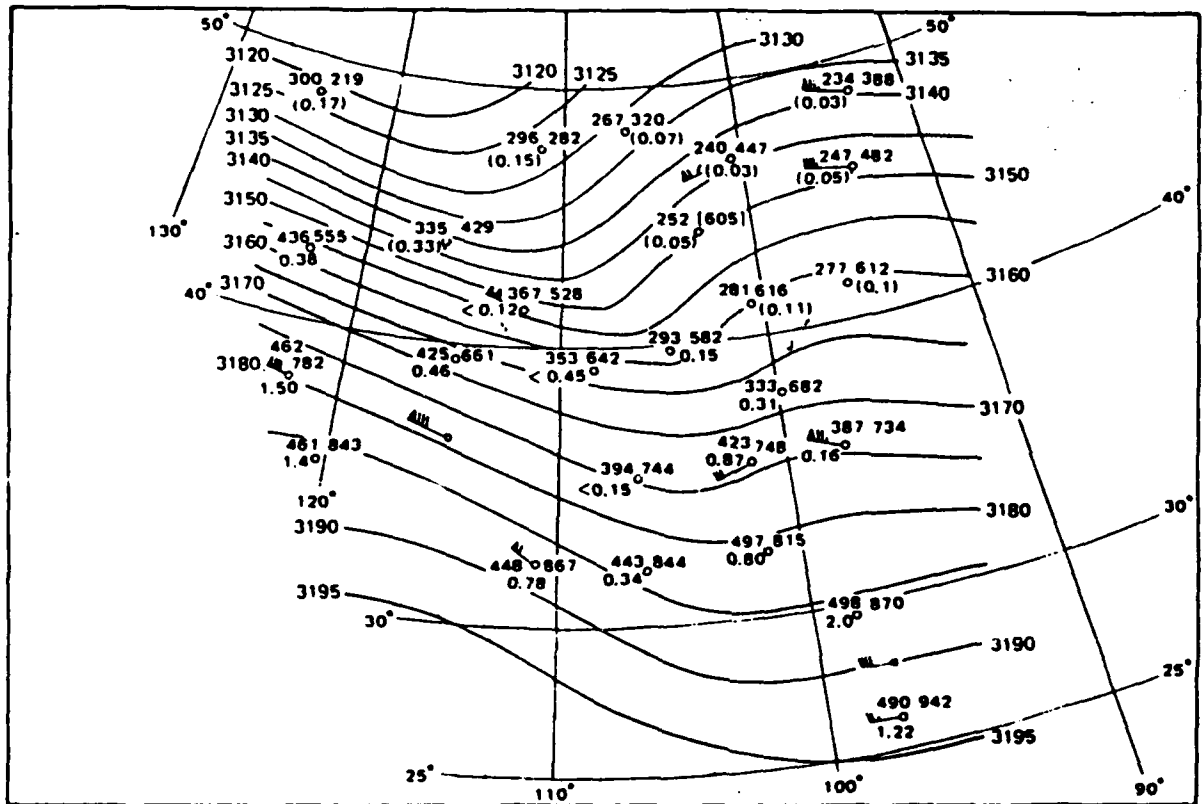


Figure 26a. Isentropic surface,  $\theta=45^\circ \text{ C}$ , 0300 GMT 8 January 1953. Numerical values to the left of each station indicate pressure (mb) and specific humidity (gm/kg); to the right are the last three digits of the Montgomery streamfunction (M). Isolines of M are labeled in units of  $10^6 \text{ m}^2 \text{ s}^{-2}$  (Danielsen and Reiter, 1960).

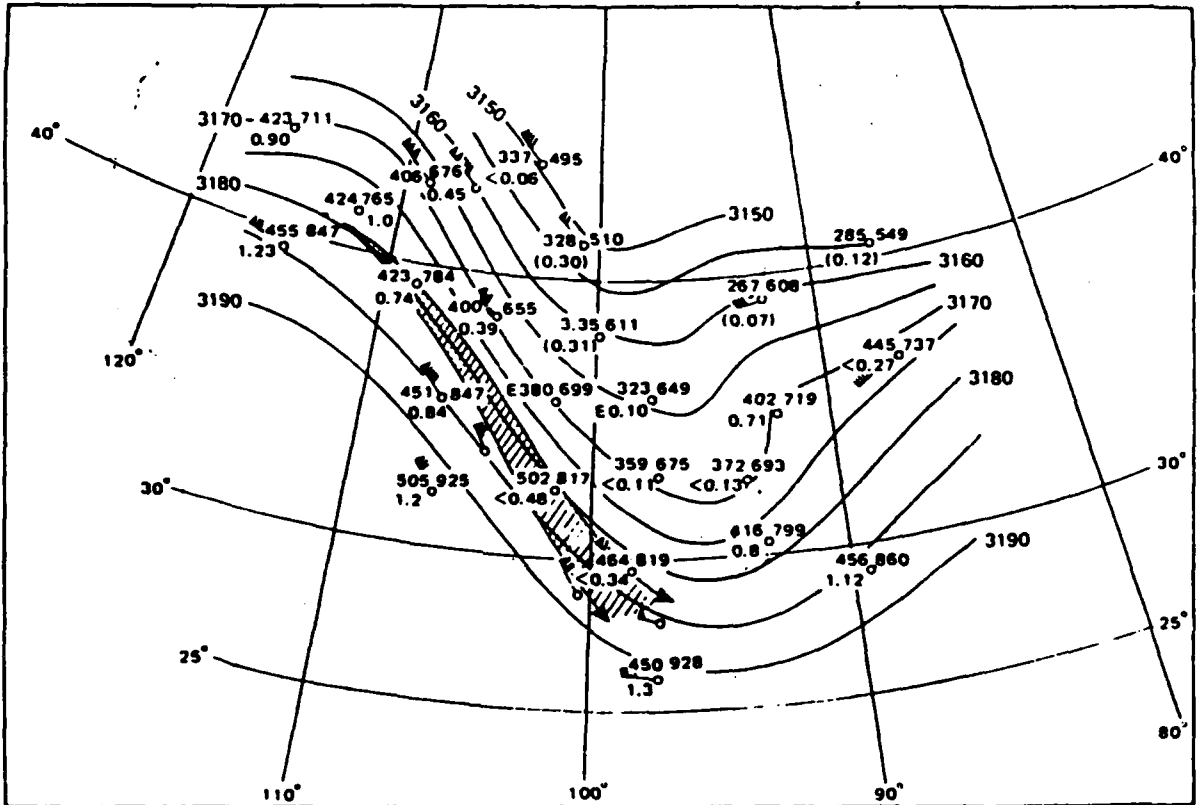


Figure 26b. Isentropic surface,  $\theta=45^{\circ}\text{C}$ , 1500 GMT 8 January 1953. Trajectories are shown for the time period 0300-1500 GMT on that day. The spread between the two trajectories allows for inaccuracies in wind reports (Danielsen and Reiter, 1960).

agrees well with the "digging" trough into the central U. S.

## 2. Explicit Approach

Petersen and Uccellini (1979) note that there are some problems with the implicit approach. The simultaneous solution of (32) and (33) for *anticyclonic* trajectories does not always converge to a unique solution. Secondly, the estimation of the local derivative term (RHS term of (32)) is only fair, at best, for the 12-hour time interval imposed by operational data availability. The basic technique applied to (32) and (33) makes it difficult to account for varying accelerations that take place along the trajectory. The explicit technique of constructing isentropic trajectories provides a better alternative that is easier to code up for a computer.

To begin with, one needs to have gridded values of  $u$  and  $v$  wind components for the initial time period and  $M$  values for both the initial and final time periods. Next, we compute the accelerations in  $x$  and  $y$  space from the inviscid equations of motion in isentropic coordinates; i.e.,

$$\frac{\Delta u}{\Delta t} = -\frac{\Delta M}{\Delta x} + fv \quad (34)$$

$$\frac{\Delta v}{\Delta t} = -\frac{\Delta M}{\Delta y} - fu \quad (35)$$

using standard finite difference techniques to compute the  $M$  derivatives. Then we compute the new  $u$  and  $v$  velocities for the parcels with

$$u^1 = u^0 + \frac{\Delta u}{\Delta t} \Delta t \quad (36)$$

$$v^1 = v^0 + \frac{\Delta v}{\Delta t} \Delta t \quad (37)$$

which are "starter" formulas used for the first time increment,  $\Delta t$ . Superscripts refer to the time step. For other than the first time step we use,

$$u^{t+1} = u^t + \Delta t \left[ \frac{3}{2} \frac{\Delta u^t}{\Delta t} - \frac{1}{2} \frac{\Delta u^{t-1}}{\Delta t} \right] \quad (38)$$

$$v^{t+1} = v^t + \Delta t \left[ \frac{3}{2} \frac{\Delta v^t}{\Delta t} - \frac{1}{2} \frac{\Delta v^{t-1}}{\Delta t} \right] \quad (39)$$

Finally, we compute the new position of the parcel with

$$x^{t+1} = x^t + \frac{1}{2}\Delta t(u^{t+1} + u^t) \quad (40)$$

$$y^{t+1} = y^t + \frac{1}{2}\Delta t(v^{t+1} + v^t) \quad (41)$$

A time step of 15-30 minutes is typically used. An M field is needed for each time step. This is done by linearly interpolating in time between the two M fields. Also, for each iteration in time one needs M derivatives in x and y space interpolated to the parcel location. One typically computes these derivatives at grid points and interpolates them to the parcel location. It is important that the interpolation scheme be accurate. Petersen and Uccellini (1979) used an overlapping polynomial technique which they describe in their paper.

The application of this explicit technique is very straightforward and yields trajectories which are nearly energy-conservative. If one has gridded fields of u, v, P, q and M for *both* time periods, it is possible to compute change fields following the parcel as well as keep track of the parcel's relative humidity. This enables you to quantitatively determine how long to "trust" the parcel trajectory, perhaps even terminating it upon saturation.

Figures 27 a-b show the isentropic charts and trajectories derived from the explicit approach from a study by Petersen and Uccellini (1979). Note how well these trajectories follow the flow.

### 3. Trajectory-Derived Variables

Once a trajectory has been calculated, it can be informative to produce change fields based on the trajectory's initial and final points. Changes in enthalpy, internal energy, potential energy, kinetic energy, pressure, and potential vorticity can be computed by using these variables' values at the end points of the parcel and plotting the "delta" value at the parcel's spatial midpoint. If enough calculations are done in this way, one can then analyze this Lagrangian-derived, irregular set of data. Much information concerning the thermodynamics and dynamics of the atmosphere can be learned in this way.

Consider the following information from an isentropic trajectory:

$$\theta = 305 \text{ K } 12 \text{ hour changes}$$

$$M_{\text{initial}} = 30500 \times 10^5 \text{ ergs/gm} \quad M_{\text{final}} = 30560 \times 10^5 \text{ ergs/mg}$$

$$P_{\text{initial}} = 250 \text{ mb}$$

$$P_{\text{final}} = 500 \text{ mb}$$

$$V_{\text{initial}} = 50 \text{ m s}^{-1}$$

$$V_{\text{final}} = 30 \text{ m s}^{-1}$$

From this information we can calculate the following "delta" values:

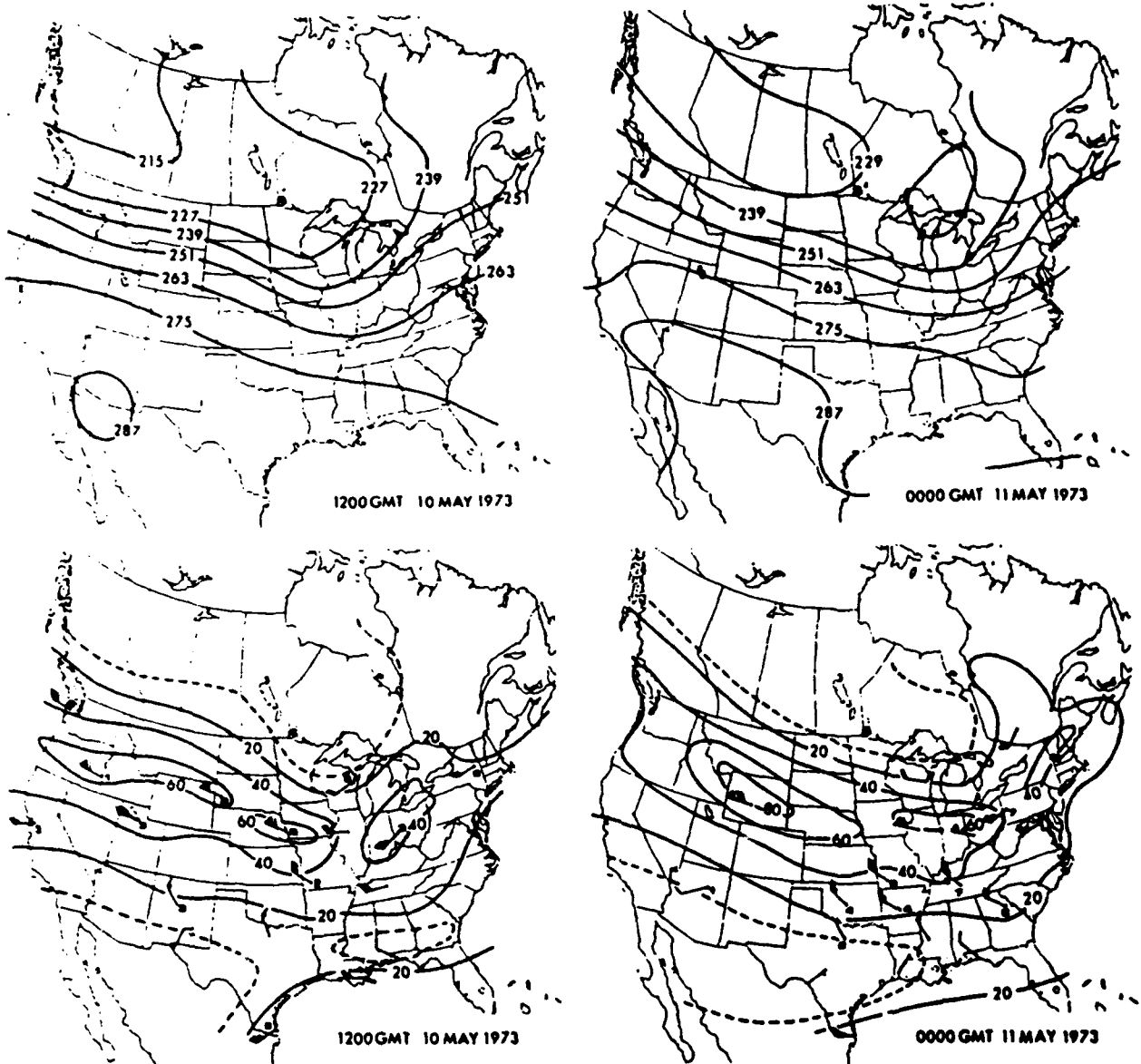


Figure 27a. 330 K isentropic surface for 1200 GMT 10 May and 0000 GMT 11 May 1973. At the top, the  $\psi$  analysis ( $275 = 3.275 \times 10^5 \text{ m}^2 \text{ s}^{-2}$ ). At the bottom, the isotach analysis ( $\text{m s}^{-1}$ ). Wind barbs represent selected station wind reports rounded to the nearest  $5 \text{ m s}^{-1}$ ; solid barb =  $50 \text{ m s}^{-1}$ , long barb =  $10 \text{ m s}^{-1}$ , short barb =  $5 \text{ m s}^{-1}$ . The number at the station is the actual last digit of the wind report (Petersen and Uccellini, 1979).

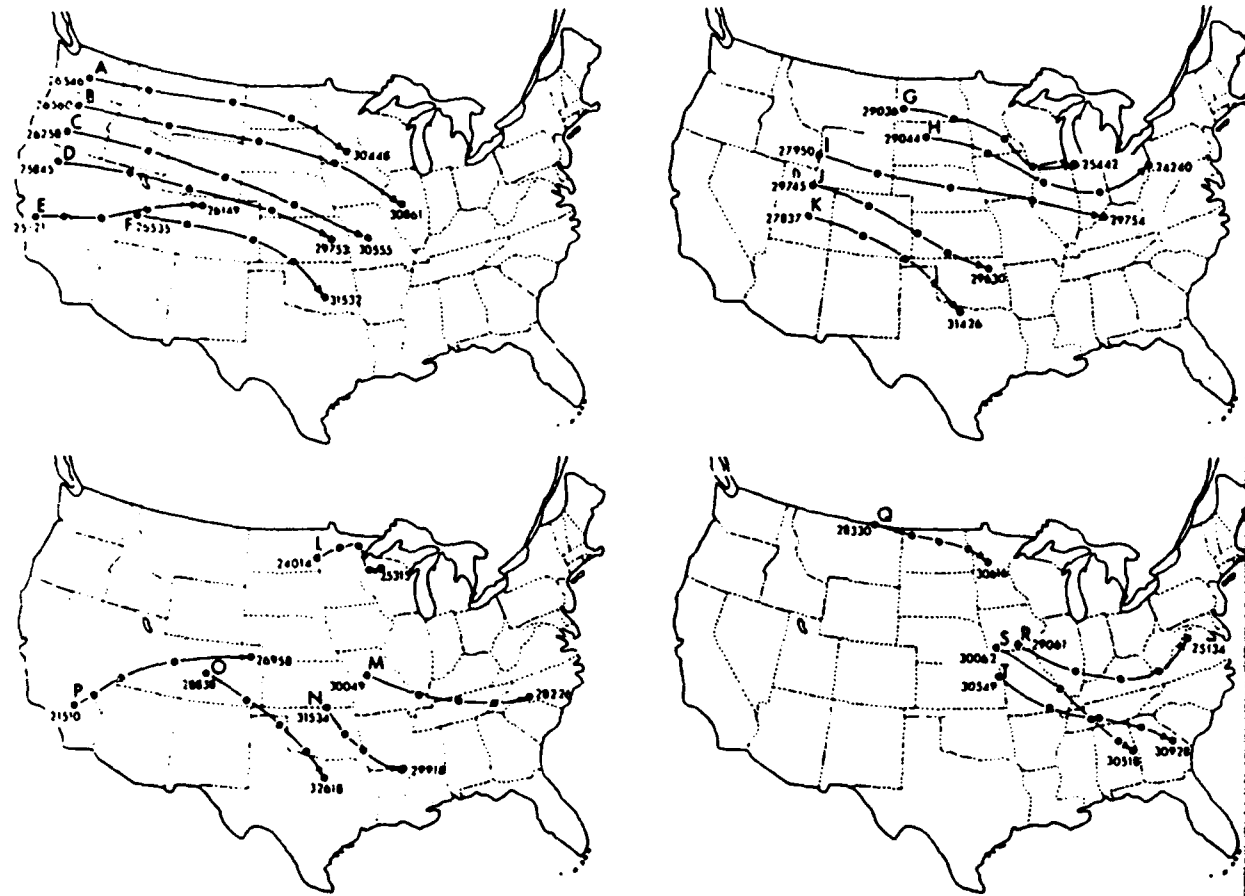


Figure 27b. Trajectories computed for 1200 GMT 10 May through 0000 GMT 11 May 1973 on the 330 K isentropic surface using discrete model technique. Positions at 3 hour intervals are indicated by the solid black dot. The initial and final wind direction and speed are indicated ( $31426 = 314^\circ, 26 \text{ m s}^{-1}$ ) (Petersen and Uccellini, 1979).

$$\Delta \text{Enthalpy} = + 45 \times 10^7 \text{ ergs/gm} \text{ since } \Delta T = + 45 \text{ K}$$

$$\Delta \text{Internal Energy} = + 32.25 \times 10^7 \text{ ergs/gm}$$

$$\Delta \text{Potential Energy} = - 45.38 \times 10^7 \text{ ergs/gm}$$

$$\text{since } \Delta M = +0.6 \times 10^7 \text{ ergs/gm}$$

$$\Delta \text{Kinetic Energy} = -0.8 \times 10^7 \text{ ergs/gm}$$

$$\omega = \Delta P / \Delta t = + 5.79 \mu \text{ bars/s}$$

At a glance we can see that this parcel warmed 45K as it descended 250 mb adiabatically, thereby increasing its enthalpy and internal energy while decreasing its potential and kinetic energies as it "crossed over" to higher M values. Note that the kinetic energy change is about an order of magnitude less than the other changes. The descent rate of  $+ 5.79 \mu \text{ bars/s}$  is substantial for the synoptic scale.

Rubino (1986) has computed various change fields for isentropic trajectories during the Atmospheric Variability Experiment-Severe Environmental Storms and Mesoscale Experiment (AVE-SESAME) I period, 1200 GMT 10-11 April 1979. Figures 28 a-c display several trajectory change fields during AVE-SESAME I for the 312 K surface (see Figure 31a for radar summary).

### B. Potential Vorticity and Tropopause Folding

It is difficult to do justice to this topic in this paper. The goal of this section is to simply acquaint the reader with some of the past and present work with respect to the topic of stratospheric extrusions or tropopause "folds". For an excellent review of this topic the reader is urged to read Keyser and Shapiro (1986).

As routine upper air soundings became available and the vertical temperature structure of the atmosphere began to be diagnosed, the concept of a tropopause "lid" capping the troposphere became entrenched in meteorological terminology. This natural inversion above the "weather sphere" appeared to preclude any vertical transport of mass between the troposphere and stratosphere. Secondly, as Reiter (1972) notes, "isobaric thinking" led to the acceptance of a jet axis as representing a discontinuity of absolute and potential vorticity. This made it difficult to envision how air masses could cross the jet axis under conservation of either of those two quantities. Therefore, the jet axis was thought to be a barrier to lateral exchange processes.

However, from the mid 1950's to this day much research documentation has shown a substantial mass exchange between the stratosphere and troposphere along tropopause "folds" or "breaks" (see Reed, 1955; Staley, 1960; Danielsen, 1968; Reiter, 1972, 1975; Shapiro, 1980; Uccellini, *et al.*, 1985). Several of these authors used stratospheric tracers of ozone, radioactivity, and potential vorticity to document airflow into the troposphere. Air descending from the stratosphere

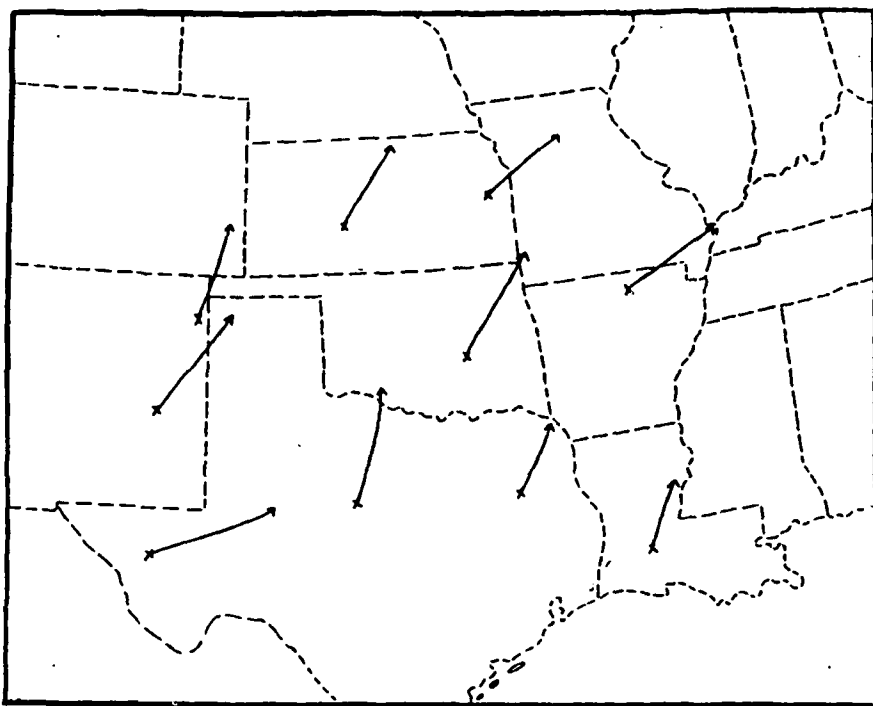


Figure 28a. 312 K 3-hour isentropic trajectories beginning 1700 GMT 10 April 1979 (Rubino, 1986).

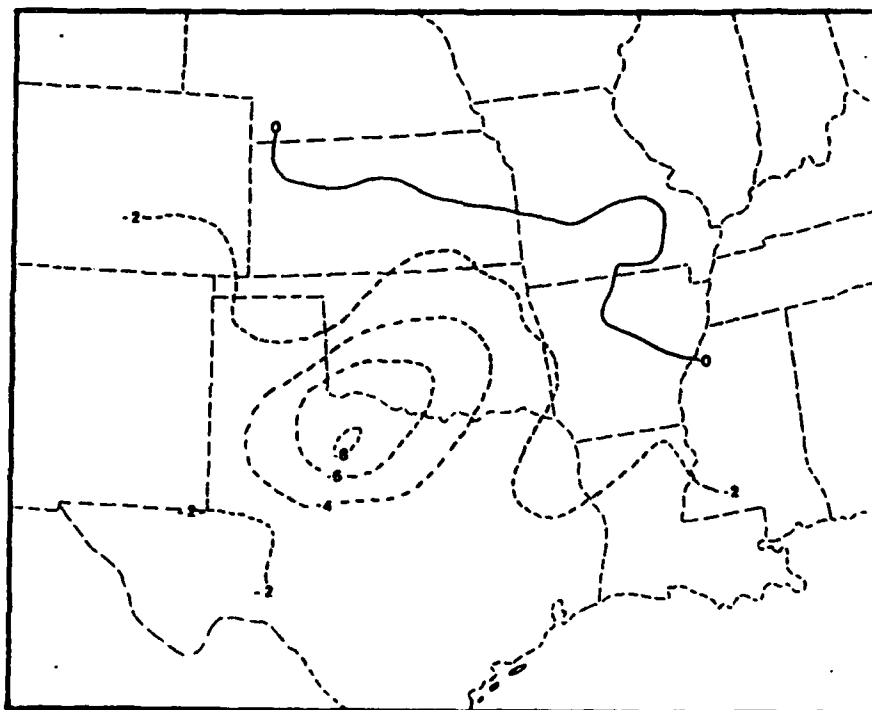


Figure 28b. 312 K 3-hour delta M field for 1700-2000 GMT 10 April 1979 (Rubino, 1986). Units are  $J/kg \times 10^3$ .

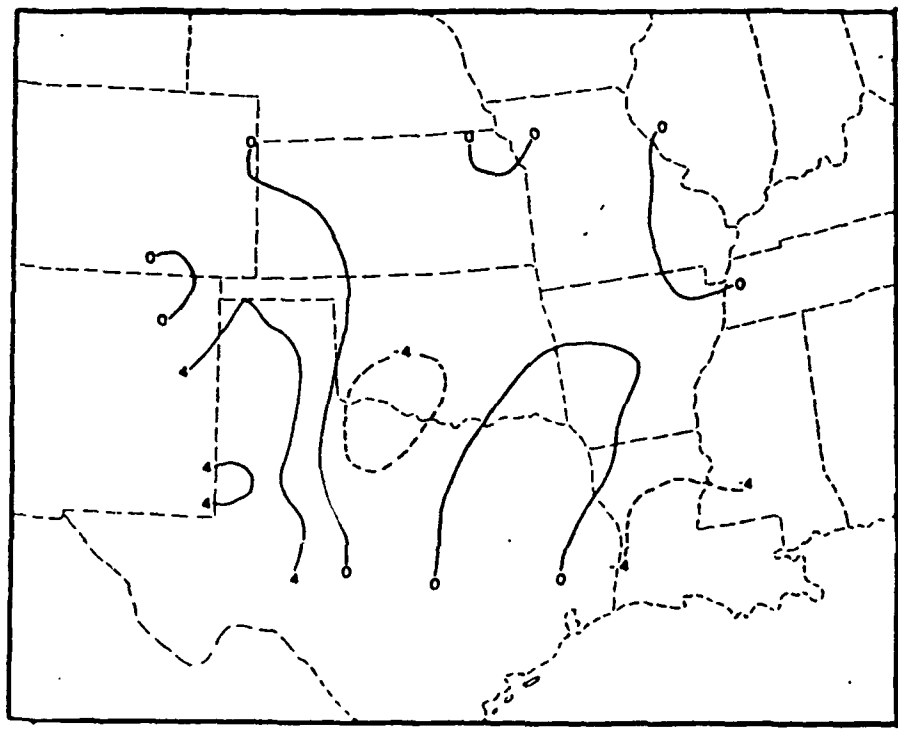


Figure 28c. 312 K 3-hour vertical motion field for 1700-2000 GMT 10 April 1979 (Rubino, 1986). Units are microbars/s.

is also characteristically "bone dry" (i.e., RH < 10%).

Figures 29 a-f display a synoptic situation during which a tropopause fold formed. The top three panels (Figure 29 a,c,e) show the rapid deepening of a mid-tropospheric wave over the central U. S. from 0300 GMT 13 December to 0300 GMT 15 December 1953. Note the intensification of the thermal gradient attendant with the developing jet streak at 500 mb. By the end of the period a hyperbaroclinic zone is established along the east coast, with wind speeds exceeding 150 knots. Cross sections taken perpendicular to the jet (Figure 29 b,d,f) diagnose the development of the tropopause fold. The strong static stability and negative wind shear help to define the stratospheric air. The tropopause is lowest where the air is coldest in the mid-troposphere. Stratospheric air sinks over the first 24-hour period and then finally extrudes into the troposphere by the last time period (Figure 29f). The stable baroclinic zone associated with the strong frontal zone is defined by both highly compacted isentropic surfaces and strong vertical wind shear. The vertical shear of the geostrophic wind is nearly zero in those areas outside the frontal zone where the isentropic surfaces are quasi-horizontal.

Uccellini, *et al.*, (1985) have documented a tropopause fold that took place during the President's Day Cyclone of 18-19 February 1979. From a forecaster's viewpoint, what is most interesting about their study is how they correlate a fold in the tropopause to subsequent explosive cyclogenesis for this east coast storm. A key diagram from their study is shown in Figure 30 a-d. In the last diagram one can identify a stratospheric extrusion from the stable baroclinic zone descending from Peoria, IL (PIA) to Appalachicola, FL (AQQ) and the high potential vorticity values along the frontal zone. Uccellini, *et al.*, (1985) show that stratospheric air descended along this zone at least 12 hours preceding cyclogenesis. It moved down to ~ 800 mb toward the east coast to an area upstream of where rapid cyclogenesis occurred. There, it experienced adiabatic mass convergence and in an effort to quasi-conserve potential vorticity vertically stretched and increased its absolute vorticity. Their work is further substantiated by ozone measurements from the Total Ozone Mapping Spectrometer (TOMS) flown aboard the Nimbus 7 satellite. TOMS measures the vertical ozone distribution in the stratosphere. A maximum in ozone concentration is positively correlated with a relatively thick stratosphere and a thin troposphere. They have shown significant positive increases in TOMS ozone measurements in the vicinity of these tropopause folds. Shapiro, *et al.*, (1982) have used the TOMS in a similar application to show how ozone maps from TOMS can locate jet streaks at tropopause levels and gauge their intensity from the intensity of the gradient of the ozone distribution. This could be a useful technique for locating jet streak activity over data sparse regions and approximating their magnitudes.

Utilizing isentropic cross sections with mixing ratio, normal wind components and potential vorticity in the operational setting may provide clues to timing the intensity and onset of significant winter storms. The author's experience is that tropopause folds are more typical with the stronger systems (central pressure < 990 mb) during the cold season. The practical application of this technique is yet to be proven--but the potential exists and the data can be computed in real-time.

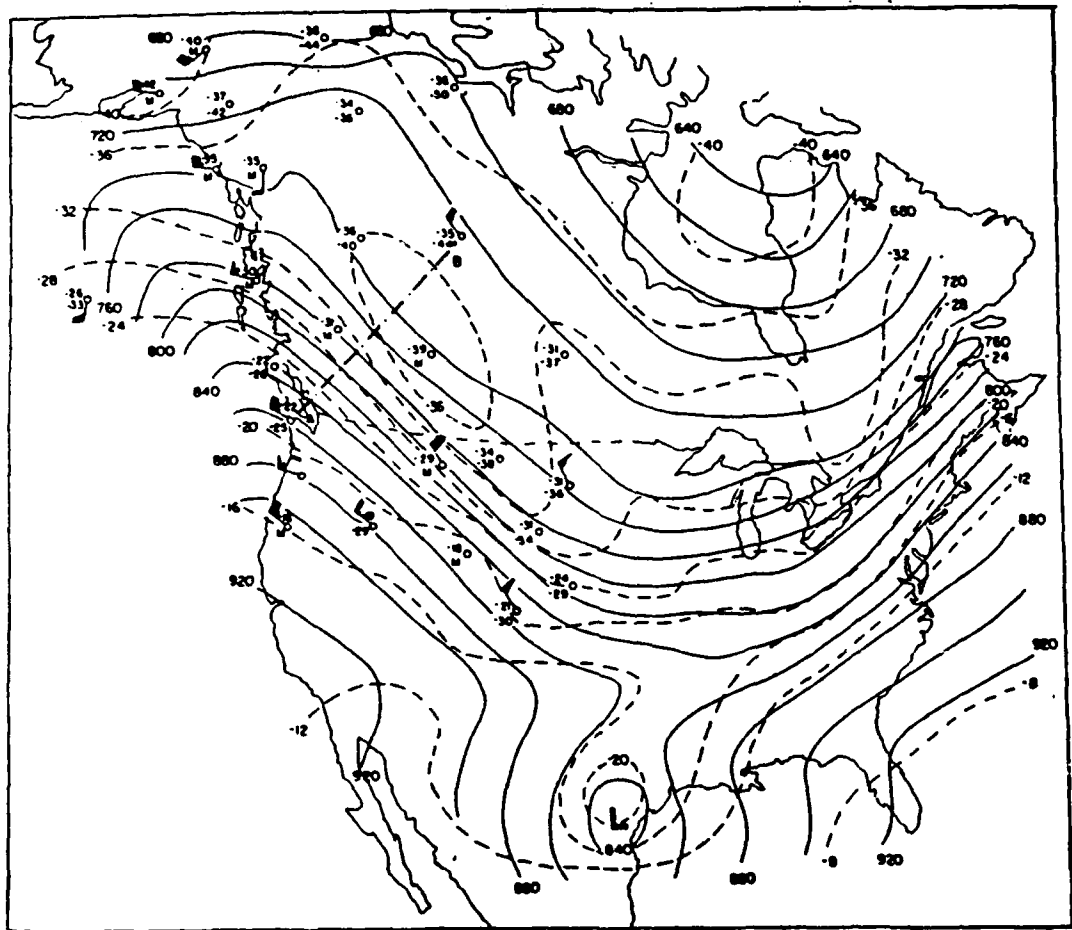


Figure 29a. 500 mb surface for 0300 GMT 13 December 1953. The chart shows contours (thin solid lines) and isotherms (thin dashed lines). Observed temperatures and dew points ( $^{\circ}\text{C}$ ) and winds are added in critical areas (Reed, 1955).

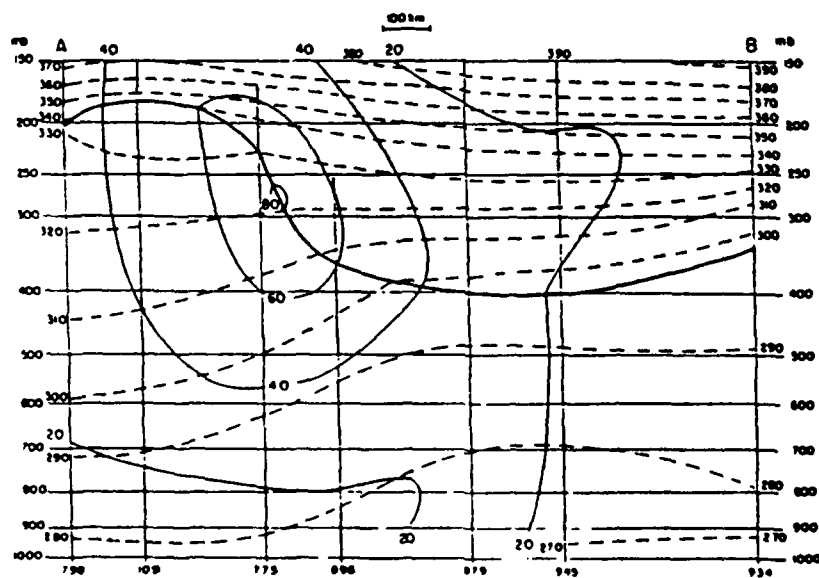


Figure 29b. Cross section along line A-B in Figure 29a. Thin solid lines give geostrophic wind speed ( $\text{m s}^{-1}$ ) normal to the section; dashed lines are isentropes. The thick solid line represents the tropopause (Reed, 1955).

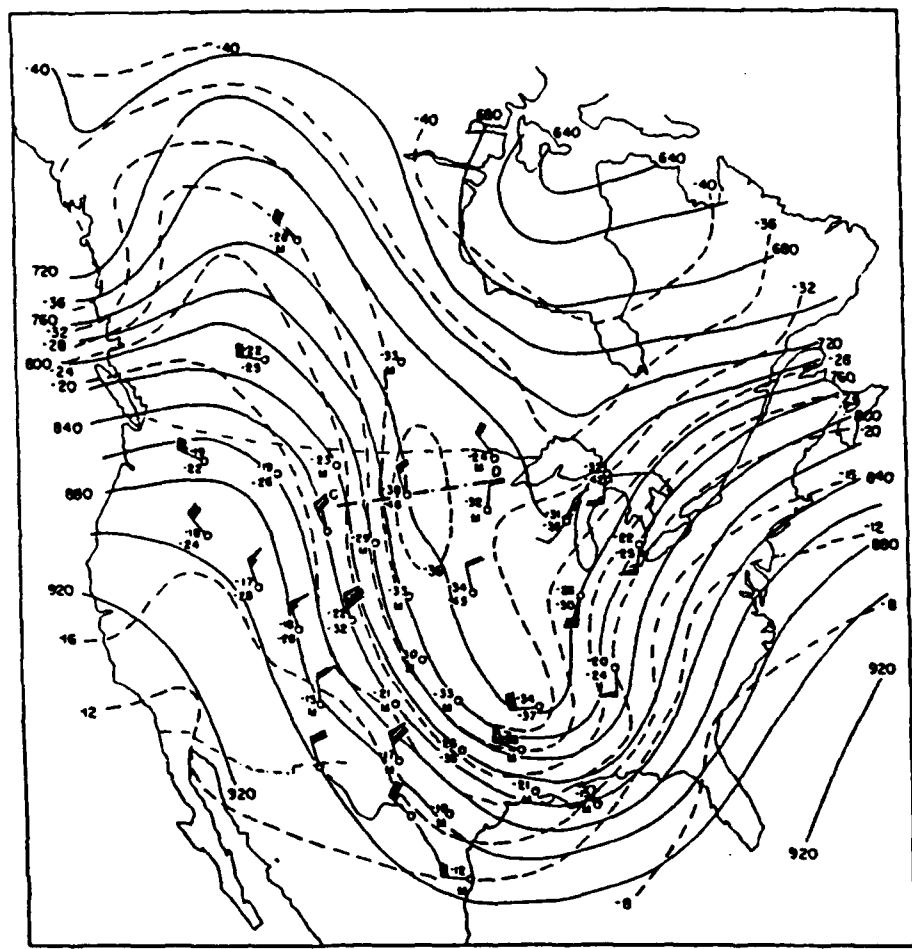


Figure 29c. 500 mb surface for 0300 GMT 14 December 1953. Notation same as in Figure 29a (Reed, 1955).

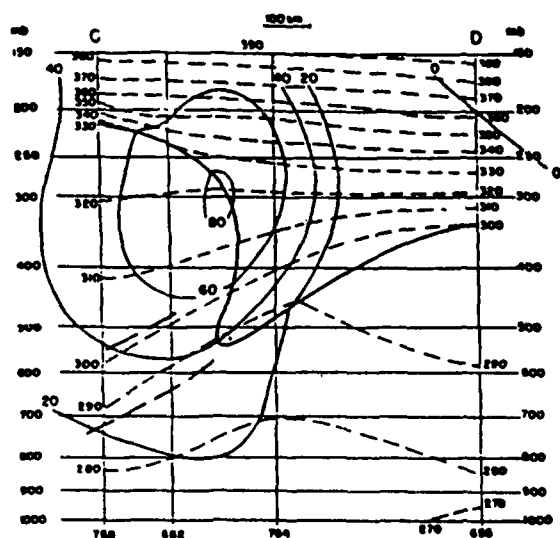


Figure 29d. Cross section along line C-D in Figure 29c. Heavy dashed lines represent boundaries of stable air; otherwise notation same as in Figure 29b (Reed, 1955).

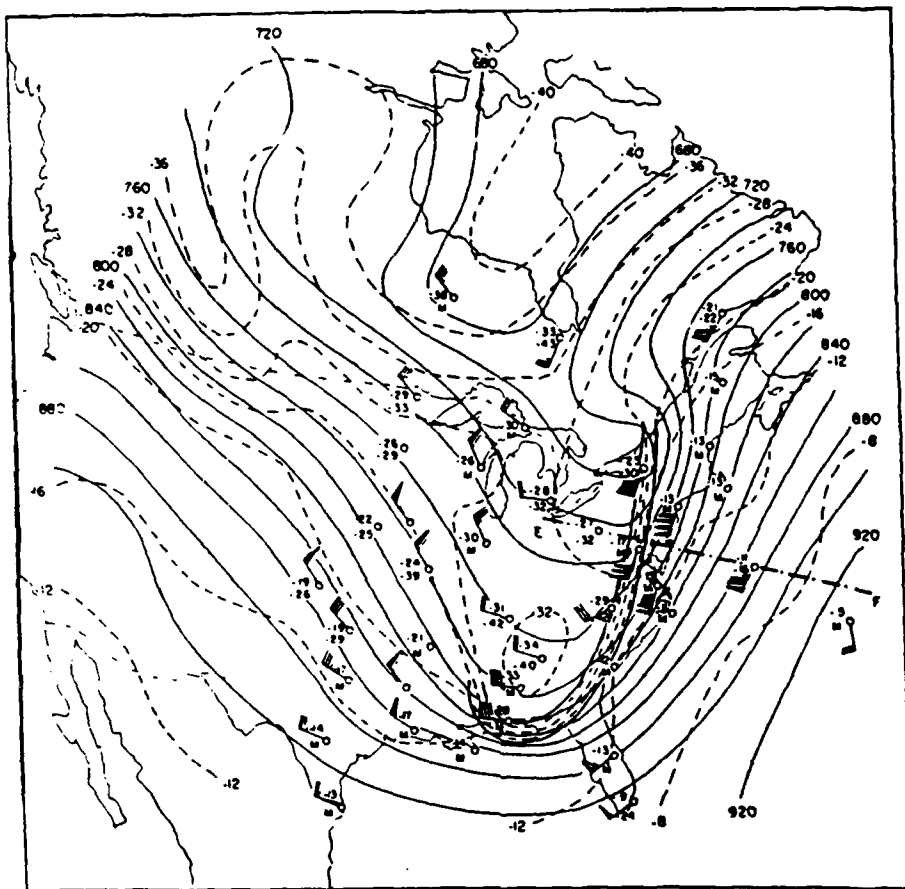


Figure 29e. 500 mb surface for 0300 GMT 15 December 1953. Heavy solid lines represent boundaries of frontal zone (Reed, 1955).

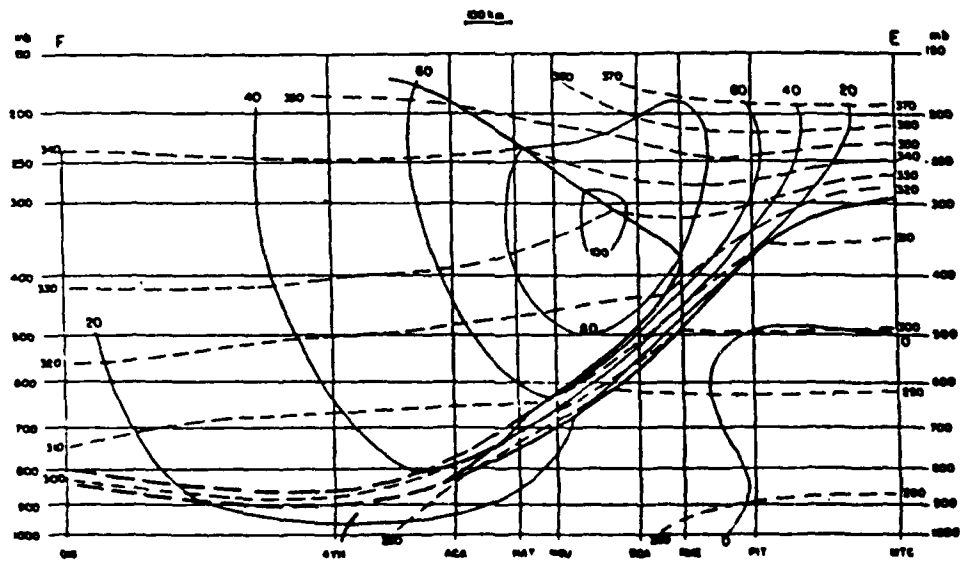


Figure 29f. Cross section along line E-F in Figure 29e. Notation same as in Figure 29b and 29d (Reed, 1955).

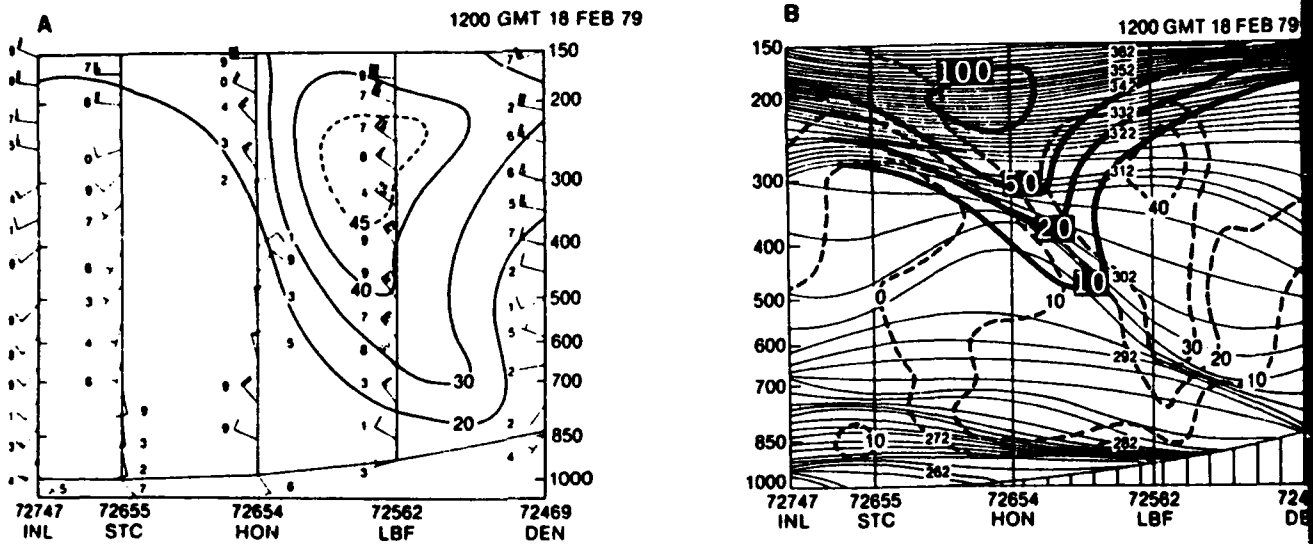


Figure 30a-b. Vertical cross section from International Falls, MN (INL) to Denver, CO (DEN) for 1200 GMT 18 February 1979. The left panel (A) is an isotach analysis for total wind speed ( $\text{m s}^{-1}$ ); wind barbs plotted with last digit of wind observation. The right panel (B) shows isentropes (solid, K); geostrophic wind (dashed,  $\text{m s}^{-1}$ ) computed from the horizontal thermal gradient in the plane of the cross section; potential vorticity,  $-(\zeta + f)/(\partial \theta / \partial P)$ , heavy solid, where  $10 = 10 \times 10^{-6} \text{ K mb}^{-1} \text{ s}^{-1}$ . Potential vorticity analysis is only shown for upper portion of frontal zone and stratosphere (Uccellini, *et al.*, 1985).

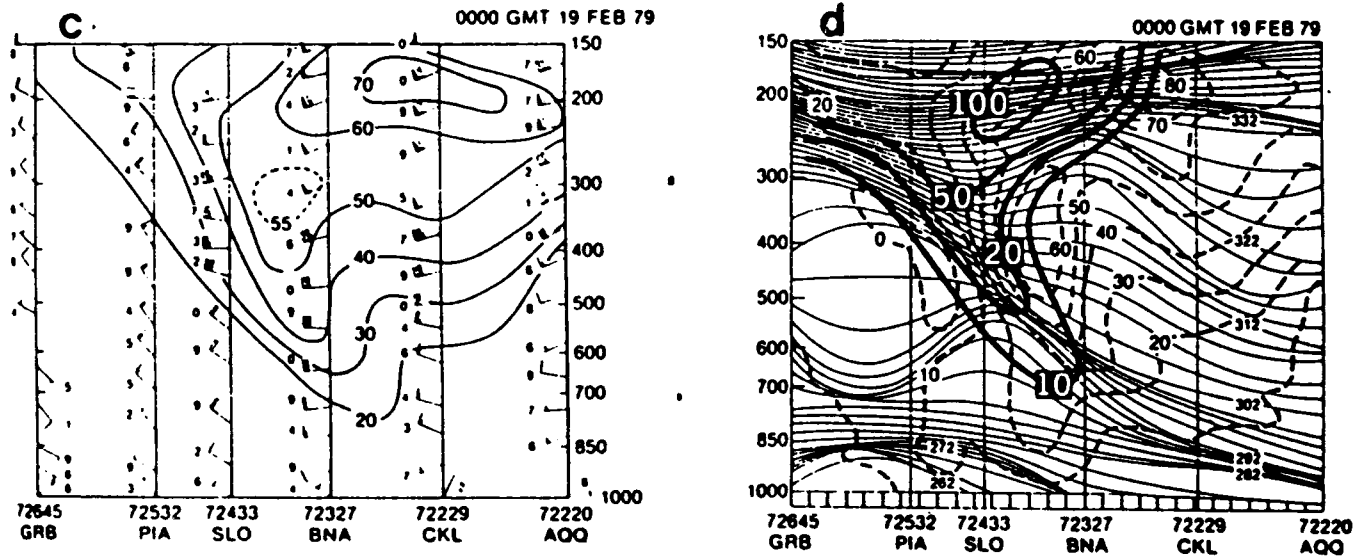


Figure 30c-d. Vertical cross sections from Green Bay, WI (GRB) to Apalachicola, FL (AQQ) for 0000 GMT 19 February 1979. Depictions same as in Figure 30a-b (Uccellini, *et al.*, 1985).

### C. Short Term Forecasting of Severe Convection Using Isentropic Analysis

Although isentropic analysis is best suited to cold season cases of cyclogenesis/frontogenesis when horizontal thermal gradients are most distinct in mid-latitudes, several authors have suggested its use in the short term forecasting of severe convection. Namias (1938) was probably the first researcher to promote using isentropic charts as an aid in thunderstorm forecasting. He emphasized the use of cross sections of potential temperature and specific humidity and "horizontal" isentropic analyses as useful charts in diagnosing and anticipating moisture patterns. He noted that, "tongues of dry and moist air may be followed from day to day by means of these charts, for it is reasonable to suppose that the major atmospheric motions are approximately adiabatic." This is especially true in the pre-convective environment before the onset of strong solar and latent heating.

More recently Wilson, *et al.*, (1980) and Moore (1985) have described analysis procedures on isentropic charts which can help forecasters diagnose severe convective threat areas on meso alpha scales of motion. Wilson, *et al.*, (1980) constructed a four panel chart consisting of:

- (1) one panel with only station models as described in Figure 16,
- (2) one panel with isopleths of Montgomery streamfunction and pressure,
- (3) one panel with isopleths of Montgomery streamfunction and stability, and
- (4) one panel with isopleths of Montgomery streamfunction and specific humidity.

A mid-level isentropic surface is chosen to help depict upward/downward vertical motion, moist/dry tongues, moisture advection, and stability. An upper level isentropic surface is chosen to diagnose jet streaks, their strength, curvature, and proximity to the possible threat area. These two isentropic surfaces may be chosen by using climatological average values or by consulting a cross section with normal wind components and specific humidity superimposed. On the mid-level isentropic surface, a dry line can be defined as the inner moisture isopleth on the dry side of the gradient while the moist tongue is taken to be the zero moisture advection line according to the M and q analysis. On the upper level isentropic surface, jet streaks are defined according to the actual wind field and the orientation and gradient of the Montgomery streamfunction.

A depiction chart (similar to a composite chart) is prepared by placing the surface front, dry line, moist tongue, and the middle and upper-level jet streak positions on one chart. Although the authors do not mention it, one could easily add the axis (or axes) of greatest instability as well. Forecast positions of these features are placed on the chart, as well. The forecast position of the surface front is taken from forecast charts while moist tongues and dry lines are forecast using 100% of the wind speed at the lower isentropic level. Jet streak positions are subjectively forecast from prognostic charts, showing continuity and relationship to the surface front. The authors then place the maximum threat area as *west* of the mid-level dry line and *east* of the surface front, and near the mid-level

jet streak. Typically the strongest convection takes place to the right (looking downstream) of the mid-level jet streak. Greatest destabilization takes place between the mid-level moisture maximum and the dry line. Since this region usually has ample low level moisture it is an area of strong convective instability.

As a follow-up to the previous study, Moore (1985) expanded on the concepts presented by the above authors. He developed five diagnostic charts based on isentropic surface data. They include charts depicting:

- (1) Montgomery streamfunction isopleths and isobars,
- (2) Adiabatic vertical motion isopleths and isohumes (specific humidity),
- (3) Horizontal moisture convergence field and low level static stability,
- (4) Low level stability flux field, and
- (5) A composite of key features--pressure ridges, upper level jet axis, and centers of upward vertical motion, minimum stability, moisture convergence, and stability flux convergence.

In his study Moore found that the threat area for AVE-SESAME I was characterized by:

- (1) thermal riding (pressure axis);
- (2) relatively low static stability;
- (3) proximity to a moist axis;
- (4) proximity to a moisture convergence maximum;
- (5) strong adiabatic upward vertical motion;
- (6) strong positive stability flux (destabilization) and,
- (7) being along the upper level jet axis, preferentially in the exit region.

The charts used in this study are shown in Figure 31a-g. Figure 31b shows the cross section used to choose the representative isentropic surfaces. Figures 31c-g are the charts described above. Note how the juxtaposition of the key thermo- and hydrodynamic features described above help depict the strong convection 3 hours later in the Texas panhandle. This was the center of the most severe activity. The west-east line of activity in Oklahoma formed north of the best "overlap" region of the parameters but was suggested by the west-east axes of adiabatic vertical motion, moisture convergence and low level stability flux.

It should be noted that these techniques are most useful during the spring and fall months when the thermo- and hydrodynamic features on isentropic surfaces are well-defined and of significant strength.

#### D. Additional Applications

There are other applications associated with isentropic analyses which have not been discussed up to this point. These applications are in the area of diagnosing and forecasting the freezing level and Clear Air Turbulence (CAT) for aviation and the overrunning convective instability for thunderstorm forecasting.

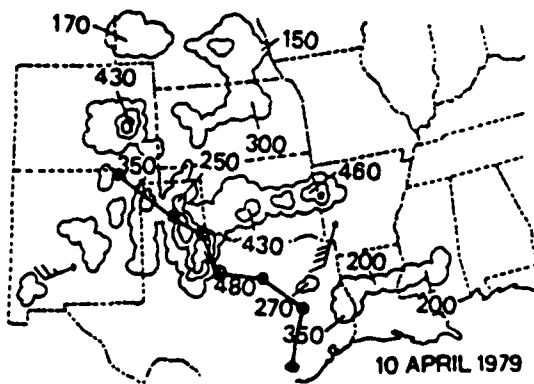


Figure 31a. National Weather Service radar summary for 2035 GMT 10 April 1979. The line shown is the cross section depicted in Figure 31b (Moore, 1985).

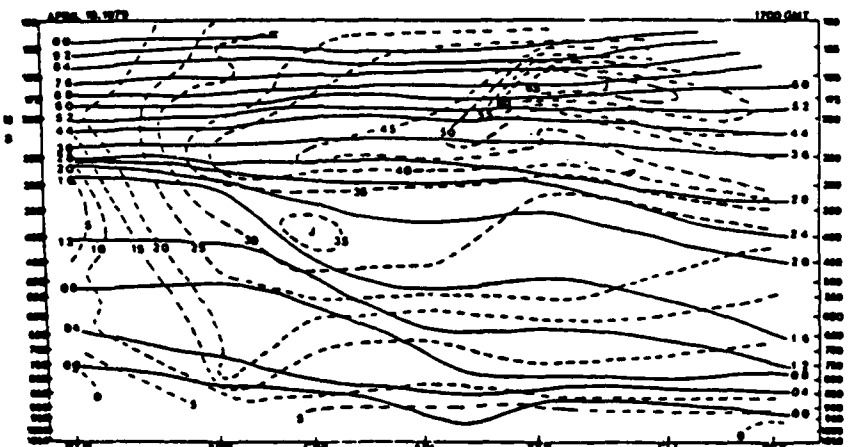


Figure 31b. Isentropic cross section for 1700 GMT 10 April 1979. The solid lines are isentropes in °K with the preceding 3 or 4 omitted. The dashed lines are isotachs of the normal wind component in  $\text{m s}^{-1}$  (Moore, 1985).

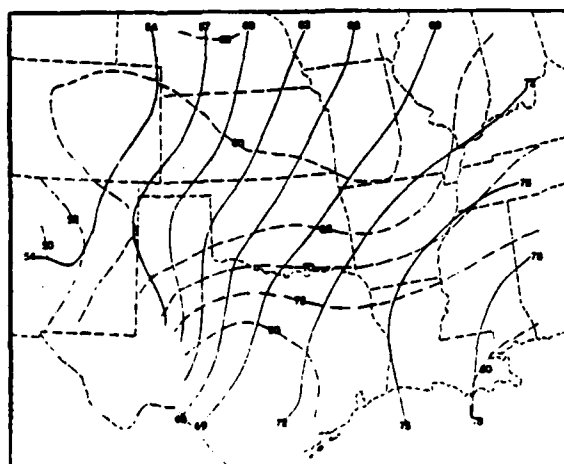


Figure 31c. The Montgomery streamfunction for 306 K surface at 1700 GMT 10 April 1979. The Montgomery streamfunction (solid) is in  $10^8 \text{ ergs/gm}$  with the preceding 30 missing. Isobars (dashed) are in tens of mb (Moore, 1985).

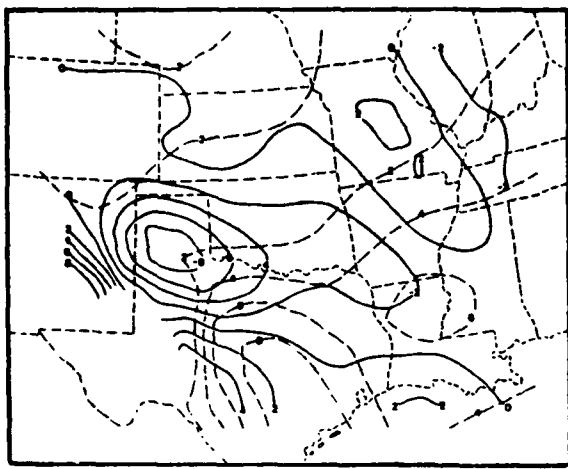


Figure 31d. Adiabatic vertical motion in microbars/s (solid) and specific humidity in gm/kg (dashed) for the 306 K surface at 1700 GMT 10 April 1979 (Moore, 1985).

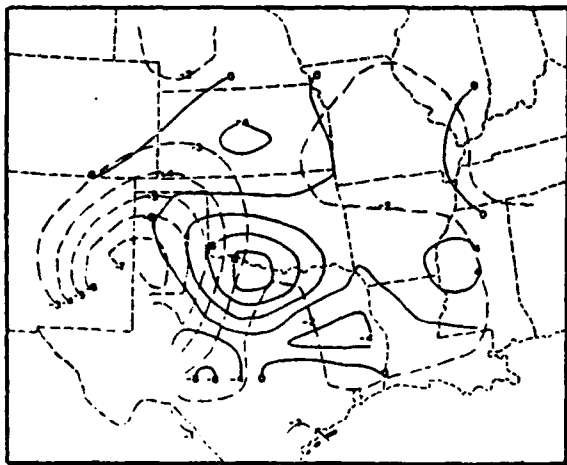


Figure 31e. Horizontal moisture convergence in gm/kg x 10 (solid) and low level stability for the 306 K surface at 1700 GMT 10 April 1979 (Moore, 1985).

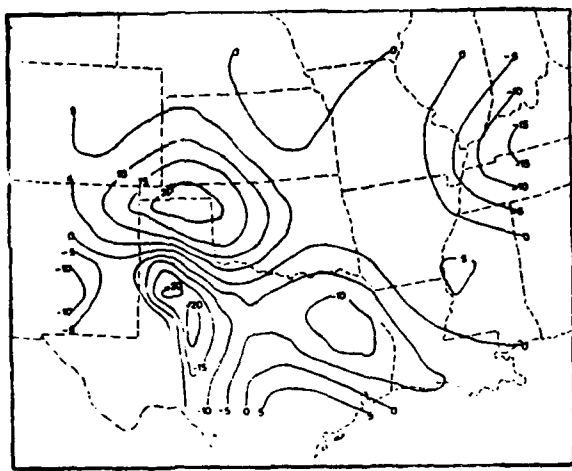


Figure 31f. Low level stability flux ( $\times 10^5$  mb K $^{-1}$  s $^{-1}$ ) for the 304-308 K layer at 1700 GMT 10 April 1979 (Moore, 1985).

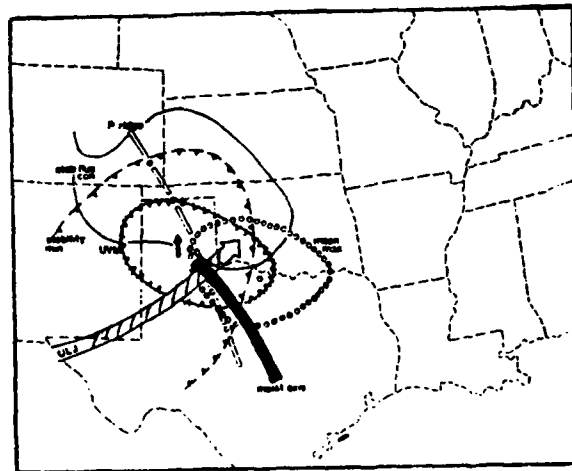


Figure 31g. Composite chart for 1700 GMT 10 April 1979 (Moore, 1985).

## 1. Freezing Level and Icing

Anderson (1984) describes a simple method for diagnosing the pressure level of the freezing level for the aviation community. From the Poisson equation (16) one can easily compute the pressure value of the  $0^{\circ}\text{C}$  isotherm on any isentropic surface. These pressure values are printed in Table 1 for  $\theta = 290\text{-}320\text{K}$ . On an isentropic chart the freezing pressure isobar could be colored blue for easy reference.

If aviation forecasters referenced this isobar to a chart showing the condensation ratio or to one showing condensation pressure and pressure, they could determine areas of possible icing conditions. Since moisture transport is more realistically depicted on an isentropic surface, these icing regions should display better continuity in space-time than on constant pressure surfaces. Even in areas of low condensation ratios, one may forecast increases in condensation ratios where significant isentropic lifting is taking place.

## 2. Clear Air Turbulence

Shapiro (1974, 1976, 1980) and Gidel and Shapiro (1979) have described and discussed CAT in relation to the level of maximum wind and the tropopause. Figure 32 shows where CAT is favored to occur with respect to a wind maximum and upper level frontal zone. The CAT region is not only found within the downward sloping frontal zone but also above the wind maximum in the upward sloping isentropic surfaces. In both regions horizontal and vertical wind shears can be quite strong. Shapiro (1974) measured, using rawinsonde data and data from a meteorologically instrumented aircraft, vertical and horizontal wind shears of  $15 \text{ m s}^{-1} \text{ km}^{-1}$  and  $25 \text{ m s}^{-1} (40 \text{ km})^{-1}$ , respectively, at about 450 mb. He states, "...though the turbulence is confined to short bursts over horizontal distances of tens of kilometers, it is encountered at several vertical levels, thus suggesting a large-scale (hundreds of kilometers) extent of the CAT patch when the turbulent-scale measurements are made along a surface contained within sloping shear layers rather than on constant pressure surfaces."

These ideas suggest that isentropic cross sections with normal wind components should be useful in diagnosing CAT. If numerical model data were available in an isentropic format, this technique could be used to forecast CAT conditions. Cross sectional analyses could be used to qualitatively evaluate the potential for CAT while actual horizontal and vertical shears with respect to  $\theta$  could be computed to assign threshold criteria.

An important consideration is that upper level frontal zones are not always easy to diagnose on constant pressure surfaces because their horizontal extent is quite limited, especially when compared to their vertical extent. Also, as Shapiro (1974) has documented, often there is a multiple structured frontal zone - jet stream system which can be resolved using cross section analysis. Figure 33 shows an example of such a complex between Albuquerque, NM (ABQ) and Oklahoma City, OK (OKC). Both frontal zones are associated with horizontal and vertical wind shear. They are easier to diagnose using the isentropic cross section than by

Table 1. Pressure values of 0°C isotherm for various isentropic surfaces  
 (Anderson, 1984)

<u>Potential Temperature (°K)</u>	<u>Pressure of Freezing Level (mb)</u>
290	809
291	800
292	790
293	781
294	772
295	762
296	752
297	745
298	736
299	727
300	719
301	711
302	702
303	694
304	686
305	678
306	671
307	663
308	656
309	648
310	641
311	634
312	627
313	620
314	613
315	606
316	599
317	593
318	586
319	580
320	576

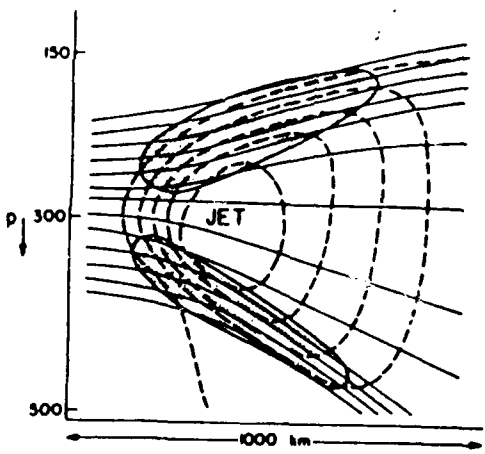
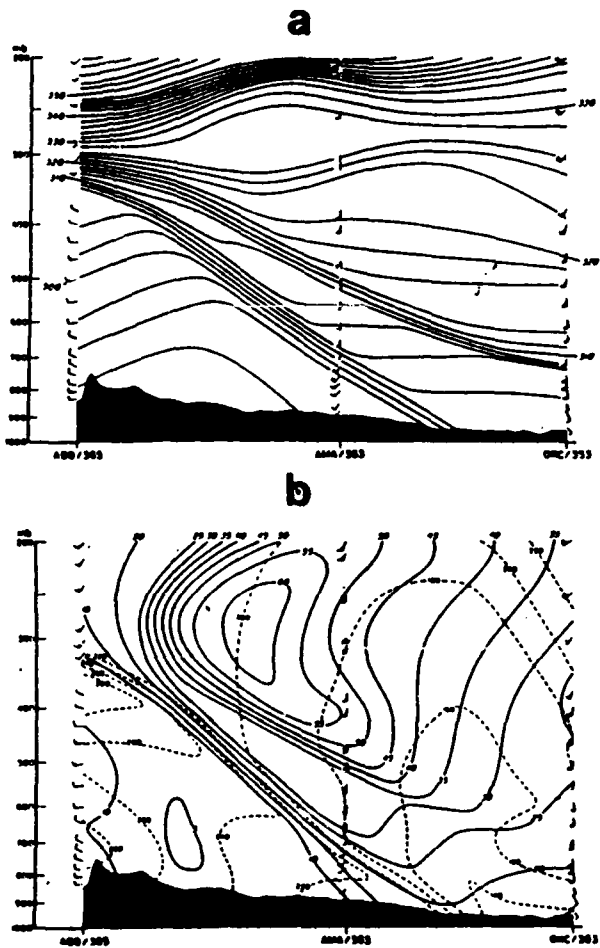


Figure 32. Schematic illustration of regions of clear-air turbulence (stippled) in the vicinity of an upper-level jet core and frontal zone. Solid and dashed lines respectively indicate potential temperature and wind speed (Shapiro, 1976).



**Figure 33.** Cross sections of potential temperature (a) and wind speed and direction (b) at 0000 GMT 20 April 1971. Isentropes ( $^{\circ}$ K), solid lines; isotachs (m/s), solid lines, isogons ( $^{\circ}$ ), dashed lines; positions of the Albuquerque, NM, Amarillo, TX, and Oklahoma City, OK rawinsonde ascents are marked along the abscissa, (Shapiro, 1974).

depending upon constant pressure analyses. This diagnosis exploits the fact that isentropic surfaces slope with the frontal zone rather than cut across it as do constant pressure surfaces. Thus, frontal characteristics, such as thermal gradients, moisture gradients, and wind shears are easier to diagnosis with a large scale data set (e.g., U.S. rawinsonde data) using an isentropic framework. On constant pressure surfaces these gradients are often poorly resolved since they can take place over mesoscale distances.

### 3. Overrunning Convection

When warm, moist unstable air (e.g., lifted indices  $< 0$ ) lies to the south of a warm frontal or similar boundary in the presence of significant low level winds (e.g.,  $> 10-15 \text{ m s}^{-1}$ ) elevated convection is likely to take place north of the boundary. Standard stability indices (e.g., lifted index, Showalter index) are unable to diagnose or even hint at this elevated instability region. An isentropic cross section with specific humidity can be useful in illustrating the presence of moisture aloft in a region of less stable air seen as a large separation of adjacent isentropes. Otherwise these elevated regions of low stability are difficult to diagnose with constant pressure analysis techniques.

A second method of diagnosing these cases of overrunning convection is through a cross section of equivalent potential temperature ( $\theta_e$ ). A typical case of overrunning convection can be diagnosed by noting regions where  $\theta_e$  isopleths "fold" over producing regions where  $\theta_e$  decreases with height. Typically warm, moist air overrides the frontal boundary at or around 800 mb and is associated with high  $\theta_e$  values. Above this layer, cooler and drier air above the frontal zone is associated with low  $\theta_e$  values. If decreases of  $\theta_e$  with height exceed 5-10 degrees K it is often significant. In the presence of isentropic uplift this instability will be released, forming imbedded convection. This kind of activity took place over Missouri and Illinois during a warm advection type snowstorm and enhanced snow totals to greater than 1 foot along a zone north of a frontal boundary. An equivalent potential temperature cross section with *parallel* wind components is shown in Figure 34 for this case. Note that low level convergence in the plane of the cross section is colocated with the stippled region above Salem, IL (SLO) to indicate convective instability. Areas south and west of SLO received heavy rain with convection while heavy snow and embedded convection took place to the north in the cold air.

THETA-E CROSS-SECTION

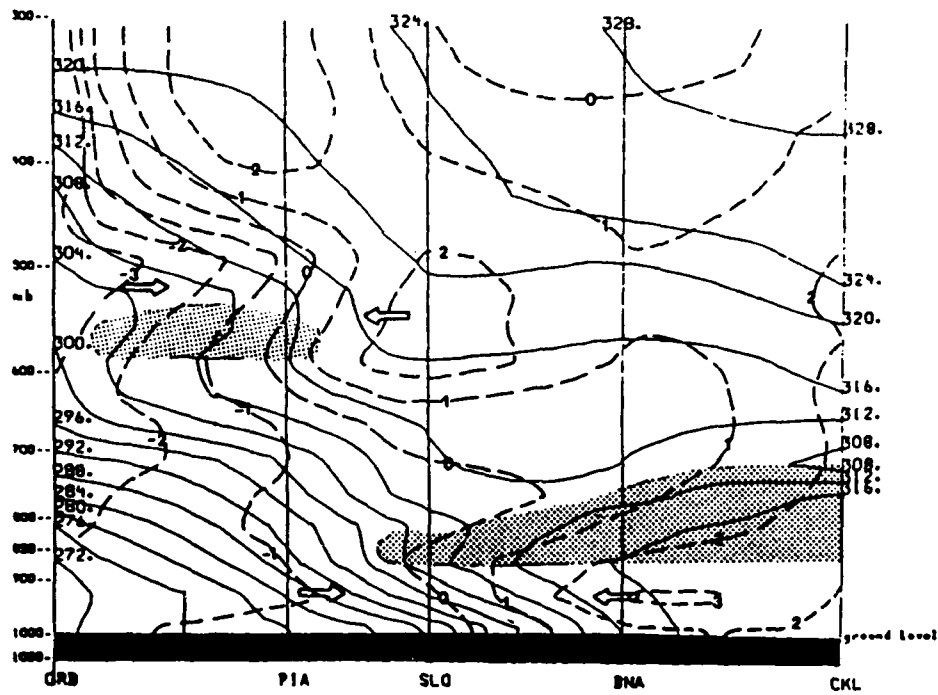


Figure 34. Cross section of equivalent potential temperature (solid lines, ° K) and wind components parallel to the plane of the cross section (dashed lines, knots). Positive values denote winds from right to left and negative values denote winds from left to right. GRB = Green Bay, WI; PIA = Peoria, IL; SLO = Salem, IL; BNA = Nashville, TN; CKL = Centerville, AL. Stippling denotes convective instability (Moore, et al., 1986).

## 5. CONCLUDING COMMENTS

The basic tools and physical concepts for using isentropic analysis techniques in the operational setting have been presented. It is now up to the reader to implement them in his/her forecasting environment so that an appreciation for how an isentropic viewpoint can help form a diagnosis may be gained. As always, experience is the best teacher. Undoubtedly one will find situations where these techniques can offer considerable insight into understanding why certain meteorological events are taking place. At other times, they may only *cloud* the issue. There are no cure-alls or quick fixes in this business. However, when used judiciously and interpreted properly it is the author's experience, shared by many others, that isentropic analysis can be used effectively *together with standard pressure analyses* to create a three-dimensional picture of atmospheric motions.

With the advent of faster computers and interactive graphic capabilities in the forecast office, the time seems right to re-introduce the isentropic viewpoint to the forecaster community. With patience and experience they will see its utility in the diagnosis and forecast process.

## 6. REFERENCES

Abbott, E. A., 1952: Flatland, A Romance of Many Dimensions. Dover Publications Inc., New York, N.Y., 103 p.

Anderson, J. F., 1984: The Use and Interpretation of Isentropic Analysis. NOAA Tech. Memo. NWS WR-188, National Weather Service Western Region, Salt Lake City, UT, 84147-0188, 40 p.

Anthony, R. W., W. E. Carle, J. T. Schaefer, R. L. Livingston, A. L. Siebers, F. L. Mosher, J. T. Young, and T. M. Whittaker, 1982: The Centralized Storm Information System at the NOAA Kansas City Complex. Preprints - Ninth Conference on Weather Forecasting and Analysis, Seattle, WA, Amer. Meteor. Soc., 40-43.

Barnes, S. L., 1973: Mesoscale Objective Analysis Using Weighted Time-Series Observations. NOAA Tech. Memo ERL NSSL-62 National Severe Storms Laboratory, Norman, OK 73069, 60 p. [NTIS Com-73-10781]

Blackadar, A. K., and J. Dutton, 1970: Tracers in the Air. *Weatherwise*, 23, 182-185.

Bleck, R., 1973: Numerical Forecasting Experiments Based on the Conservation of Potential Vorticity on Isentropic Surfaces. *J. Appl. Meteor.*, 12, 737-752.

Browning, K. A., 1986: Conceptual Models of Precipitation Systems. *Weather and Forecasting*, 1-2, 23-41.

Burger, D., 1965: Sphereland, A Fantasy About Curved Spaces and an Expanding Universe. Barnes and Noble Books, Harper and Row Publishers, New York, 208 p.

Byers, H. R., 1938: On the Thermodynamic Interpretation of Isentropic Charts. *Mon. Wea. Rev.*, 66, 63-68.

Carlson, T. N., 1980: Airflow Through Midlatitude Cyclones and the Comma Cloud Patterns. *Mon. Wea. Rev.*, 108, 1498-1509.

Carr, F. H., and J. P. Millard, 1985: A Composite Study of Comma Clouds and Their Association with Severe Weather over the Great Plains. *Mon. Wea. Rev.*, 113, 370-387.

Danielsen, E. F., 1959: The Laminar Structure of the Atmosphere and its Relation to the Concept of the Tropopause. *Arch. Meteor. Geophys. Bioklim. Atol.*, Ser. A, 11, 232-293.

\_\_\_\_\_, E. F., and E. R. Reiter, 1960: Bemerkungen zu E. Kleinschmidt: Nichtadiabatische Abkühlung im Bereich des Jet-Stream. *Beitr. Phys. Atmos.*, 32, 265-273.

\_\_\_\_\_, E. F., 1961: Trajectories: Isobaric, Isentropic and Actual. *J. Meteor.*, 18, 479-486.

\_\_\_\_\_, E. F., 1966: Research in four-dimensional Diagnosis of Cyclonic Storm Cloud Systems. Rep. No. 66-30, Air Force Cambridge Research Lab., Dept. 66-30, Bedford, MA, 53 p. [NTIS AD 632 668].

\_\_\_\_\_, E. F., and R. Bleck, 1967: Moist Isentropic Flow and Trajectories in a Developing Wave Cyclone. Rep. No. 67-0617, Air Force Cambridge Research Lab., Dept. 67-0617, Bedford, MA, 34 p. [NTIS AD 670 847].

\_\_\_\_\_, E. F., 1968: Stratospheric-Tropospheric Exchange Based on Radioactivity, Ozone and Potential Vorticity. *J. Atmos. Sci.*, 25, 502-518.

Doswell, C. A., 1986: The Human Element in Weather Forecasting. *Nat. Wea. Dig.*, 11, 6-18.

Duquet, R. T., 1964: Data processing for Isentropic Analysis. Tech. Report No. 1, Contract AT (30-1)-3317, Pennsylvania State University, State College, PA, 33 pp. [Available from Pennsylvania State University, Dept. of Meteorology, University Park, PA 16802].

Dutton, J. A., 1976: The Ceaseless Wind. McGraw-Hill, Inc., New York, 579 p.

Edson, H., 1966: Technique Development Reports - 1966. Technical Report 188, Air Weather Service (MAC), USAF, 135-143.

Eliassen, A., and E. Raustein, 1968: A Numerical Integration Experiment with a Model Atmosphere Based on Isentropic Coordinates. *Meteorologist Annale*, 5, 45-63.

Gidel, L. T., and Shapiro, M. A., 1970: The Role of Clear Air Turbulence in the Production of Potential Vorticity in the Vicinity of Upper Tropospheric Jet Stream Frontal Systems. *J. Atmos. Sci.*, 36, 2125-2138.

Haagenson, P. and M. A. Shapiro, 1970: Isentropic Trajectories for Derivation of Objectively Analyzed Meteorological Parameters. NCAR Technical Note NCAR/TN-149+STR, Boulder, CO, 30 p.

Hess, S. L., 1959: Introduction to Theoretical Meteorology. Holt, Rinehart and Winston, New York, p. 30-34.

Holton, J. R., 1972: An Introduction to Dynamic Meteorology. Academic Press, New York, p. 69-73.

Homan, J. H., and R. A. Petersen, 1985: The Use of a Simplified Isentropic Model for Nowcasting Convective Development. Preprints - Fourteenth Conference on Severe Local Storms, Indianapolis, IN, Amer. Meteor. Soc., 394-397.

\_\_\_\_\_ and L. W. Uccellini, 1987: Winter Forecast Problems Associated with Light to Moderate Snow Events in the Mid-Atlantic States on 14 and 22 February 1986. *Weather and Forecasting*, 2, 206-228.

Hoskins, B. J., and F. P. Bretherton, 1972: Atmospheric Frontogenesis Models: Mathematical Formulation and Solution. *J. Atmos. Sci.*, 29, 11-37.

Koch, S. E., M. DesJardins, P. J. Kocin, 1983: An Interactive Barnes Objective Map Analysis Scheme for Use with Satellite and Conventional Data. *J. of Climate and Appl. Meteor.*, 12, 1487-1503.

Kocin, P. J., L. W. Uccellini, and R. A. Petersen, 1981: The Role of Jet Streak "Coupling" in the Development of the 10-11 April Wichita Falls Tornado Outbreak. Preprints - Twelfth Conference. Severe Local Storms, San Antonio, TX, Amer. Meteor. Soc., 560-563.

Little, C. D., 1985: Isentropic Plotter. NOAA Eastern Region Computer Programs and Problems, NWSA ERCP-No. 29, NOAA, U.S. Dept. of Commerce, 10 p.

Moore J. T. and M. F. Squires, 1982: Ageostrophic Winds and Vertical Motion Fields Accompanying Upper Level Jet Streak Propagation During the Red River Valley Tornado Outbreak. Preprints - Ninth Conference on Weather Forecasting and Analysis, Seattle, WA, Amer. Meteor. Soc., 424-429.

Moore, J. T., 1985: A Diagnostic, Isentropic Analysis Package for the Short Term Prediction of Severe Convective Threat Areas. Preprints - Fourteenth Conference on Severe Local Storms, Indianapolis, IN, Amer. Meteor. Soc., 127-130.

Moore, J. T., 1986: The Effect of Diabatic Heating/Cooling on Vertical Motions in the Severe Storm Environment. Preprints - Eleventh Conference on Weather Forecasting and Analysis, Kansas City, MO., Amer. Meteor. Soc., 211-216.

Moore, J. T., P. D. Blakley, and C. A. Zacher, 1986: Thunderstorms with Snow: The Paralyzing Midwest Snowstorm of 30-31 January 1986. Submitted to Weatherwise.

Montgomery, R. B., 1937: A Suggested Method for Representing Gradient Flow in Isentropic Surfaces. *Bull. Amer. Meteor. Soc.*, 18, 210-212.

Namias, J., 1938: Thunderstorm Forecasting with the Aid of Isentropic Charts. *Bull. Amer. Meteor. Soc.*, 19, 1-14.

\_\_\_\_\_, J., 1939: The Use of Isentropic Analysis in Short Range Forecasting. *J. Aeronaut. Soc.*, 5, 295-298.

\_\_\_\_\_, J., 1940: An Introduction to the Study of Air Mass and Isentropic Analysis. Amer. Meteor. Soc., Boston, MA, edited by Robert G. Stone, 232 p.

Oliver, V. J., and M. B. Oliver, 1951: Meteorological Analysis in the Middle Latitudes. Compendium of Meteorology, Amer. Meteor. Soc., Boston, MA, 715-727.

Palmen, E., and C. W. Newton, 1969: Atmospheric Circulation Systems. Academic Press Inc., New York, Vol. 13, 195-227 p.

Petersen, R. A. and L. W. Uccellini, 1979: The Computation of Isentropic Trajectories Using a "Discrete Model" Approach. *Mon. Wea. Rev.*, 107, 566-574.

\_\_\_\_\_, R. A., 1986: Detailed Three-Dimensional Isentropic Analysis Using an Objective Cross-Sectional Approach. *Mon. Wea. Rev.*, 114, 719-735.

Reed, R. J., 1955: A Study of a Characteristic Type of Upper-Level Frontogenesis. *J. Meteor.*, 12, 226-237.

Reiter, E. R., 1972: Atmospheric Transport Processes, Part 3: Hydrodynamic Tracers. Atomic Energy Commission Critical Review Series, [NTIS TID-25731/LA] Springfield, VA 22161, 212 p.

\_\_\_\_\_, E. R., 1975: Stratospheric-Tropospheric Exchange Processes. *Review of Geophysics and Space Physics*, 13, 459-474.

Rossy, C. G., et al., 1937: Isentropic Analysis. *Bull. Amer. Meteor.* 18, 201-209.

Rubino, J. T., 1986: The Diagnosis of Adiabatic Forcing in the Severe Storm Environment Using Isentropic Trajectories M.S. Thesis, St. Louis University, 119 p.

Saucier, W., 1955: Isentropic Analysis. Chap. 8 in Saucier, W., Principles of Meteorological Analysis, Chicago, IL, Univ. of Chicago Press, 438 p.

Shapiro, M. A., 1974: A Multiple Structured Frontal Zone-Jet Stream System as Revealed by Meteorologically Instrumented Aircraft. *Mon. Wea. Rev.*, 102, 244-253.

\_\_\_\_\_, M. A., 1976: The Role of Turbulent Heat Flux in the Generation of Potential Vorticity of Upper Level Jet Stream Systems. *Mon. Wea. Rev.*, 104, 892-906.

\_\_\_\_\_, M. A., 1980: Turbulent Mixing within Tropopause Folds as a Mechanism for the Exchange of Chemical Constituents between the Stratosphere and Troposphere. *J. Atmos. Sci.*, 37, 994-1004.

\_\_\_\_\_, M. A., A. J. Krueger, and P. J. Kennedy, 1982: Nowcasting the Position and Intensity of Jet Streams Using a Satellite-Borne Total Ozone Mapping Spectrometer. *Nowcasting*, K. A. Browning, Ed., Academic Press, 137-145.

Spilhaus, A. F., 1938: Isentropic Airplane Flights--A Suggestion. *Bull. Amer. Meteor. Soc.*, 19, 279-280.

Staley, D. O., 1960: Evaluation of Potential Vorticity Changes near the Tropopause and the Related Vertical Motions, Vertical Advection of Vorticity, and Transfer of Radioactive Debris from Stratosphere to Troposphere. *J. Meteor.*, 17, 591-620.

Uccellini, L.W., 1976: Operational Diagnostic Applications of Isentropic Analysis. *Nat. Wea. Dig.*, 1, 4-12.

\_\_\_\_\_, L. W., and D. R. Johnson, 1979: On the Coupling of Upper and Lower Level Jet Streaks and Implications for the Development of Severe Convective Storms. *Mon. Wea. Rev.*, 107, 682-703.

\_\_\_\_\_, L. W., D. Keyser, K. F. Brill and C. H. Wash, 1985: The President's Day Cyclone of 18-19 February 1979: Influence of Upstream Trough Amplification and Associated Tropopause Folding on Rapid Cyclogenesis. *Mon. Wea. Rev.*, 113, 962-988.

Wilson, L. J., Siok, S. and B. Marois, 1980: Operational Application of Isentropic Analysis to the Diagnosis of Severe Convective Weather Threat Areas. Preprints - Eighth Conference on Weather Forecasting and Analysis, Denver, CO, Amer. Meteor. Soc., 166-173.

\_\_\_\_\_, L. J., 1985: Isentropic Analysis - Operational Applications and Interpretation, third edition. Edited for Training Branch by James Percy. Atmospheric Environment Service, Canada, 35 p.

**DISTRIBUTION**

AWS/DN, Scott AFB, IL 62225-5008.....	10
AWS/DO, Scott AFB, IL 62225-5008.....	3
OL-B, HQ AWS, Langley AFB, VA 23665-5000.....	1
CACDA, OL-E, HQ AWS, ATZL-CAW, Ft Leavenworth, KS 66027-5300.....	1
OL-G, HQ AWS, NHC Rm 631, 1320 S Dixie Hwy, Coral Gables, FL 33146-2976.....	1
OL-H, HQ AWS (ATSI-CD-CS-SWO), Ft Huachuca, AZ 85613-7000.....	1
OL-I, HQ AWS (ATD0-WE), Ft Monroe, VA 23651-5000.....	1
AFOTEK OL-NX, 1313 Halley Circle, Norman, OK 73069-8476.....	1
Det 1, HQ AWS, Pentagon, Washington, DC 20330-6560.....	1
Det 2, HQ AWS, Pentagon, Washington, DC 20330-5054.....	1
AFSCF/WE, PO Box 3430, Sunnyvale AFS, CA 94088-3430.....	1
Det 8, HQ AWS, PO Box 4239N, Las Vegas, NV 89030.....	1
Det 9, HQ AWS, PO Box 12297, Las Vegas, NV 89112-0297.....	1
1WW/DN, Hickam AFB, HI 96853-5000.....	2
20WS/DN, APO San Francisco 96328-5000.....	1
30WS/DN, APO San Francisco 96301-0420.....	1
2WW/DN, APO New York 09012-5000.....	2
7WS/DN, APO New York 09403-5000.....	1
28WS/DN, APO New York 09127-5000.....	1
31WS/DN, APO New York 09130-5000.....	1
3WW/DN, Offutt AFB, NE 68113-5000.....	2
9WS/DN, March AFB, CA 92518-5000.....	1
11WS/DN, Elmendorf AFB, AK 99505-5000.....	1
24WS/DN, Randolph AFB, TX 78150-5000.....	1
26WS/DN, Barksdale AFB, LA 71110-5002.....	1
4WW/DN, Peterson AFB, CO 80914-5000.....	2
2WS/DN, Andrews AFB, MD 20334-5000.....	1
5WW/DN, Langley AFB, VA 23665-5000.....	2
1WS, MacDill AFB, FL 33608-5000.....	1
3WS/DN, Shaw AFB, SC 29152-5000.....	1
5WS/DN, Ft McPherson, GA 30330-5000.....	1
25WS/DN, Bergstrom AFB, TX 78743-5000.....	1
AFGWC/SDSL, Offutt AFB, NE 68113-5000.....	1
AFGWC/WF, Offutt AFB, NE 68113-5000.....	1
USAFAETAC, Scott AFB, IL 62225-5438.....	1
7WW/DN, Scott AFB, IL 62225-5008.....	2
6WS, Hurlburt Field, FL 32544-5000.....	1
15WS/DN, McGuire AFB, NJ 08641-5002.....	1
17WS/DN, Travis AFB, CA 94535-5000.....	1
MAC/SCOOS, Scott AFB, IL 62225-5000.....	1
JSOC/Weather, P.O. Box 70239, Fort Bragg, NC 28307-5000.....	1
3350 TECH TG/TTGU-W, Stop 62, Chanute AFB, IL 61868-5000.....	5
AFIT/CIR, Wright-Patterson AFB, OH 45433-6583.....	1
AFCSA/SAGW, Washington, DC 20330-5000.....	1
NAVOCEANCOMDET, Federal Building, Asheville, NC 28801-2723.....	1
NAVOCEANCOMFAC, NSTL, Bay St Louis, MS 39529-5002.....	1
COMNAVOCEAN, NSTL, MS 39529-5000.....	1
NAVOCEANO, ATTN: Code 9220 (Tony Ortolano), Bay St Louis, MS, NSTL 39522-5001.....	1
NEPRF, Monterey, CA 93943-5106.....	1
Naval Research Laboratory, Code 4323, Washington, DC 20375.....	1
Naval Post-Graduate School NC4(63rd), Monterey, CA 93943-5100.....	1
Naval Eastern Oceanography Ctr, U117 McCAdy Bldg, Attn: Clim Section (AG2 Kopera),	
NAS Norfolk, Norfolk, VA 23511-5000.....	1
Naval Western Oceanography Ctr, Box 113, Attn: Tech Library, Pearl Harbor, HI 96860-5000.....	1
Naval Oceanography Command Ctr, COMNAVMAR Box 12, FPO San Francisco, CA 96630-5000.....	1
AFGL Library, Attn: SULLR, Stop 29, Hanscom AFB, MA 01731-5000.....	1
Atmospheric Sciences Laboratory, White Sands Missile Range, NM 88002-5501.....	1
U.S. Army Missile Command, ATTN: AMSMI-RD-TE-T, Redstone Arsenal, AL 35898-5250.....	1
Technical Library, Dugway Proving Ground, Dugway, UT 84022-5000.....	1
NCDC Library (D542X2), Federal Building, Asheville, NC 28801-2723.....	1
DTIC-FDAB, Cameron Station, Alexandria, VA 22304-6145.....	2
NBS Pubs Production, Rm A-536, Admin Bldg, Gaithersburg, MD 20899.....	1
AUL/LSE, Maxwell AFB, AL 36112-5564.....	1
AWSTL, Scott AFB, IL 62225-5438.....	100